UNIVERSIDADE DA BEIRA INTERIOR
Engenharia

Design of MECSE Nanosatellite Mechanical Subsystem

Ana Rita Moreira Azevedo

Dissertação para obtenção do Grau de Mestre em
Engenharia Aeronáutica
(Ciclo de Estudos Integrado)

Orientador: Doutor Pedro Vieira Gamboa
Co-orientador: Mestre Tiago Alexandre Rebelo

Covilhã, outubro de 2017

Dedication

This Master Dissertation is dedicated to the memory of my beloved grandfather Joaquim Moreira.

Acknowledgments

I would like to express my gratitude to my advisor at UBI, Professor Pedro Vieira Gamboa for his precious help and support. I appreciated his advices and his confidence in me.

Many thanks go to my advisor at CEiiA, Engineer Tiago Rebelo who dedicated his precious time helping me and keeping me in the right path. I would also like to thank CEiiA for the unique opportunity to enrich me as a person and as a professional. Moreover, this gratitude includes CEiiA's team: Paulo Figueiredo and André João. I have no words to describe your kindness and everything you have done to help me finish this thesis, you were essential during this path.

Thank you all whom helped me during this thesis, especially a huge thanks to my friends: Jorge Monteiro, Carlos Mendes, Beatriz Fernandes, Fábio Ventura, Guilherme Azevedo, Wesley Fernandes and Gonçalo Pardal for listening to me when I most needed.

I am forever thankful to my mother Inês, who was present during the good and bad days and encouraged me to be a better person, to my father, Vitor, who always supported my choices and adventures, to my grandmother, Firmina, who always had kind words of support during this journey and finally to my grandfather, Joaquim, who taught me that only strong man cry.

Resumo

Magnetohydrodynamics/Electrohydrodynamics CubeSat Experiment (MECSE) é o primeiro CubeSat a ser desenvolvido na Universidade da Beira Interior (UBI), resultando da colaboração do C-MAST (Centro de Ciências e Tecnologia Mecânica e Aeroespacial) e o CEiiA (Centro de Engenharia e Desenvolvimento de Produto). A missão do MECSE é criar uma plataforma para a futura validação da teoria que afirma que um campo electromagnético permite diminuir a espessura da camada de plasma e, como tal, permitir comunicações durante a reentrada atmosférica, evitando a chamada fase de *blackout*.

De modo a dar forma à missão, foi necessário o desenvolvimento do produto CubeSat que respeite os requisitos ciêntificos bem como as limitações de produção e regulação espacial, promovendo assim a viabilidade técnica. Esta dissertação de mestrado tem como objectivo o desenvolvimento preliminar do Subsistema Mecânico do MECSE, cuja configuração assegura a fiabilidade estrutural durante o lançamento e em órbita.

A abordagem adotada para o design do Subsistema Mecânico do MECSE foi a de primeiro definir os diferentes requisitos de projeto. Depois da definição dos subsistemas necessários, os componentes e respectivos requisitos de hardware foram escolhidos com base em missões semelhantes. O projeto também apresenta requisitos de design que foram estabelecidos tendo por base as especificações de design de Cubesats e as especificações da plataforma de lançamento P-POD. Depois da definição de requisitos, o material para a estrutura primária foi escolhido. Um estudo de *trade-off* foi realizado em que se comparou várias propriedades dos materiais (p.ex condutividade térmica, condutividade elétrica, maleabilidade, entre outros) e a liga de alumínium 7075 T6 foi a escolhida para a estrutura primária do MECSE.

A aeronave deve resistir a um conjunto de cargas mecânicas sem deformar permanentemente com uma determinada margem de segurança devido às incertezas do valor associado às cargas durante o lançamento. Análises em elementos finitos validaram a capacidade do MECSE em resistir às cargas estáticas lineares e às temperaturas estáticas durante o lançamento e em órbita. Os componentes foram avaliados e foi concluído que todos os componentes com exceção das *Side Frames* deveriam ter a sua espessura reduzida, pois apresentavam uma margem de segurança alta para tensão e deformação.

Um estudo de impacto térmico foi realizado e foi possível concluir que os subsistemas terão o seu envelope de operação condicionado pelo ângulo entre o plano de órbita e o vetor solar. De forma a aumentar o envelope de operações, é recomendada a aplicação de aerogel.

Palavras-chave

Nanosatélite, CubeSat, Magnetohydrodynamics/Electrohydrodynamics CubeSat Experiment, MECSE, Subsistema Mecânico do MECSE, Análises de elementos finitos em CubeSats, Impacto Térmico.

Abstract

Magnetohydrodynamics/Electrohydrodynamics CubeSat Experiment (MECSE) is the first CubeSat being developed at the University of Beira Interior (UBI) and it is an under development Nanosatellite resulting from the collaboration between C-MAST (Center for Mechanical and Aerospace Science and Technologies) and CEiiA (Centre of Engineering and Product Development). MECSE's mission is to create a benchmark for the future validation of the theory that an Electromagnetic field can re-shape the layer of plasma surrounding a spacecraft, and therefore allow communications during the so-called atmospheric re-entry Radio Frequency (RF) blackout phase.

When it comes to scientific space research there is a need to create a bridge between the scientific goals and the engineering feasibility. In order for the mission to take shape, the development of the product CubeSat shall meet scientific requirements as well as production limitations and space regulations. This master dissertation aims to preliminarily develop MECSE's Mechanical Subsystem. In this work, a Mechanical Subsystem configuration that ensures the structural reliability during launch, as well as on orbit was developed.

The approach adopted for the design of MECSE's Mechanical System was to, first, define the different project requirements, and then, COTS hardware components were selected based on similar previous missions and their requirements were specified. The project also presents Design Requirements that were specified based on the CubeSat Design Specifications, and the launch platform P-POD. Finally, the materials for the primary structure of the CubeSat had to be selected. A trade-off was performed comparing several material properties (e.g. thermal conductivity, electrical conductivity, workability and others) and the aluminum alloy 7075 T6 was chosen.

The spacecraft must sustain a set of mechanical loads without permanent deformation, with a certain margin of safety to prevent the uncertainties in the loading values during launch. A finite element analysis validated the capacity of MECSE to sustain the linear static loads and static temperature during launch and on-orbit.The components were evaluated and, with exception of the Side Frames, the primary structural components should have their thickness reduced, since they presented high margins of safety to stress and strain.

The thermal impact study showed that the subsystems will have their envelope of operations conditioned by the angle between the orbit plane and the solar vector. In order to increase the envelop of operations it was recommended the use of aerogel.

Keywords

Nanosatellite, CubeSat, Magnetohydrodynamics/Electrohydrodynamics CubeSat Experiment, MECSE, MECSE Mechanical Subsystem , CubeSat's Finite Element Analysis, Thermal Impact.

Contents

List of Figures

List of Tables

Abbreviated Terms

NOT UPDATED

AM	Additive Manufacturing
AOCS	Attitude and Orbit Control Subsystem
ASAT	Anti-Satellite Weapons
CAD	Computer Aided Design
CAE	Computer Aided Engineering
CCCs	Carbon-Carbon Composites
CDH	Computer and Data Handling Subsystem
CDS	CubeSat Design Specification
C-MAST	Center for Mechanical and Aerospace Science and Technologies
COTS	Commercial Off-The-Shelf
CSK	CubeSat Kit
DAR	Deviation Waver Approval Request
DOF	Degree of Freedom
ECSS	European Cooperation of Space Standardization
EMB	Electrical Management Boards
EPS	Electrical Power Subsystem
ESA	European Space Agency
FDM	Fusion-Deposition Modeling
FEA	Finite Element Analysis
FEM	Finite Element Method
FoS	Factors of Safety
GNC	Guidance, Navigation and Control
GNSS	Global Navigation Satellite System
HMS	High Margin of Safety
ISIS	Innovative Solutions in Space
ITO	Indium Tin Oxide
LV	Launch Vehicle
MECSE	Magnetohydrodynamics/Electrohydrodynamics CubeSat Experiment
MEMS	Micro-Electro-Mechanical Systems
MFS	Multifunctional Structure
MLI	Multi-Layer Insulation
MMCs	Metal-Matrix Composites
MMS	Mechanical Subsystem and Structures
MS	Margin of Safety
NASA	National Aeronautics and Space Administration
PDE	Partial Differential Equations
P-POD	Poly Picosatellite Orbital Deployer
PSB	Power Management Board
PMCs	Polymer-Matrix Composites
QSL	Quasi-Static Loads
RF	Radio Frequency
RBF	Remove Before Flight

S/C	Spacecraft
SMS	Structure and Mechanisms Subsystem
SRS	Shock Response Spectra
SPC	Single Point Constraint
STK	STK
TCS	Thermal Control Subsystem
TE	Maximum Time of Eclipse
TS	Maximum Time of Sunlight
TTC	Telemetry, Tracking and Control Subsystem
U	Unit = $10cm \cdot 10cm \cdot 10cm$
UBI	Universidade da Beira Interior

Nomenclature

A_{Earth}	Area Facing the Earth
A_{Sun}	Area facing the Sun
A_{Total}	Total Area of the Spacecraft
CTE	Coefficient of Thermal Expansion
E	Modulus of Elasticity
F	Vector of Loads
F_{cy}	Transverse Tensile Yield Strength
F_{tu}	Longitudinal Ultimate Tensile Strength
F_{ty}	Longitudinal Tensile Yield Strength
G	Shear Modulus
G_{Earth}	Earth IR Constant
G_{Sun}	Sun Radiant Constant
$h_{Mission}$	Orbit's Altitude
I	Area Moment of Inertia
K	Stiffness Matrix
K_L	Load Factor
K_M	Modeling Factor
K_{MT}	Material Factor
KR	Rotational Stiffness
L_{eff}	Column's Effective Length
L_i	Low Frequency Dynamic Load Factor
M	Bending Moment
n	Number of orbits
N_i	Combined Load Factor
P	Orbital Period
$P1$	Maximum Principal Stress and Strain
$P3$	Minimum Principal Stress and Strain
P_{cr}	Critical Load
$\overline{q}$	Heat Flow Rate Vector
Q_{Albedo}	Reflected Solar Absorption Heat
Q_{Earth}	Emitted Heat from Earth
$Q_{Internal}$	Internal Heat Generated from Satellite's components
Q_{Sat}	Total Energy Input to Satellite
Q_{Solar}	Solar Absorption Heat
ρ	Density
R_{Earth}	Earth Radius
R_i	High Frequency Random Vibration Load Factor
S_i	Steady State Load Factor
T	Temperature
u	Displacement Vector
v	Orbital Velocity
y	Distance from neutral axis

Greek

α	Absorptivity
$\alpha_{Mission}$	Orbit's semi major axis
α_{Sun}	Solar Absorptivity
β	Orbit Beta Angle
γ_{Earth}	Gravitational parameter
ε	Strain
ε	Emissivity
η_{Min}	Minimum Safety Factor
σ	Boltzman Constant
σ	Stress
σ_{cr}	Buckling Stress
σ_{P1}	Maximum Principal Stress
σ_{P3}	Minimum Principal Stress
$\sigma_{Von-Mises}$	Extreme Von-Mises Stress
τ_{xy}	Shear Stress

Chapter 1

Introduction

1.1 Motivation

Traditionally, the space industry produced large and sophisticated spacecraft projected by engineering teams during several years with high budgets within the reach of only few government-backed institutions, making it impracticable for the Academic institutions. However, over the last decade, the space industry experienced an increased interest towards smaller missions and recent advances in MEMS (Micro-Electro-Mechanical Systems) technology, spurred the development of missions based on the CubeSat standard [3]. In fact, components have been reduced to minimum physical limitations through changes in micro packaging techniques which allowed miniaturization

The CubeSat program was developed with the goal of providing universities with the opportunity to launch educational satellites as secondary payloads, ensuring that CubeSats have a set of interfaces with the launch vehicles that minimize the risks to the payload [3, 4]. Yet, their use has rapidly spread within academia, industry, and government agencies (e.g. European Space Agency (ESA), the National Aeronautics and Space Administration (NASA), among others) due to their low-cost and rapid development which allows the launch to occur within normally two years since the project starts [3].

Commercial companies are also developing their own CubeSats, using cost effective access to space to accomplish their mission requirements. Clearly, CubeSats started to transition from being solely educational and technology demonstrative platforms to offer opportunities for low-cost scientific missions with high potential value in terms of scientific return and commercial revenue [3, 5].

Magnetohydrodynamics/Electrohydrodynamics CubeSat Experiment (MECSE) as many CubeSats presents educational purposes, but also presents scientific purposes as it aims to create a benchmark for the future validation of the theory that an Electromagnetic field can re-shape the layer of plasma surrounding a spacecraft and, therefore, allow communications during the so-called atmospheric re-entry Radio Frequency (RF) blackout phase [6, 7]. Continuous communications, real-time telemetry and GNSS signal reception are essential parameters that ensure the accomplishment of manned and unmanned space missions. For that reason, the mitigation of the RF blackout is essential in the design of re-entry space vehicles. Solutions that may solve or attenuate this issue are of high priority in scientific and technological agendas [6, 7].

This work aims to create a platform that allows the integration of all the required systems and payload for the MECSE mission, and to create a modular structure for CubeSats which proves to be cost effective and provide fast access to space.

1.2 State-of-the-Art

An artificial satellite[1] is by definition an artificial body intentionally placed in orbit around a planet to collect information or to enable communications. The World's first artificial satellite, Sputnik 1, was launched in 1957 by the Soviet Union and since then, dozens of countries have launched satellites [8]. PoSAT-1 is the first portuguese satellite and it was mainly used for military communications.

The mission is the objective of the satellite, which is imposed by the stakeholders' needs. There is a wide range of missions. Figure 1.1 details applications and some examples of satellite's missions.

	Communications and Navigation	Applications	Science	Education and Training	Exploration	Resource Utilization	Military	Other
Applications	Telephone	Weather	Earth monitoring	CubeSats	Moon	Materials processing	Surveillance	Space tourism
	TV (commercial)	Earth resources	Telescopes (visible, UV, IR, X-Ray, gamma ray, Radio)	Training missions	Planets and Satellites	Solar power satellites	Reconnaissance	Burial in space
	TV (direct broadcast)	Fire detection	Particle detection	Educational satellites Student viewing and tracking	Asteroids	Asteroid mining	Tactical	Space Colonies
	Satellite Radio	Oceanography	Magnetic fields		Comets	Atmosphere mining	Comm.	Lunar colonization
	Store and Forward	Disaster monitoring	Planetary		Beyond the Solar System Human and unmanned fly-bys, orbiters,	Lunar resource utilization	Space surveillance	Mars colonies
	Space-to-Space	Search and Rescue	SETI			Mars in-situ propellants	Missile warning	Space Stations
	Relay Satellites	Crop monitoring	Solar		Surface Rovers	He^3 from Lunar Regolith	Nuclear detection	Technology demonstration
	Military Comm	Global warming	Biological		Lunar/Mars sample return		ELINT	Technology tests
	Navigation (air, ships, cars, people)	Warning of space hazards	Materials research				SIGINT	Spacecraft repair, refurbishment,
	Amateur Radio	Commercial cargo/vehicle tracking					IMINT	Tugs, OTVs
		Ice flows					SDI	Tethers
		Orbital debris monitoring					Space-based laser	Prayer Wheel
							ASATs	Interstellar Travel
							Wind measurements	
Examples	IntelSat	LandSat	Hubble	StarShine	Apollo	Industrial Space Facilty	DSP	Sputnik
	Direct TV	SPOT	Chandra	EDUSAT	Galilio	SPS	FLTSATCOM	Celestis
	OrbComm	SeaSat	COBE	AAUSat	Cassini		MILSTAR	ISS
	Iridium	NPOES	IRAS	OUFTI-1	Voyager		GPS	MIR
	GlobalStar	GOES	JWST	PLUME	Mariner		BSTS	SkyLab

Figure 1.1: Space Missions Applications [8].

[1] In the next sections of this dissertation the term satellite will always refer to artificial satellite.

Satellites can also be classified by their mass [9]. Their different classes are presented in Table 1.1.

Table 1.1: Classification of Satellites per Mass ([9])

Category	Mass Range [kg]
Large Satellite	>1000
Medium Satellite	500-1000
Minisatellite	100-500
Microsatellite	10-100
Nanosatellite	1-10
Picosatellite	0.1-1
Femtosatellite	<0.1

Small Satellites are defined as satellites weighting less than 500 kg [8]. Even with small space-crafts, there is a large variety of size and mass (Table1.1). Small Satellites have been used since the beginning of the space program due to the limitations of size and capability of launch systems [8]. Typically, small satellites are simpler than larger satellites and have only a single payload and limited capacity, but in recent years due to the microminiaturization of consumer electronics, the capacity of small satellites has increased while maintaining a low budget. Over the last 50 years, more than 860 microsatellites (10–100 kg), 680 nanosatellites (1–10 kg), and 38 picosatellites (0.1–1 kg) have been launched worldwide [10]. 471 CubeSats with a size of 1U and larger have been launched until August 2016 with several different missions [10]. The 3U spacecrafts represent the largest fraction of all launches (57% share), while the 1U vehicles represent about 29% of all launches.

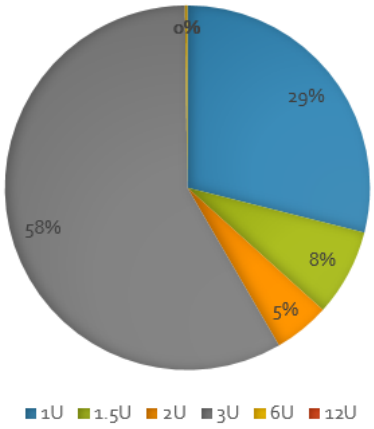

Figure 1.2: Percentage of Launches for each CubeSat Size [5].

1.2.1 CubeSat

A CubeSat is a cube with the dimension of 10x10x10 cm and a mass of up to 1,33 kg [4].The CubeSats' size is measured in units (U) and the form factor has been extended, ranging from 1U up to 6U. Larger sizes have been proposed but are not yet standardized (Figure 1.3). The standardization for the design of Pico/Nanosatellites has the purpose of reducing the cost and development time while increasing accessibility to space [4]. The CubeSat Project started in 1999, as a collaboration between Prof. Jordi Puig-Suari from California Polytechnic State University and Prof. Bob Twiggs from Stanford University [4].

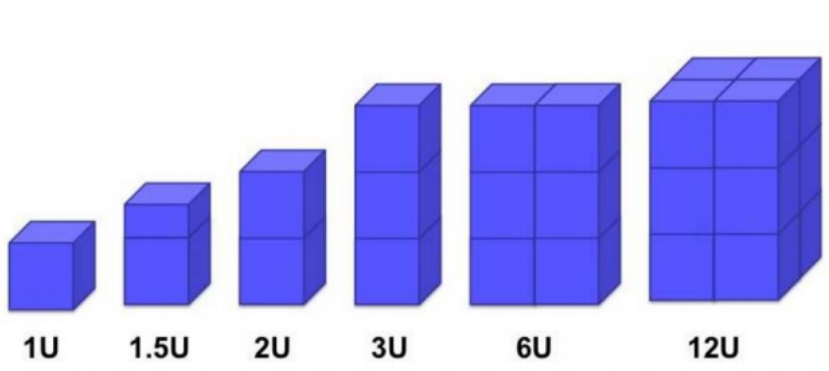

Figure 1.3: CubeSat Form Factor [5].

CubeSats missions are widespread and range from space environmental studies to telecommunications. Some missions also aim to demonstrate the efficiency of a newly developed system in space 1.2.

Table 1.2: CubeSat Missions [8]

Name	Type	Organization	Mission	Launch Year
Aeroclube 2	1U+	Aerospace Corporation	Education and Technology Testing	2002
DTUsat	3U	Standford University and Quake Finder	Earthquake Detection	2003
CUTE-1	1U	Tokyo Institute of Technology	Education, Separation System Demonstration, Technology Testing and Amateur Radio	2003
CanX-1	1U	University of Toronto	Technology Demonstration	2003
UWE-1	1U	University of Wuerzburg	Technology Demonstration	2005
COMPASS-1	1U	University of Applied Science at Aachen	Technology Demonstration	2008
SwissCube-1	1U	Ecole Polytechnique Fédérale de Lausanne	Upper Atmospheric Science Research	2009
RAX	3U	University of Michigan, Ann Arbor, MI, SRI International, Menlo Park and CA	Bi-static Radar measurement of Plasma Formation in Earth's Ionosphere	2010

1.2.2 General CubeSat Specification

Cal Poly [4] updates and distributes a document named CubeSat Design Specification (CDS) that describes all the requirements that a CubeSat shall meet. The document is divided in mechanical, electrical and operational requirements. In order to design the CubeSat's structure, some of the mechanical and general requirements shall be taken into consideration. The Waiver Process [2] is also described in the documents. The document also defines the testing requirements that the CubeSat shall meet in order to be launched. The requirements consist on random vibrations, thermal vacuum bake-out, shock testing, visual inspection, qualification, protoflight and, at last, qualification [4].

1.2.3 CubeSat Subsystems

It is convenient to subdivide the spacecrafts into functional subsystems. It is also important to recognize that the satellite itself is only a systen within a larger system [11]. A CubeSat can be broken down into three physical parts: the ground segment, the space segment and the launch segment (Figure 1.4).

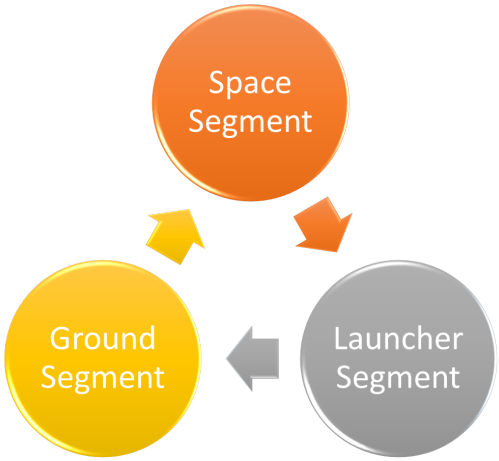

Figure 1.4: Segments of a CubeSat.

The launch vehicle transports the spacecraft to orbit. The ground segment enables commands to be sent up to the vehicle and enables status and payload information to be returned to the ground. The space segment can be divided into two modules: the payload, and service module. The first is the mission's specific equipment, and the second consists of subsystems that allow the correct functioning of the payload [8]. The service module can be divided into 6 subsystems, Figure 1.5, the Telemetry, Tracking and Control subsystem (TTC), the Command and Data Handling subsystem (CDH), the Attitude and Orbit Control subsystem(AOCS), the Electrical Power subsystem (EPS), the Thermal Control subsystem (TCS) and the Mechanical Subsystem and Structures (MSS).

[2] Developers will fill out a Deviation Waver Approval Request (DAR) if there is a violation of any requirements of the Poly Picosatellite Orbital Deployer (P-POD) or the CubeSat Specifications

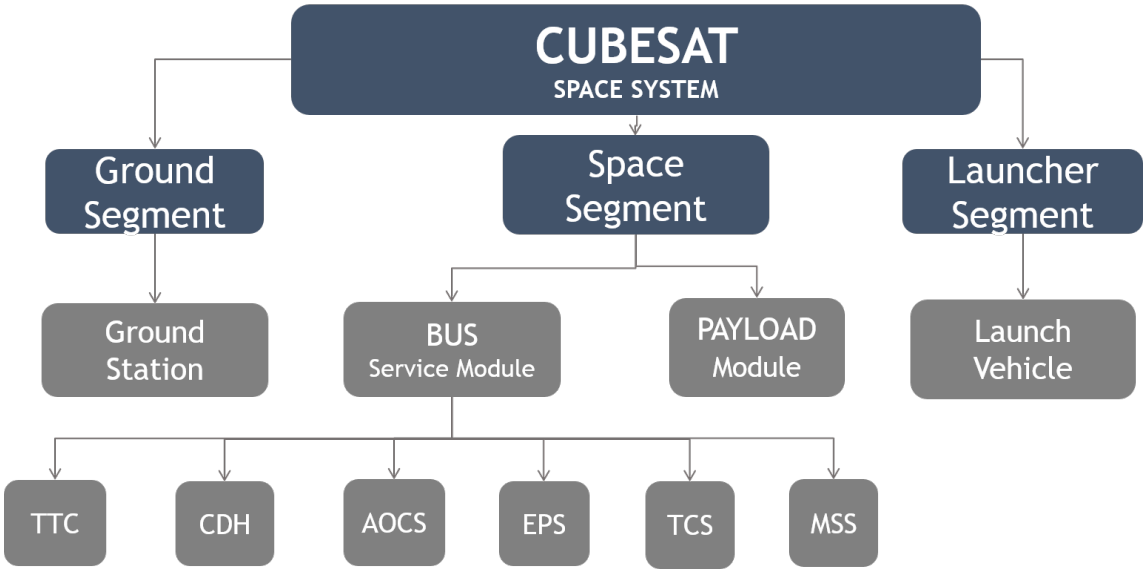

Figure 1.5: Architecture Diagram of the CubeSat Ground Segment, Space Segment, Launch Segment and each one with its own Subsystems.

Each satellite has many subsystems and each of them has a role to play ion-board the satellite. In practice, each satellite subsystem is assigned to one team of experts because each of the modules belong to one field of expertise [11]. On the other hand, there are connections between the various subsystems. Therefore, each team works in coordination with other teams to complete the tasks of each subsystem. In order to understand the connections between them, it is required to understand each subsystem individually.

1.2.3.1 Telemetry, Tracking and Control Subsystem (TTC)

Telemetry, Tracking and Control subsystem (TTC) is an essential subsystem of a spacecraft as it enables the transmission of data and telemetry to the Ground Station, it receives commands from Earth and transfers information to one another through the transmission of electromagnetic signals, typically at radio frequencies (RF). The process of sending information towards the spacecraft is called uplink or forward link and the opposite process is called downlink or return link. Uplink consists of commands and ranging tones whereas downlink consists of status telemetry, ranging tones and may even payload data. The mission data includes both the spacecraft engineering data and the sensor/instrument data generated by the payload, Figure 1.6.

Most of the early CubeSat missions used VHF and UHF radio frequency communications with typical data rates of 1.2 and 9.6 Kbps [12, 13]. However, the DICE 1.5U CubeSat mission launched in 2011 was able to achieve an higher data rate of 3 Mbps on UHF band [14]. Additionally, several CubeSat missions achieved higher data rates of up to a few Mbps through S-band communication systems [13]. These low rates are a major limiting factor for making cutting-edge miniaturized science instruments compatible with the CubeSat standard since the payload will generate significantly more data than it could possibly be downlinked at these rates [15]. Communication systems using higher bands such as X-band started to become compatible with CubeSat standards enabling much greater downlink capabilities for CubeSats [16]. Additionally, CubeSats' compatible high-speed Ka-band communication systems are also gradually becoming available, which will improve CubeSat data rates by orders of magnitude in the near future [17].

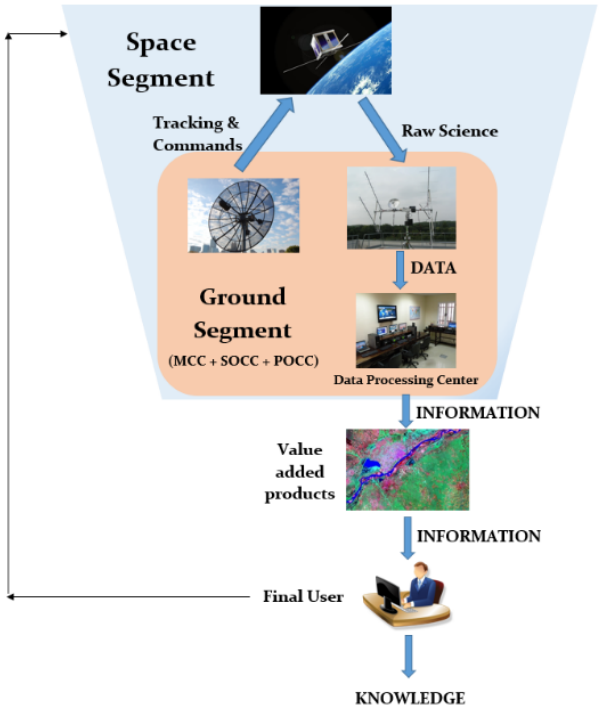

Figure 1.6: Functional relationship between space segment, ground segment and final user in a CubeSat mission [18].

1.2.3.2 Computer and Data Handling Subsystem (CDH)

The Computer and Data Handling Subsystem is responsible for receiving, decoding, and distributing commands to other subsystems as well as gathering, and storing housekeeping and mission data, Figure 1.7, for onboard use or downlink to the user. In general, Commercial off-the-shelf (COTS) microcontroller technologies enable high performance capabilities although with higher vulnerability to space radiation [12, 19].

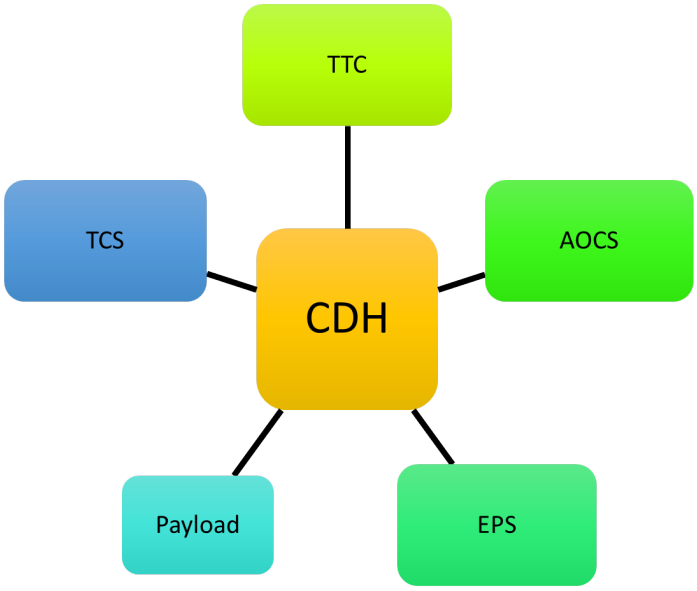

Figure 1.7: CDH dependency on Subsystems [8].

CubeSat onboard storage data can be as low as several Kbs or Mbs and depending on the mission requirements the total storage capacity could be increased up to hundreds of GBs by taking advantage of commercial flash memory technologies [3]. Overall, the CubeSat command and data handling subsystem is already relatively mature with a wide range of available options [3].

1.2.3.3 Attitude and Orbit Control Subsystem (AOCS)

The Orbit Determination and Control Subsystem (ODCS) measures and maintains the position of the satellite's center of mass as a function of time, while the Attitude Determination and Control Subsystem (ADCS), measures and maintains the satellite's orientation about its center of mass. AOCS combines the attitude sensors (e.g. star trackers, Sun sensors, Earth sensors, and magnetometers) that provide the knowledge of the vehicle's dynamics providing accurate and unique solution for the attitude state as a function of time [8]. Spacecraft may use actuators such as reaction wheels, magnetorquers, and thrusters to stabilize and orient spacecraft in a desired direction.

Figure 1.8 presents the major components of a general AOCS. The links between components identify the major interactions and the arrows indicate that there is a cause-effect relationship. In summary, if the main structure of the spacecraft is subjected to time-varying torques, it responds with attitude motion that will be detected by the sensors. Outputs from the sensors are sent to the on-board and the ground station computers and the information is used to determine the torques that should be applied to the structure to correct its orientation and attitude.

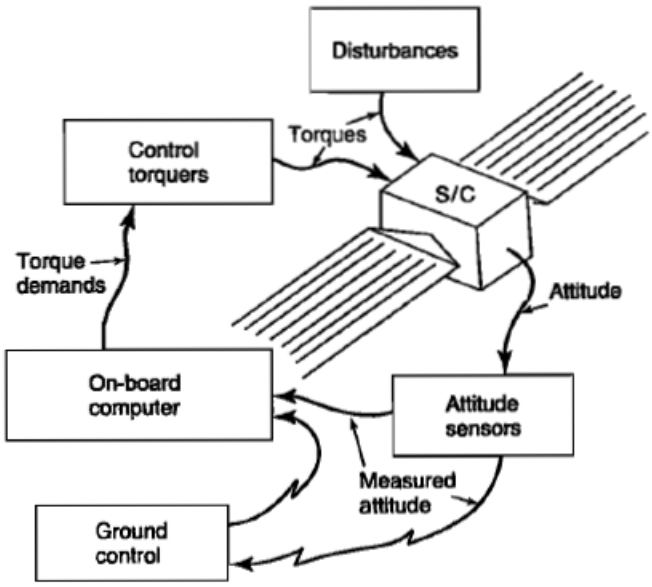

Figure 1.8: Block Diagram for an AOCS [20].

CubeSat's AOCS has been improved over the last decade due to the development of miniaturized hardware. Additionally, several companies are offering integrated units for precise 3-axis control, which combine different Guidance, Navigation and Control (GNC) components into a single package. Overall, CubeSat AOCS subsystem is a relatively mature subsystem with numerous flight proven components available in the market [21].

1.2.3.4 Electrical Power Subsystem (EPS)

Electrical Power Subsystem (EPS) is the source of power to whole subsystems, Figure 1.9. Nothing on the spacecraft works without electrical power [8].

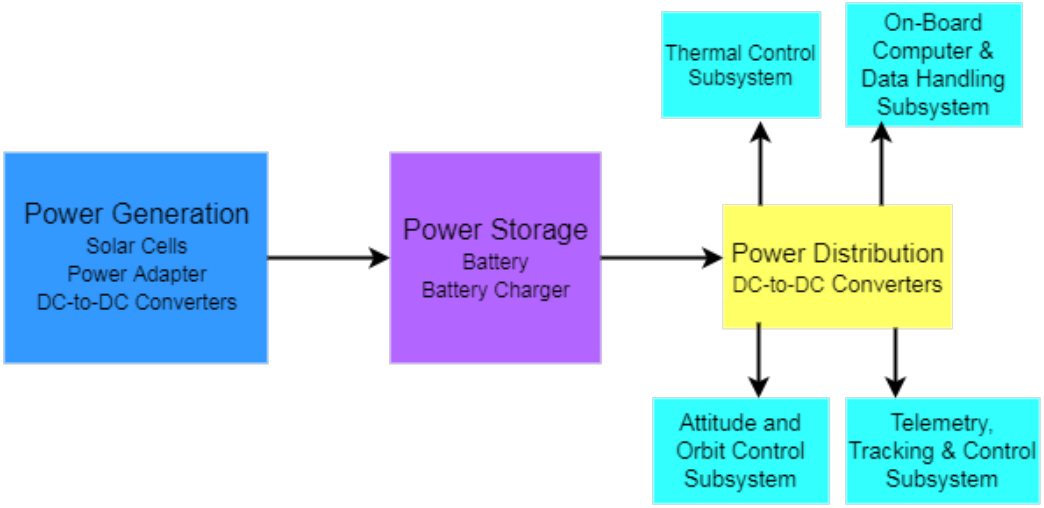

Figure 1.9: General Layout of EPS [adapted from reference [22]].

Photovoltaic solar cells are the primary power source for CubeSats and given the CubeSat surface area constraints, solar cells can be either deployable or body-mounted depending on the mission's power requirements [8, 16].

Additionally, spacecraft requires on-board energy storage capacity in order to provide power during the eclipses periods as well as to satisfy peak power requirements of the avionics that can be achieved using batteries. There is a wide range of battery types available in the market, such as high energy density lithium ion and lithium polymer batteries that can be used as primary or secondary power source for CubeSat missions [16].

Power distribution, regulation and control systems are often custom built by spacecraft designers based on their systems' requirements. Nevertheless, there are several options of power management systems in the CubeSat market provided by companies such as Clyde Space [23], and GomSpace [24], among others.

1.2.3.5 Thermal Control Subsystem (TCS)

In orbit, spacecrafts experience extreme temperature fluctuations over short time periods and while facing the Sun the temperature can reach over $+120°$C, whereas in eclipse the temperatures can get well below $-120°$C [25]. Hence thermal control is critical for the satellite's survival and its payload. It is the task of the structural designer to ensure survivability and functionality of both structural and nonstructural components [1].

The thermal budget of the spacecraft is influenced by external heat inputs from direct sunlight (which is the most important external heat source), sunlight reflected from the Earth or other planets and moons (albedo), and infrared (IR) energy emitted from a surface in addition to heat generated by internal components of the satellite [26]. The thermal control of the spacecraft

is attained by balancing the heat inputs against the energy emitted by the satellite [1, 8]. The temperature may be regulated based on mission requirements by two techniques, the Passive or the Active Thermal Control [1].

Passive thermal control uses no power input and can be accomplished by a variety of techniques such as Multi-Layer Insulation (MLI), Thermal Coating, Sun Shields, Louvers, Heat Pipes, Radiators and Thermal Straps. The passive approach has significant advantages such as no power consumption, low mass, low volume and low cost, which makes it a particularly attractive choice for CubeSats given their constraints [1, 16, 27].

Active thermal control systems rely on power input for operation. Figure 1.10 represents the typical transmission of heat and data between subsystems when using the active thermal control system. The structure receives heat from the radiation and emits heat from the radiance surfaces to space. The subsystems dissipate heat as they do not convert the entire energy that powers them, releasing this power in the form of heat loads to the structure. On the other hand the structure transmits the heat received from the radiance to the subsystems. The temperature sensors will sense the change on the temperature and transmit that information to the OBC. The OBC will activate the TCS, which will increase or decrease the subsystem's temperature. The active control systems include thermal straps, heaters and cryocoolers [8, 16].

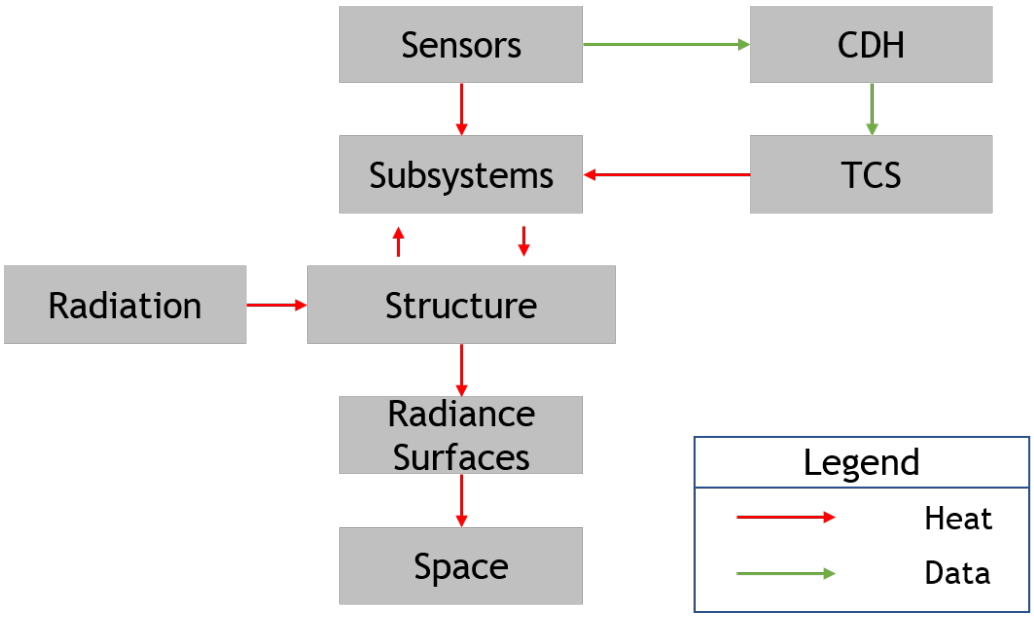

Figure 1.10: Transmission of Heat between Subsystems and Communications between the TCS and CDH subsystems.

Traditionally, thermal insulation could be combined with active control systems for a more effective and precise thermal regulation [16]. Several other technologies are under development, as for example active cryocoolers which are potentially compatible with CubeSat platforms (although none of them have flown on CubeSats to date) (Sunpower,Inc [28]; Northrop Grumman [29]; Lockheed Martin Space Technology and Research Lab [30], among others).

The temperature gradient across a small satellite is typically not significant, hence, CubeSats do not tend to use active thermal control methods due to the spacecraft's power limitations [8]. The heat pipes and other mechanisms as flight modes are also not normally use. Small satellites

cannot manage easily their internal temperature with electric heating or thermostats as they have a large surface area to volume ratio. The normal solution consists on the use of coatings and insulation minimizing the cold and hot cases. Depending on the needs of the thermal control, there are different types of coatings (e.g. black painting, white painting, among others) with different emissivities, Figure 1.11.The TCS subsystem will be surveyed in more detail in the next chapter.

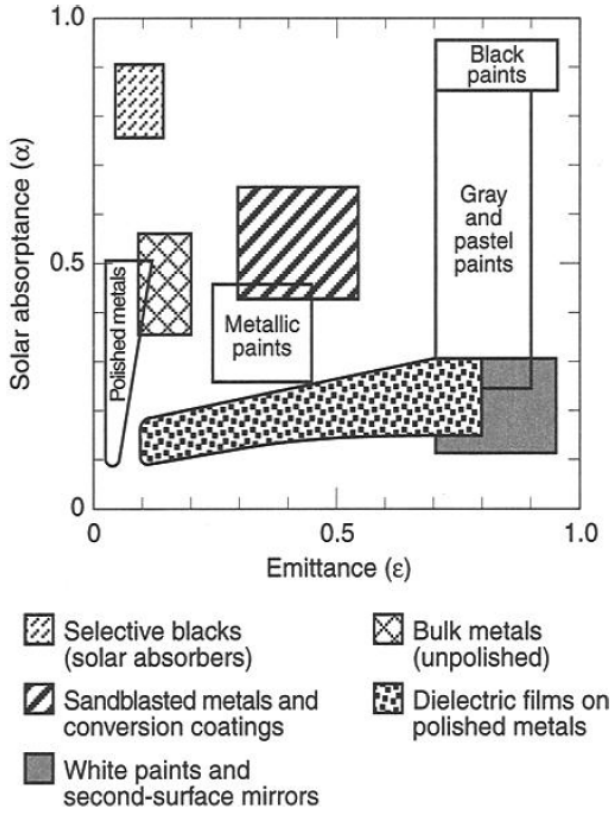

Figure 1.11: Surface Properties according to the type of Finish [1].

1.2.3.6 Mechanical Subsystem and Structures

The Structure is the primary skeleton of a spacecraft, which mechanically supports all spacecraft's subsystems while functioning as thermal and radiation shielding for sensitive components [8, 31]. Customized and off-the-shelf structures are the two main options for a CubeSat structure. The main advantage of off-the-shelf structures is their simplicity and flight heritage. On the other hand, customized structures may be more suitable for some missions that need to adapt the structural connections with payloads and/or subsystems, although they require extensive testing that will increase the cost budgets and the time of delivery [31]. Typically, CubeSat structures are made from aluminum and due to the improvement of the 3D printing, CubeSat structures fabricated with this technique are garnering some interest among developers, and have already been used on several missions [16].

Commercial Off-The-Shelf Structures

Regarding acquisition of COTS[3] structures specially built for CubeSats, the market has multiple suppliers of COTS, such as: Pumpkin Incorporated (USA), Innovative Solutions in Space (Netherlands), Clyde Space (UK), Nano Avionics, among others.

Pumpkin Incorporated presents the CubeSat Kit (Figure [32]) which has the entire structure and all the necessary components to allow satellite developers to concentrate on the mission's specific goals [32]. This structure is very rigid and it keeps the weight to a minimum. The structure is available to purchase in standard formats (1U, 2U or 3U) and also in 0,5U or 1,5U forms.

Figure 1.12: CubeSat Kit [32].

Innovative Solutions in Space (ISIS) offers a generic primary satellite structure based on the CubeSat standard [33]. Comparing ISIS with Pumpkin, it provides a less complex structure. ISIS structure features a modular design which involves the assembly of several small components. This satellite structure also contains a secondary structure that incorporates the circuit board stack to enhance the structural integrity of the CubeSat. Due to the characteristics of this structure the stack can be vertical or horizontal, allowing the customer to choose the most suitable stacking method for each particular mission. ISIS provide formats of 1U, 1.5U, 2U, 3U, 6U, 8U and 12U, Figure 1.13.

[3]COTS- Commercial Off-The-Shelf is a term used to describe the purchase of packaged solutions which are then adapted to satisfy the needs of the purchasing organization, rather than the commissioning of custom made or bespoke solutions

Figure 1.13: ISIS Form Factors [32].

Clyde Space structures are designed to allow the stack of printed circuit boards (PCB) to be mounted directly onto a set of rods housed in the structure end plate [23].The structure is also compatible with the CubeSat Standards and is available in 1U, 2U and 3U formats, Figure 1.14.

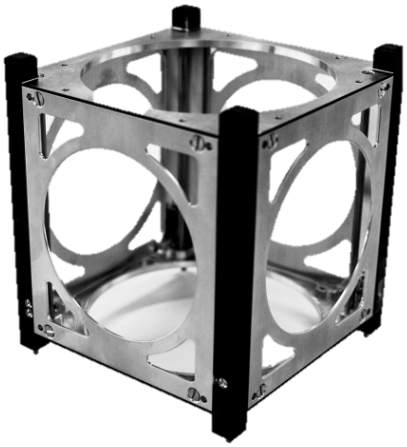

Figure 1.14: Clyde Space 1U Format [23].

Nano Avionics developed a modular Nanosatellite structure [34], which allows a high level of freedom in the spacecraft configuration. The avionics and payload are built as a single 1U building blocks that are mounted into the primary structure. These structures are available in 1U, 2U and 3U formats, Figure 1.15.

Figure 1.15: CubeSat Kit [34].

The Structure and Mechanisms subsystem will be surveyed in more detail in the next chapter as it is the focus of this dissertation.

1.3 MECSE Project

Magnetohydrodynamics/Electrohydrodynamics CubeSat Experiment (MECSE) is an under development Nanosatellite resulting from the collaboration between C-MAST from University of Beira Interior (UBI) and CEiiA.

MECSE's mission is to create a benchmark for the future validation of the theory that an Electromagnetic field can re-shape the layer of the plasma surrounding the spacecraft, and therefore allow communications during the so-called atmospheric re-entry Radio Frequency (RF) blackout phase [6]. The RF blackout is caused by a highly dense plasma layer attenuating or reflecting the electromagnetic waves used for telecommunications. During the spacecraft's atmospheric re-entry, a shock wave is formed in front of the vehicle, causing air compression and heating [35]. At hypersonic velocities, the increase of temperature will excite the gas molecules' internal energy modes, which will cause reactions of dissociation and ionization, forming a plasma layer around the vehicle. The moment the plasma frequency exceeds the transmitting frequency, the communication signal will be cut-off. Even when the signal frequency exceeds the plasma frequency, the quality of the communication is still damaged.

C-MAST is researching the magnetic window manipulation method and considers that it would be possible to reduce the plasma density in a localized region through electromagnetic manipulation of the flow using the Hartmann flow approach [6]. The interaction between the flow and the imposed magnetic field will generate a Lorentz force, with magnitude proportional to the pressure gradient and opposite direction. The opposite force will reduce the maximum velocity of the fluid leading to a decrease in the viscous boundary layer [36].

Continuous communications, real-time telemetry, and GNSS signal reception are essential parameters that ensure the accomplishment of manned and unmanned space missions. For that reason, the mitigation of the RF blackout is essential in the design of re-entry space vehicles. Solutions that may solve or attenuate this issue are a high priority in scientific and technological

agendas.

CEiiA designs, implements and operates innovative products and systems for technology intensive markets and has recently started to explore space-related fields. CEiiA's mission is to promote a more competitive industry, and to achieve this, CEiiA connects companies, universities, and public entities in different countries [37]. CEiiA aims to fast-forward the portuguese space industry, therefore they accepted the challenge to support the development of MECSE due to its important and innovative mission objectives. A team of experienced engineers has been supporting the project technically and financially, which allows the materialization of MECSE concept

1.3.1 Mission Objectives

The objectives of this challenging mission are:

- Study the formation of Plasma in LEO by collecting data for different altitudes;
- Validate the theory that an electromagnetic field can manipulate the plasma layer.

In order to fulfill the objectives of the mission, the payload will be divided in three groups: PL01-ENVISENSE, PL02-LP and PL03-EMG. PL01-ENVISENSE is constituted by environmental sensors which aim to measure environmental parameters (e.g. temperature and pressure). The PL02-LP aims to measure the density of the plasma layer around the vehicle, therefore this payload will have sensors as for example Langmuir Probes. PL03-EMG aims to generate the electromagnetic field, so an electromagnetic generator will integrate this payload. The different payloads are still under-development, therefore for this master dissertation, they were considered as blackboxes and their electromagnetic and thermal effects on the subsystems were not taken into account in this work.

1.4 Objectives

CEiiA, challenged the author of this thesis to design and develop a modular mechanical subsystem for MECSE that would allow a cost effective and fast access to space. The aim of this dissertation is that the mechanical subsystem can further be developed and become a platform for the validation of MECSE mission and also create a platform that can be used in other missions by different entities.

The objectives established to set up the research strategy baseline for this dissertation are:

- Investigate the different Standards for the Design of a CubeSat;
- Select and Define the layout of the required Subsystems's hardware;
- Design MECSE Mechanical Subsystem;
- Perform Steady State Structural and Thermal Analysis on MECSE;
- Analyze the preliminary thermal impact on the subsystems.

Although each subsystem is being designed independently, it is important to remember that each component is only one part of the complete satellite. Ergo, to maintain a high level of integration between the various subsystems, continuous communication and discussion is maintained between the designers of the individual subsystems. This report focuses on the structural design and configuration of MECSE, and it was developed at the same time as the mission analysis and CubeSat's management system, therefore along the dissertation some assumptions are done to perform a feasible structural design study. The development of a CubeSat is an iterative process therefore, after the definition of the subsystems hardware the Mechanical Subsystem shall be evaluated and the necessary changes shall be performed.

1.5 Thesis Outline

This master dissertation is divided in four chapters:

Chapter 1 presents the author's motivation to design the mechanical subsystem of MECSE, a state-of-the-art and objectives of this master thesis.

Chapter 2 has the purpose of reviewing several important concepts for the design of a satellite. It contains information about design procedures, operation conditions, methods of attachment, materials, manufacturing processes, structural and analysis.

Chapter 3 will detail the process of configuration of a satellite, the mission and design requirements for MECSE project, the process of the structural design of MECSE and the electronics and their functionalities.

Chapter 4 will explain the Static Finite Element Analysis performed on MECSE considering the launch phase and evaluation of the thermal impact on the subsystems.

Chapter 2

Background

This chapter contains a review of important theoretical aspects for the objectives of this dissertation focusing on the the process of design, structural subsystem analysis and thermal control subsystem analysis. These concepts are very important to aid in the decisions further made on this dissertation.

2.1 Design Procedure

The process of designing and developing a spacecraft is characterized by the fact that it is a single and "one-off" time product, that has to be produced within a given amount of time [38] due to the project budgets. The structural design process consists of three phases: conceptual design, preliminary design and detail design [39].

During the Conceptual Phase, feasibilities, costs and risks estimations are established for one or more spacecraft configurations and the main objective is to select a viable concept and optimize it as much as possible.

Once the concept phase has been defined, more iterations in the process are required to select materials, dimensions and structures [39]. Computer simulations are performed and physical models are constructed and tested. This constitutes the Preliminary Design Phase [39]. The final phase is the Detail Design Phase, the product is prepared for production. The project is described in full detail and manufacturing processes are outlined. Detailed drawings, bills of materials, and detailed costs' estimations are prepared. Typically, in this phase a prototype is built for testing [39].

The structural design of a spacecraft is an iterative process that starts with the initial spacecraft concept and nominally ends only shortly before shipment to the launch site (Figure 2.1). In such a multi-disciplinary project it is essential to specify the number of design reviews to continuously evaluate the interaction of all the separate design factors and subsystems [11, 40]. In fact, the design process benefits greatly from concurrent engineering with other subsystems [40].

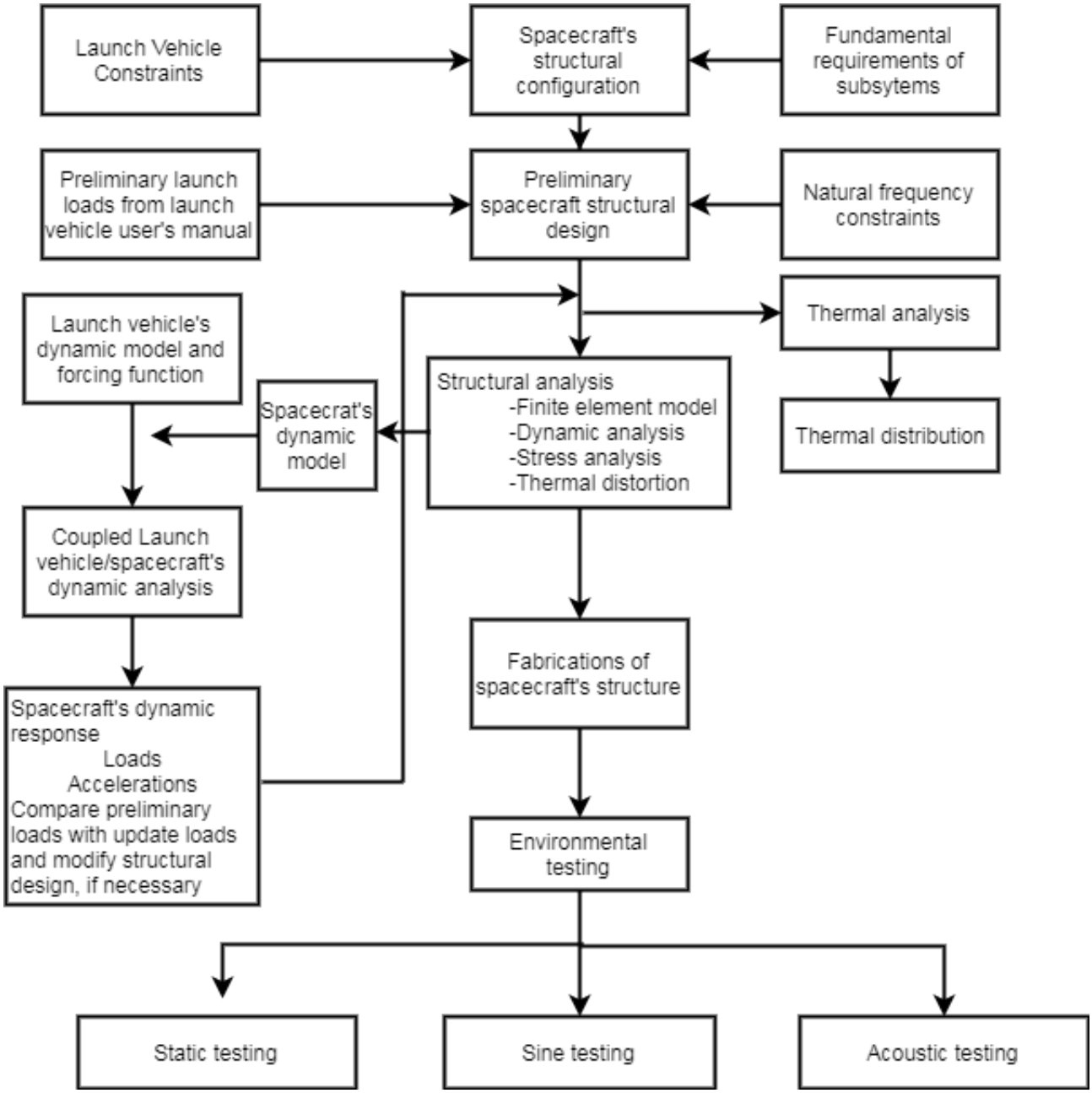

Figure 2.1: Design procedure of a Satellite [40].

The first step in the structures engineering process for any project should be the gathering of all the project requirements and relevant information that need to comply with the demands concerning the material properties,the manufacturing process, the reliability of the space vehicle, the lifetime, the maintenance, the manageability, among others [11].

A crucial factor for the structural design is the operational conditions (whether temperature loads or mechanical loads) the spacecraft will be exposed during all the phases of its mission [11].

2.1.1 Operation Conditions

The operation conditions can be subdivided in several areas of interest: conditions on Earth, during launch, and while on-orbit. These conditions drive the design requirements of the space-

craft's structure [11].

The launch vehicle's contractor provides a User's Manual that defines the mechanical loads that the CubeSat will be subject to while on the contractor's facilities and during launch [41].

2.1.1.1 Launcher

The configuration of the interface between the launch system and the satellite must be determined to understand the conditions that the spacecraft must withstand. Several different static (constant with time) and dynamic loads (varying with time) that vary with the stages of the launch affect the structure of the spacecraft [42].

The launch is divided in stages. A typical ascension profile is presented in Figure 2.2. The first stage of the launch (lift the satellite from the ground) generates the highest load factors on the satellite. During the launch, the rocket engines produce very harsh vibrations, that propagate throughout the structure of the launch vehicle and are then transmitted to the satellite through the interfaces. The engines produce high level of acoustic noise, which generates high acoustic loads and broadband random vibrations. In addiction to these loads, the satellite is subjected to shock waves loads produced by pyrotechnic devices used for the ignition and separation of the various stages of the launch vehicle.

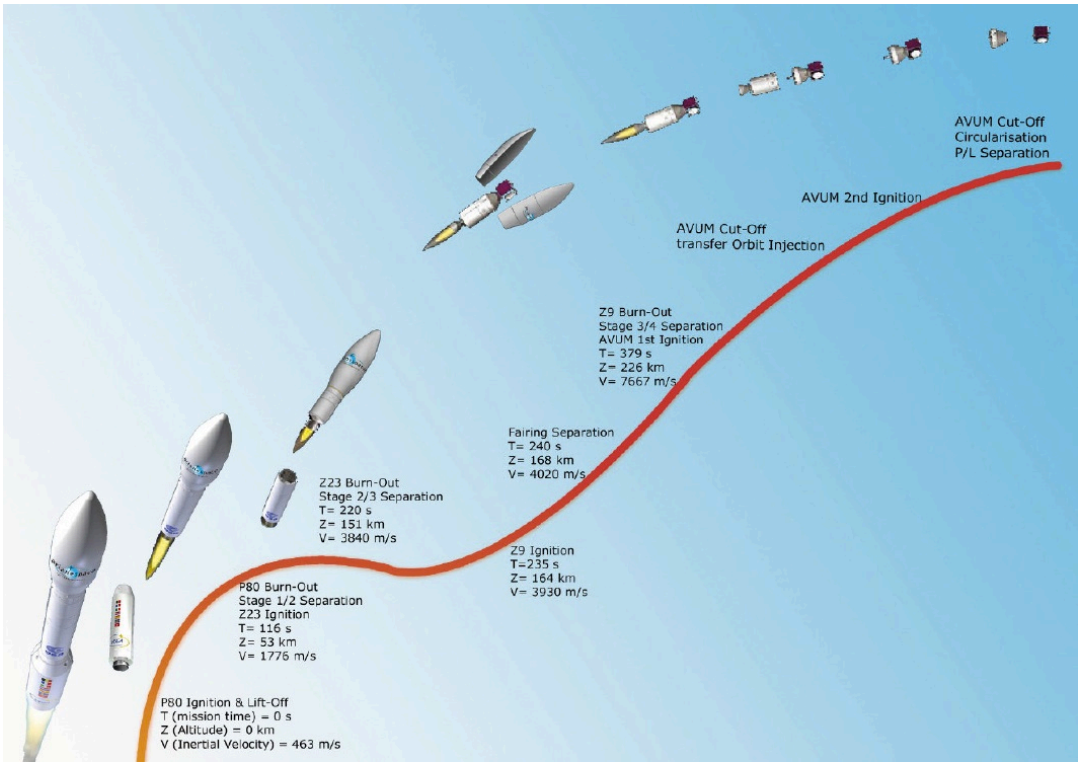

Figure 2.2: Typical Ascent Profile of VEGA [43].

At any point during the flight, the spacecraft can be subjected at the same time to a combination of high/low frequency, acoustic, quasi-static and shock loads in all axes. The next subsections will overview how the launch vehicle mechanical environment is translated into load specifications [41].

Quasi-Static Loads

These low frequency dynamic loads are produced due to several phenomena, including wind loadings, asymmetric vortex shedding, asymmetric ignition and pressure oscillations during the earliest stages of launch to buffer during transonic flight and resonant burn-induced axial excitation throughout the first stage.

The Quasi-Static Loads (QSL) are obtained by the launch agency. In some cases, these loads are presented in the form of an envelope diagram which gives vertical versus lateral loads [41]. The QSL are applied at the satellite in static analysis and must be considered during the preliminary sizing of the structure.

The capacity of the satellite's structure to withstand these loads without failure is demonstrated via structural analysis and testing. In the testing of QSL, a sinusoidal load is applied to the prototype at a low frequency within the limits of the maximum displacement of the shaker. This test can be carried out as a sine sweep, similar to a sine test, at a constant frequency with amplitude varying with time as a sine burst or as a half sine pulse [41].

Acoustic and Random Loads

Some phenomena occurring during launch produce intense vibrations, producing a broadband of excitations and the characteristics of the oscillations lose the typical sinusoidal behavior that is associated to low frequency excitation to become much more random in nature [41]. The spacecraft has to be able to withstand without failure these vibrations. Loads of this type are transmitted to the spacecraft in two ways:

- Vibration through the satellite to the launch vehicle interfaces;
- Acoustic energy absorbed by the external surfaces of the satellite.

For small spacecraft random vibrations are more significant than acoustic loading [41]. The random vibration loads are defined as a power spectral density profile. The acoustic loads should be described using direction and intensity.

Sine Loading

During launch the vehicle will experience low frequency dynamic loads, that can be approximated by sinusoidal functions. There are lateral modes and longitudinal modes of vibration, if the vehicle can not comply with the requirements concerning its lowest resonance frequency the loads experienced by the satellite may exceed the QSL, and this type of situation should be avoided, so the satellite must be designed to withstand sinusoidal loads over the range specified by the launch agency [41].

Shock

During the flight, shocks are normally produced by mechanisms as those used to separate the various stages of the launch vehicles or fairing jettisoning. These systems in general use explosive charges as actuators and have the final purpose of breaking the connection with a mechanism [41]. This explosion produces a rapid transient shock (load) that is characterized by a very high acceleration (few thousand g) and very high frequency (thousands of Hz) oscillations

rapidly damped.

Shock environments are specified using Shock Response Spectra (SRS) which is a method to capture the severity or damaging potential of a shock. The SRS produces a curve that gives the acceleration as a function of the frequency and where each point represents the maximum acceleration response of a single degree of freedom system. Shocks in general are not of great concern to the primary structure of the vehicle, except if there is some brittle material (e.g. ceramics) where it can produce fractures and cracks [41].

Figure 2.3 resumes all the static and dynamic loads the spacecraft will be subject to by frequency range.

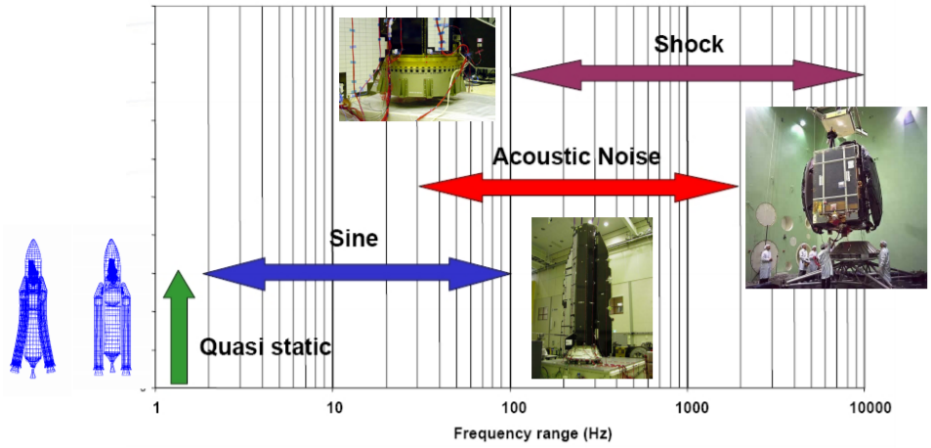

Figure 2.3: Static and Dynamic Environment Specifications (Typical Range) [44].

2.1.1.2 On-Orbit Conditions

Given the mission orbit parameters, operational conditions' requirements can be derived from the space environment [8].

Orbital Beta Angle

The satellite's inclination is the starting point for the investigation of a parameter of interest to the thermal analysys [8]: the orbit beta angle β. The orbit beta angle, Figure 2.4 is the angle measured between the orbit plane and the solar vector and has values between $\pm$ 90 degrees.

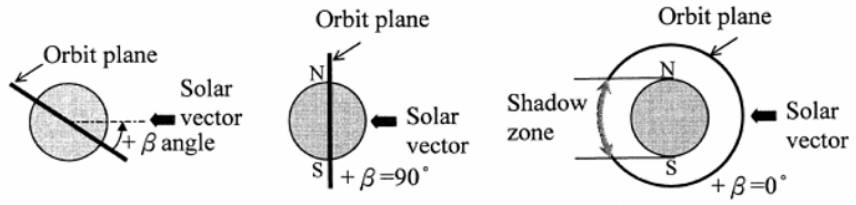

Figure 2.4: Beta Angle Representation [45].

A satellite's eclipse fraction depends on β and varies continuously because of the orbit nodal regression and the change in the Sun's right ascension and declination over the year [45]. Viewing

from the Sun, the beta angle is positive if the satellite is revolving counter clockwise and negative if the satellite is revolving clockwise. The satellite is exposed to more sunlight per orbit as beta angle increases [in absolute value], and eventually reaches constant sunlight exposure when beta angle is at 90 degrees. At a high beta angle the satellite may get overheated if it is not properly controlled.

Altitude

Altitude is another important parameter. Using this parameter it is possible to determine the orbit's semi-major axis $\alpha_{Mission}$, the orbital velocity v and the period P.

$$v = \sqrt{\frac{\gamma_{Earth}}{\alpha_{Mission}}} \quad (2.1)$$

$$\alpha_{Mission} = R_{Earth} + h_{Mission} \quad (2.2)$$

The standard gravitational parameter(γ_{Earth}) has a value of 3.986 $\cdot 10^5\ km^3/s^2$ and the Earth's radius (R_{Earth}) has a value of 6378 km.

$$P = 2\pi\sqrt{\frac{\alpha^3_{Mission}}{\gamma_{Earth}}} \quad (2.3)$$

The number of orbits in one day (n) can also be obtained by equation

$$n = \frac{86400}{P} \quad (2.4)$$

Using these equations, the general orbital parameters can be calculated. Those are important to understand the maximum time of eclipse TE (Equation 2.7) and of sunlight TS (Equation 2.5) that help determine the conditions of the spacecraft during the time intervals [8].

$$TS = \frac{2\rho}{360} \cdot P \quad (2.5)$$

where

$$P = sin^{-1}(\frac{R_{Earth}}{R_{Earth} + h_{mission}}) \quad (2.6)$$

And,

$$TE = P - TS \quad (2.7)$$

Incident Radiation

While on-orbit the satellite is under three main heat sources [42, 46], Figure 2.5.

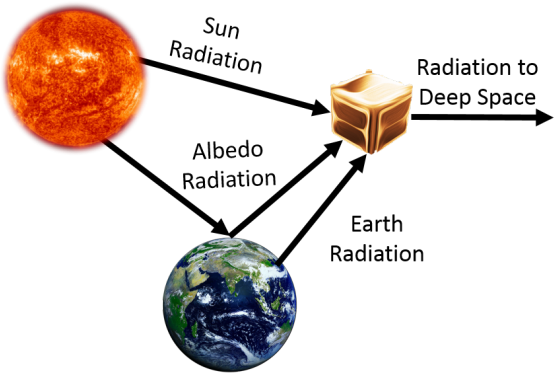

Figure 2.5: Space Thermal Environment [adapted from [26]].

The sun's radiation is the greatest source of energy incident on most space vehicles [26]. Due to Earth's orbit, the Sun's radiation reaching LEO orbit varies by $\pm$ 3.5% depending on the Earth's distance from the Sun. During summer (northern hemisphere) the intensity reaches a minimum 1372 W/m^2 and during winter solstice a maximum of 1417 W/m^2. This value is assumed to be in average 1367 W/m^2 [46].

The radiation that is reflected off the Earth is known as Albedo and is usually expressed as a percentage of incident sunlight that is reflected back into space. It is highly variable from 5% to 100%, but in average is 30% [46].

In table 2.1 it is possible to find a summary of the heat sources explained above.

Table 2.1: Summary of Heat Sources

Heat Source	Value
Direct Solar Flux	1367 [W/m^2]
Albedo	0.3
Earth IR	230 [W/m^2]

2.2 Mechanical Design

2.2.1 Structures

The structural design of a satellite is a complicated iterative process that contains a selection of configuration, materials, design, analysis and testing [11]. It is dependent on the design requirements set by the other subsystems like power, propulsion, communications and thermal. All of the subsystems will have hardware and electronics mounted internally and/or externally and the structure must provide a "safe" environment for their operation.

The internal configuration must both depend on the dimensions and the weight of the different subsystems and consequently has to impose restrictions on these same subsystems. The design process starts at a conceptual stage with design specifications which are based on mission requirements. In general the specifications include the accommodation of payload and subsystems, launch requirements, environmental protection, thermal and electrical paths, good stiffness, mass efficiency and high reliability. The structural design process also provides inter-

face to each individual unit or equipment in order to aid the integration sequence.

Structures and Mechanisms include all components connected to the launcher, satellite structure and the moving parts associated with it. The structure provides a strong supporting framework to house payloads, instruments and satellite subsystems, especially through the stresses of launch [40].

The function of the Mechanical Subsystem is to provide a simple sturdy structure that survives to launch loads while providing an easily accessible data and power bus for debugging and assembly of components [42]. The structure is the most basic component and the most restrictive component of the CubeSat and consequently influences the design of all other subsystems which have to fit inside or to be mounted on it. A satellite structure is defined as a combination of members, beams or plates held together by screws, rivets or similar fasteners [31].
Structures are divided in three categories [42]:

Primary Structure

It is the major load path between the spacecraft's components and the launcher. It carries shear, axial loads, bending moments and torsion and it provides access to install and service components during ground operations and maintenance [31, 40, 42]. In the case of Small Satellites, it consists of the base plate, upper frame, base block case, lower frame and the mounting plate. The primary structure is usually designed to survive steady-state accelerations and transient loading during ground operation, launch, and space operation. This category of structures may need to maintain a particular alignment among the payload, sensors, and antennas to achieve dynamic positional stability. When the primary structure fails, it is almost always catastrophic.

Secondary Structure

It includes support beams, antenna dishes, and solar panels. Most of the considerations for the primary structures also apply to the secondary structure but the load factors used to design the primary structure often are not suitable for the design of the secondary structure. For this structure acoustics, launch and on-orbit thermal cyclic loading are important as well, but it is not as well protected from thermal environments as in the case of the primary structure. The solar panels during launch will respond to acoustics at the same time they are excited by transients and steady-state accelerations. The failure of this structure does not affect the integrity of the spacecraft, but it can have a significant impact on the global mission [31, 40, 42].

Tertiary Structure

It includes component housing, mounting brackets, cable support brackets and connector panels. For most of these structures, base-driven vibrations are the harshest environment and fatigue life is the driving requirement. Most random vibrations for this type of satellite are induced at the launch vehicle interface. Spacers of a thermally nonconductive material are used to isolate devices from thermal stresses [31, 40, 42].

2.2.1.1 Conventional Structures

Conventional spacecraft integrates four basic primary structural designs [31, 42, 47]:

- **Skin-frame Structures** (Figure 2.6) use an internal skeletal network of axial and lateral frames to mount exterior skin panels [48]. The skin reinforces the structure supporting the shear forces induced by the interior members, and the frames support bending, torsion and axial forces. The skin is reduced to save mass, but it can not be too reduced as thin skin creates structural instability. Intermediate frames are used to mount equipment or increase the buckling strength of the skin and stringers. Removable panels might be needed as the internal access is difficult. A solution to mount components in the case of this structure is the use of sandwich and isogrid panels [31, 42, 47, 48];

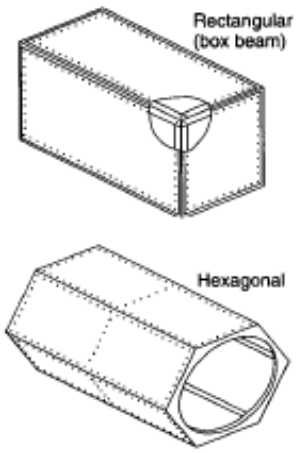

Figure 2.6: Skin-frame Structure [48].

- **Skin-stringer Structures** (Figure 2.7) are designed applying axial and lateral frame members attached to an outer skin. This type of structure is similar to the previous one, but skin-stringer refers to circular cylinder configurations. Typical connection methods include fasteners and/or rivets. It also needs removable panels or framed cutouts. Interior components are usually mounted on the walls at locations along the stringer assembly [31, 42, 47];

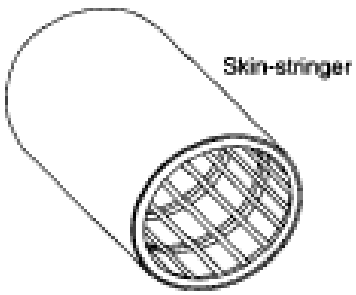

Figure 2.7: Skin Stringer Structure [48].

- **Truss Structures** (Figure 2.8) use an array of members that support axial loads. Truss members are arranged typically in arrays of triangles to increase the stability [48]. The members are manufactured using extruded tubes or open shapes made of composite, metallic or sheet metal materials. Trusses are mass-efficient when the members are configured into rectangular or triangular cross-sectional assemblies, but they become less efficient

when the cross-section is more circular or hexagonal [48]. Buckling is usually the critical failure mode for this type of structure. The design of trusses creates stress concentrations at interface mounting points, as separation systems. The absence of shear panels facilitate the access to the payload, but it is not helpful to the spacecraft if it requires body mounting solar cells. This structure is easier to machine and to assemble individual members [31, 42, 47, 48];

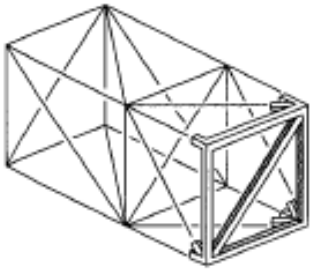

Figure 2.8: Truss Structure [48].

- **Monocoque Structures** (Figure 2.9) are axisymmetric shells that do not contain any stiffeners or frames. Shells are manufactured using metallic or sandwich panels with curved sections formed by rolling. The strength of the monocoque cylinders is usually limited by its buckling strength [48]. The shells are more efficient when the loads are distributed uniformly throughout the structure. Components are normally mounted to the walls with fasteners. To achieve a uniform load distribution, the mating structure must be either a monocoque cylinder or a stiff transition adapter. The use of sandwich construction results in a light structure and isogrid shells can also be made at a relatively low weight. This structure is less efficient than the cylindrical skin-stringer [31, 42, 47, 48].

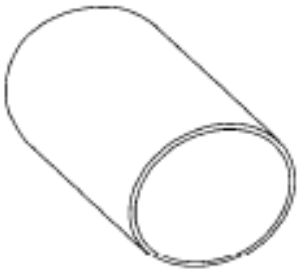

Figure 2.9: Monocoque Structure [48].

2.2.2 Methods of Attachment

To attach structural modules, mechanical fastening hardware,welding and adhesive bonding are the main methods [42].

Fastening

A fastener is a hardware that is used for creating non-permanent joints. The basis of a fastener is a screw thread. Based on the application area of the fastener, the head portion of the fastener is available in various shapes and sizes [42, 49]. Fasteners have standard sizes and

standard thread geometries. These add damping to a structure, but they show a significant loss of stiffness and premature failure in brittle materials because of the stress concentration introduced at fasteners locations. They are suitable for many structures and mechanisms made of materials with high ductility [42]. There are several fasteners types. In Figure 2.10 it is possible to find some examples and their advantages and disadvantages.

Fastener Type	Advantages	Disadvantages
Solid Rivet	Lowest cost, weight Good performance in fatigue	Non-removable Low tension High noise during installation
Lockbolt	High shear, clamp-up High reliability Low noise during installation	Non-removable Moderate cost, weight Limited tension (some types) Low fatigue
Hi-Lok	Same as lockbolt but somewhat lower cost and weight	Same as lockbolt but somewhat lower cost and weight
Shear Bolt	High shear Low cost Removable	Low tension Low fatigue Moderate cost, weight
Tension Bolt	High shear, tension, clamp-up High reliability Removable	High cost, weight No flush surface

Figure 2.10: Advantages and disadvantages of each fastener type [50].

Welding

Welding is a permanent process of joining two materials by applying intense heat and sometimes pressure. Often, welding is a very economical method of attachment, but it is limited to joining similar weldable structures [42]. It can produce distortions and fissures in some materials [42].

Adhesive Bonding

Adhesive Bonding is widely used for bonding face sheets to honeycomb, to join polymer-matrix composites, to electrically isolate solar cells from the structure that will support them and to separate dissimilar metals that are vulnerable to galvanic corrosion [42]. With adhesive bonding, loads are distributed over the joined region and not locally at fasteners. Therefore weight can be saved as well as a longer fatigue life can be achieved. It can add structural damping and join dissimilar materials, but it can not be disassembled. It shows a limited shelf life, and in some cases, adhesives are toxic and require specific ventilation [42].

2.2.3 Materials

Satellite Structural designs use several different materials and the two most typical materials used in space applications are the metal alloys and advanced composite materials. The material selection is a significant step in designing a satellite structure, and in the case of small satellites, it becomes even more important since small changes in the structure can result in precious space for other subsystems [38]. Materials are selected based on:

- Density;
- Specific Strength;
- Specific Stiffness;

- Corrosion Resistance;
- Fracture Resistance;
- Fatigue Resistance;
- Thermal Expansion;
- Thermal Conductivity;
- Machinability;
- Cost.

2.2.3.1 Metal Alloys

Metals are commonly homogeneous and isotropic, so they have the same properties at every point and in every direction.

Aluminum alloys have a density of $\rho = 2700 - 2900 kg/m^3$, modulus of elasticity $E = 70 GPa$, at a temperature range $T \leq 200 - 350°C$ [38] are the most widely used metallic materials in spacecraft manufacturing. The aluminum alloy presents high strength to weight ratios, high ductility and ease of machining. The stiffness to weight ratio is comparable to steel, however, the strength to weight ratio is typically higher. The disadvantages include low hardness and a high coefficient of thermal expansion (CTE). The alloys are typically tempered to increase the material strength. For space applications the typical alloys are: 6061, 7075, 2024 and 7005 [8,16,51].

Titanium ($\rho = 4500 - 4800 kg/m^3, E = 115 - 120 GPa$ at a temperature range $T \leq 500°C$) [38] alloys are applied where high strength materials or high strength at high temperatures are required. They have high strength to weight ratios, low CTE and great resistance to corrosion. But, titanium alloys are hard alloys to machine, and some have reduced fracture resistance. Ti-6Al-4V which contains 6% aluminum and 4% vanadium, is the most popular among titanium allows for aerospace applications [42, 51].

Beryllium ($\rho = 1850 - 2300 kg/m^3$, $E = 190 GPa$, temperature range $T \leq 600°C$) [38] is used in high stiffness applications. It has a specific modulus of 6 times the specific modulus of aluminum. This type of material is nonisotropic and therefore has low ductility and fracture toughness in its short-grain direction. Beryllium is an expensive material, difficult to machine, requires special machining equipment and it is toxic [42, 51].

Steel ($\rho = 7800 - 8000 kg/m^3$, $E = 185 - 200 GPa$) [38] is normally used where low-volume strength and stiffness are important. It provides high wear resistance, it is weldable and easy to machine. However, it is not efficient for structural stability as it provides low buckling strength vs. weight. Austenitic stainless steel is the most abundant steel alloy used in spacecraft. It is often used for fasteners and mechanisms [42].

2.2.3.2 Advanced Composite Materials

A composite material consists of a matrix (metal, epoxy) and reinforcement fibers (carbon, graphite). The efficiency of structures made of composite is a result of their high specific modulus and unique load path. The flexural shear loads are transferred from the matrix to the axial

loads on the high strength fibers, creating a light and stiff structure. The most widely used discontinuous composite is aluminum reinforced with silicon carbide particles [42].

Polymer-Matrix Composites (PMCs) are the most commonly used continuous fiber composites in space. Their matrix consists of two polymers, the thermoplastics, and the thermosets. The thermoplastics can be melted and solidified several times, but the thermosets are not reusable after curing. Generally, composites have a large development cost, and extensive testing is required for fiber composite flight hardware to verify the structural integrity [38, 42].

Metal-Matrix Composites (MMCs) are becoming available with possible applications to small spacecraft frames and components [16]. Aluminum alloys reinforced with silicon carbine, alumina or boron particles increase stiffness and strength. However, this type of material shows poor ductility and toughness properties and is more expensive than the conventional options [38, 42].

Carbon-Carbon Composites (CCCs) are typically used in applications requiring extreme temperatures (up to about $1650\,^{\circ}\mathrm{C}$) and when combined with active cooling these can be used in structures exposed to temperatures as high as $3300\,^{\circ}\mathrm{C}$. Although these materials have high thermal resistance, they are highly susceptible to oxidation [38, 42].

2.2.4 Manufacturing

To make the shape of a structure, the materials are subjected to processes of manufacturing, which include primary forming processes (like casting and forging), material removal processes (turning, drilling, milling, among others), finishing processes (such as polishing) and joining processes (e.g. welding). Viewing manufacturing as a system provides a way of identifying which factors, whether internal or external, are important and so aid decision making about choosing a particular manufacturing process in a particular situation [52] . The choice of which material and which process to use is not trivial. Factors such as consumables for manufacturing equipment, the amount of scrap produced, the speed of the process, the energy required and so on, all must be considered in order to make a sensible decision about the best way of making the final product.

2.2.4.1 Machining

It is a process that is used to describe several removal processes in which tools remove material from a piece to produce the desired shape. Machining requires attention to many details for the workpiece to meet the specifications set out in the blueprints. Machining also presents challenges to achieve the correct finish or surface smoothness on the workpiece [53]. Almost all materials (metal, plastic, composite, wood) can be machined, therefore this process is considered versatile. On the other hand, as the material is removed and discarded to obtain the final structure, in some cases it is not most economical choice and in some cases this process requires a long time until the final structure is finished which also increases the costs of manufacturing [53].

The three principal machining processes are classified as turning, milling and drilling [53].

- **Turning** operations are operations that rotate the workpiece as the primary method of moving metal against the cutting tool. Lathes are the main machine tool used in turning. Lathes can be used to create a desirable external diameter by rotating a metal workpiece, so that a cutting tool can cut the metal away, creating this way a smooth surface matching the required diameter and surface finish required by the blueprints [53].

- **Milling** operations are operations in which a rotating tool with multiple cutting edges is moved slowly relative to the material to generate a plane or straight surface. The direction of the feed motion is perpendicular to the tool's axis of rotation. Milling machines are the principal machine tool used in milling [53].

- **Drilling** operations are operations in which holes are produced or refined by the contact of a rotating cutter with the workpiece. Drilling operations are done primarily in drill presses but sometimes on lathes or mills. A drill can be used to remove metal in the shape of a cylindrical hole.The tools that may be used for various types of metal removal are milling machines, saws, and grinding machines [53].

2.2.4.2 Mechanical Forming

The processes of mechanical forming or plastic forming are characterized by causing changes in shape without appreciable volume variations. The roll forming is characterized by the action of a bending moment that cause the change in shape of the plate [53]. Forming process can be classified into two types as cold working and hot working.

The cold working deforms the material at a temperature below the recrystallization temperature of the work metal. With this process, the strength and the hardness increases due to the strain hardening, but on the other hand, the ductility decreases. It is possible to achieve a good surface finish and high dimensional accuracy with this process [53].
The hot working deforms the material at a higher or equal temperature to the recrystallization temperature of the work metal. In hot working, the refinement of the grain size occurs, thus, improving mechanical properties. This process requires much less bending force, but the final formed surface does not present a good surface finish and accurate dimensions [53].

2.2.4.3 Additive Manufacturing

Additive Manufacturing (AM) also called 3-D printing is a manufacturing technique in which the material is added and joined layer by layer. This technology is not just a different way to manufacture components but rather offers a new way of re-conceptualize space architectures [54]. A design can be conceived in Computer Aided Design (CAD) and printed on-demand enabling the fabrication of complex mechanical structures that could not be manufactured through traditional techniques [55].

Initially, the AM technology was used as a method of rapid prototyping [56], but recently the development of manufacturing techniques provided promising material properties and finishes from AM manufacturing parts. Although AM is advancing rapidly, this technology is still relatively young and it is important to have a clear understanding of the relation material-structure

in order to ensure consistency in production [56].

Additive manufacturing has typically much less waste than traditional machining methods because it uses nearly all the primary material to create the part resulting in virtually no waste [8]. The use of AM for spacecraft manufacturing is creating many new possibilities in design and fabrication in cases where previously it was impossible to manufacturefor what had previously been impossible.

Currently, the development of CubeSats is an active area of AM for space applications. Many CubeSats are being built with several structures and components produced with additive manufacturing materials, simplifying the construction and reducing the mass [16].

Typically, CubeSat structures are made from metal therefore, in this dissertation only the AM using metallic alloys will be considered.

Powder Bed Fusion

It represents a group of technologies that use polymer or metal powders contained in a build container or vat. The material is bound selectively using typically a laser or an electron beam. There is a moving platform in a build chamber that moves downward after each single layer is fabricated where parts are built in. Figure 2.11 represents the Power Bed Fusion process.

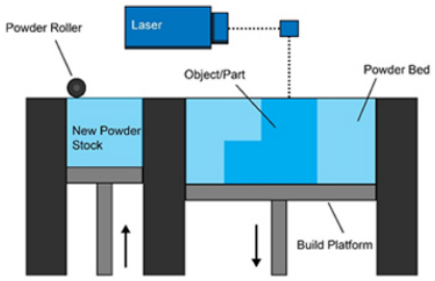

Figure 2.11: Power Bed Fusion Process [57].

Directed-Energy Deposition

In this technology three-dimensional shapes are constructed using lasers or electron beams directly at the build surface, with material fed onto the build region to coincide with the incident energy source. A powder feed or wire feed system is used to deliver material into the built zone. There are two processes in this technology, laser-engineered net shaping and direct manufacturing. The laser-engineered net shaping uses a laser with a powder feed system enabling the deposition of one or more materials simultaneously. The direct manufacturing uses an electron beam and a wire feed system. Figure 2.12 represents the Directed-Energy Deposition process.

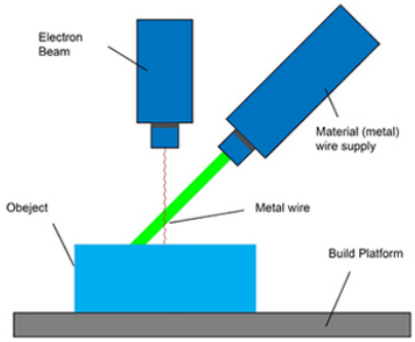

Figure 2.12: Directed-Energy Deposition Process [58].

2.3 Structural Analysis

There are three methods to solve any engineering problem [59, 60], the classical, the numerical and the experimental.

Classical Methods attempt to solve field problems directly by forming governing differential equations based on fundamental principles of physics.The principal advantage of classical methods is the high degree of problem insight provided by solutions of this type, but this method is only applicable for simple cases of geometry, loading and boundary conditions. Consequently, these solutions bear little resemblance to most practical engineering problems [59, 60].

Numerial Methods address a broad range of problems. These methods are applicable even if a physical prototype is not available but the results can not be believed blindly and certain results must be validated by experiments or analytical methods, as the results are based on assumptions [59, 60].

Experimental Methods attempt to solve problems by experimenting on a prototype, therefore it is only applicable if a prototype is available. A minimum of three or five prototypes shall tested to obtain as acquired results, therefore, this method is expensive and time consuming [59, 60].

In the case of a satellite it is required to perform experimental methods, but in an early stage of the project experimental methods are not viable, as the model is constantly changing. Therefore, for this master thesis the most viable method is the numerical method, more precisely the Finite Element Method (FEM) because the geometry is too complex for a classical method and the design is still in a preliminary phase for the manufacture of a prototype.

2.3.1 Finite Element Method (FEM)

The Finite Element Method (FEM) is a numerical technique used to determine the approximated solution for Partial Differential Equations (PDE) on a defined domain (ω). Any continuous object has infinite degrees of freedom and it is not possible to solve the problem in this format, so the FEM reduces the degrees of freedom from infinite to finite with the help of discretization or meshing, dividing the structural model into nodes and elements. The calculations are made at

a limited number of nodes and to get the value of a variable (e.g. displacement, among others) between the calculation point, FEM uses an interpolation function [59, 60].

2.3.2 Plate Theory

A plate is a three dimensional solid body [61] for which the thickness is small compared with the surface dimensions. The thickness is usually constant but may be variable and is measured normal to the middle surface of the plate. The midsurface of the plate is the locus of the points located half-way between the two plate surfaces, it is a plane, Figure 2.13.

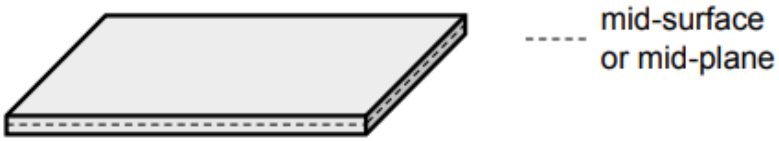

Figure 2.13: Thin Plate [61].

The plates can be classified in 3 groups:

- Thin plates with little deflection;
- Thin plates with big deflection;
- Thick plate

A plate is considered thin when the ratio of thickness and its smaller side is inferior than $\frac{1}{20}$ [61]. Plates in a plane stress state are also called membrane or lamina state, this occurs if external loads act on the plate midsurface. Under these conditions the distribution of stress and strains across the thickness may be seen as uniform, and the three dimensional problem can be reduced to two dimensions.

Historically, the first model of thin plate bending was developed by Lagrange, Poisson and Kirchhoff. It is known as the Kirchhoff plate also called Classical Theory. The classical assumptions of thin plate behavior for a linear static analysis are [60, 61]:

- A thin plate is one in which the thickness is much less than the next larger dimension;
- The deflection of the plate's midsurface is small compared with its thickness;
- The midsurface remains neutral during bending-this applies to lateral loads, not in-plane loads;
- The normal to the midsurface remains normal during bending.

The basic finite element equation to be solved for thin plates experiencing static loads can be expressed as [60]:

$$K \cdot u = F \quad (2.8)$$

where K is the stiffness matrix of the structure (an assemblage of individual element stiffness matrices). The vector u is the displacement vector and F is the vector of loads applied to the structure. Equation 2.8 represents the equilibrium of external (right-hand side) and internal forces (left-hand side) [60].

Once the unknown displacements of the elements are calculated, the strains can be achieved by the derivation of the displacement$\varepsilon = \dot{u}$. Knowing the strains, stress can be calculated by using the constitutive relations for the materials. For linear static analysis where the displacements are in the elastic range, i.e.: the stresses, σ, are assumed to be linear functions of the strains, ε, Hooke's law can be used to calculate the stresses. Hooke's law can be stated as:

$$\sigma = C \cdot \varepsilon \quad (2.9)$$

where C is the elasticity matrix of the material.

For structural analysis, stiffness is a very important property. Generally the loads a spacecraft is submitted to are known, but the displacement those loads create are unknown. If the stiffness matrix is formulated for a given shape, like line, quadrilateral, or tetrahedron, then the analysis of any geometry could be performed by meshing it and then solving Equation 2.8.

2.3.3 Analysis Methods

Analysis methods are generally divided in three categories, static, transient and random vibration analysis [60].

Static analysis are used to predict distribution of loads and displacements in a structure due to slowly varying applied forces [60]. This type of analysis is also used for thermal loads, which arise from temperature changes in the structure.

Transient analysis are used to predict loads resulting from applied forces that are rapidly varying and are deterministic functions of time [60].

Random vibration analysis deals with applied forces that are not deterministic but are known only in terms of statistical average properties. This type of analysis predicts statistical averages of loads in the structure resulting from applied random forces [60].

For this dissertation, the focus of the studies will be on the static analysis methods, therefore the remaining categories will not be explored.

2.3.3.1 Static Load Analysis

Static load analysis is appropriate for load events in which the applied forces vary slowly with time. These forces have much lower frequency than the natural frequencies of the structure, so a dynamic response is not induced. These events are called quasi-static [62, 63]. The objective of static load analysis is to define the resulting load distribution throughout the structure. This load distribution may be defined using tools such as free body diagrams in simple cases.

Finite element analysis is recommended for complicated or redundant load paths [62, 63]. When performing static analysis with load factors, inertial ("G") forces are applied to the structure along the various axes. Inertial forces in all three axes (including rotations, if appropriate) shall be applied simultaneously, including sign combinations [62, 63]. Interface boundary conditions shall be consistent with the coupled configuration. Static analysis is also used to predict forces

and displacements due to specified temperature variations. The thermal strain caused by the specified temperatures, along with the system constraints, results in the predicted forces and displacements.

2.3.4 Load Analysis

In most cases, structural loads are dependent not only on the external environment but also on the structural properties of the spacecraft or payload. This means the sizing of structural members can influence the loads. At the same time, the sizing is often governed by the need to withstand the loads. As a result, structural design and loads analysis are normally an iterative process [62]. The primary steps in a typical launcher-spacecraft load cycle analysis process are presented in Figure 2.14

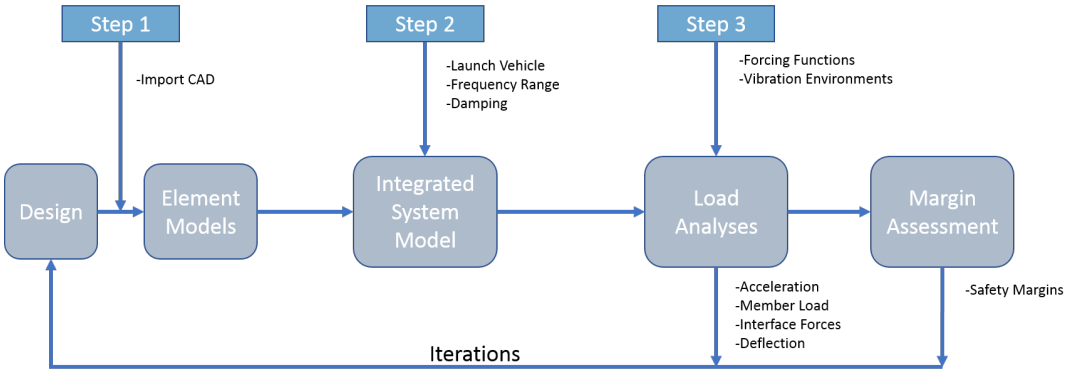

Figure 2.14: Load Cycle Analysis Process [62].

The steps in this process are described as follows:

- Step 1: Finite element models of elements comprising the spacecraft are developed from structural properties and geometry. For the first load cycle, the properties and geometry of the initial design shall be used. For subsequent load cycles, these models are updated.
- Step 2: The spacecraft element models are combined with models of launch vehicle elements to form an integrated system model.
- Step 3: Forcing functions representing the specific flight environments are applied to the integrated system model to obtain the spacecraft structural response. Appropriate uncertainty factors are applied at this time and the results of these analysis shall be used to update/revise the design load data set as required and are subsequently used for structural margin assessment.

The logic and sequence of the spacecraft loads analysis process depend on many factors strictly related to the general design, development and verification plan. The whole process and the specific sequences within the load's cycles are strongly dependent on the project and on the phase and maturity of the project itself. Still, some milestones can be identified for the early stages of the project [62, 63]:

- Identification of structure architecture;
- Dimensioning by preliminary loads assumptions. In particular for the primary structure by using the load factors taken from the launch vehicles user's guides;

- Development of preliminary FEM, in particular to verify stiffness;
- Definition of technical specifications for equipment and identification of pre-qualified units;
- Frequency response analysis at spacecraft level, simulating the sine vibration test, for the evaluation of the structural response and for the preliminary definition of the primary notching;
- Preliminary Launcher/Spacecraft coupled load analysis.

2.3.4.1 Factors of Safety

The Factors of Safety (FOS) are a coefficient by which the design loads are multiplied in order to account for uncertainties in the statistical distribution of loads, uncertainties in structural analysis, manufacturing process, material properties and failure criteria. The determination of an appropriate safety factor is a delicate matter requiring strong engineering experience. However, standards such as the one created by the European Cooperation for Space Standardization (ECSS) states that several factors should be taken into account [62, 64], Table 2.2.

Table 2.2: Minimum Required Safety Factor

Factor	Value
Modeling Factor [K_M]	1.25
Material Factor [K_{MT}]	1.25
Load Factor [K_L]	1
Minimum Safety Factor[η_{Min}]	1.56

2.3.4.2 Margin of Safety

In order to address the suitability of a particular structure the Margin of Safety shall be computed. The Margin of Safety (MS) is computed using equation 2.10 and its result gives the value of how much additional strength the structure has [65].

$$MS = \frac{Allowable of the Material}{Applied Load} - 1 \quad (2.10)$$

Reference [66] defines that MS>0.2 to the ultimate and yield stress and strain.

In the computation of MS the following minimum FOS shall be used for standard metallic materials 2.3

Table 2.3: FOS for Standard Metallic Materials [62]

FOS	Value
Yield Stress FOS	1.25
Ultimate Stress FOS	1.5
Minimum Fatigue FOS	4 cycles

A structure meets its criteria for strength analysis if its margin of safety is greater than or equal to zero [65].

2.3.5 Failure Modes

Since the largest stresses in the structure are sufficiently less than the yield strength of aluminum, it is assumed that the most likely cause of failure will be either buckling or bending, both are discussed below [67].

2.3.5.1 Buckling

The failure of a structural column by buckling is typically attributed to an axial compressive load that generates lateral deflections. This implies that the buckling load is a compressive load at which the column becomes unstable.

$$\sigma_{cr} = \frac{P_{cr}}{A} = \frac{\pi^2 EI}{AL_{eff}^2} \quad (2.11)$$

where σ_{cr} represents the buckling stress, P_{cr} is the critical load, EI is the flexural rigidity for bending in the xy plane, A is the cross-sectional area and L_{eff} is the column's effective length.

2.3.5.2 Bending

When a beam with a straight longitudinal axis is loaded by a lateral force, the axis is deformed into the deflection curve of the beam. The bending stress of a beam is represented by:

$$\sigma_x = \frac{-My}{I} \quad (2.12)$$

where M is the bending moment, y is the distance from the neutral axis and I is the area moment of inertia of the beam. This equation is called the flexure formula and shows that the stresses are directly proportional to the bending moment and inversely proportional to the moment of inertia of the cross section.

2.4 Thermal Analysis

As stated before, static analysis is also used to predict forces and displacements due to specified temperature variations. The thermal strain caused by the specified temperatures, along with the system constraints, results in the predicted forces and displacements. Overall thermal control of a spacecraft is achieved by balancing the heat emitted by the body against the incident heat loads and the internal heat generated by the various subsystems (subsystem's electronic hardware never convert the entire energy that powers them, the power that is not converted is released in the form of heat loads.) [1]. Using the energy equilibrium the surface of a satellite shall satisfy the following equation [1, 68]:

$$Q_{Sat} = Q_{Solar} + Q_{Albedo} + Q_{Earth} + Q_{Internal} \quad (2.13)$$

where Q_{Sat} is the total energy input to satellite. The Q_{Solar} is the solar absorption heat, Q_{Albedo} is the reflected solar heat from planet and Q_{Earth} represents the emitted heat from Earth. $Q_{Internal}$ represents the internal heat generation from satellite's components.

When $Q_{Sat} = 0$ the surface is in equilibrium (no heating nor cooling occurring). When $Q_{Sat} < 0$ the surface is cooling and when $Q_{Sat} > 0$ the surface is warming.

$$Q_{Solar} = G_{Sun} \cdot A_{Sun} \cdot \alpha_{Sun} \quad (2.14)$$

G_{Sun} represents the sun radiant constant, A_{Sun} area facing the sun and α_{sun} the Solar Absorptivity.

$$Q_{Albedo} = G_{Sun} \cdot \alpha_{sun} \cdot \alpha \cdot \frac{R_{Earth}^2}{(R_{Earth} + h)^2} \cdot A_{Earth} \cdot \sum \frac{1 + \vec{E'} \cdot \vec{N_i}}{2} \quad (2.15)$$

α is the Albedo Coefficient, $R_{Earth} = 6371$ km is the Earth Radius, h is the Altitude of the satellite and $\sum \frac{1+\vec{E'} \cdot \vec{N_i}}{2}$ is used as exposition correction factor for heat flux coming from Earth and it has a value of 3, meaning the spacecraft receives three times the heat flux coming from Earth Radiation and Albedo [68].

$$Q_{Earth} = G_{Earth} \cdot \alpha_{IR} \cdot \frac{R^2}{(R + h)^2} \cdot A_{Earth} \cdot \sum \frac{1 + \vec{E'} \cdot \vec{N_i}}{2} \quad (2.16)$$

G_{Earth} is the Earth IR Constant and A_{Earth} is the Area facing the Earth.

$$Q_{Sat} = \sigma \cdot \varepsilon \cdot A_{Total} \cdot T^4 \quad (2.17)$$

σ is the Boltzman Constant ($\sigma = 5.67 \cdot 10^{-8}$), ε is the emissivity, A_{Total} represents the total area of the spacecraft and T is the temperature of the spacecraft.

2.4.1 Heat Transfer

In general there are three main heat transfer modes [69]: conduction, radiation and convection. In space due to the low residual pressure, only conduction and radiation are present.

Conduction is governed by Fourier's Law [69]:

$$\overline{q} = -K\overline{\bigtriangledown} T \quad (2.18)$$

where $\overline{q}$ is the heat flow rate vector, K is the thermal conductivity and T is the temperature.

Radiation is governed by Stefan-Boltzmann's Law [69], the black-body irradiance is proportional to the fourth power of its temperature.

$$E = \sigma \cdot T^4 \quad (2.19)$$

where σ is the Stefan-Boltzmann constant, that has a value of $5.6 \cdot 10^{-8} W/m^2K^4$ [68].
The radiated energy of a black-body depends on its temperature, but a real body can absorb, reflect and transmit radiation energy. As there is no perfect black-body in practice, the emissivity $\varepsilon(l)$ is defined as the ratio of the energy emitted by a surface to the radiation from an ideal black surface at the same temperatures, this ratio varies from 0 to 1.

Absorptivity and emissivity can be hemispherical or directional and either total or spectral [68]. The second Kirchhoff's law states that for a given direction q, directional spectral absorptivity and emissivity are equal.

$$\varepsilon(q,l) = \alpha(q,l) \quad (2.20)$$

Chapter 3

Satellite Configuration Design

There are many considerations to take into account when designing a satellite's structure. Synthesizing these considerations into a design specification allow to ensure that the final design fulfill all the design objectives. Currently MECSE is between phase 0 and phase A of the project development (Figure 3.1). Therefore, the requirements presented in this chapter for the project are still being defined by the different teams responsible for each field of study.

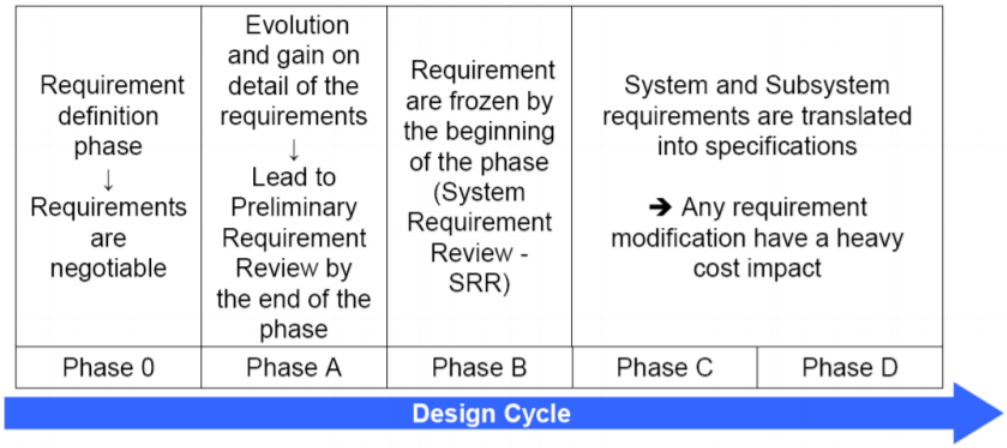

Figure 3.1: Requirements Evolution [44].

Along this chapter, assumptions about the hardware for each service module are done based on the state-of-the-art from previous missions, so the design team may have a base to develop a feasible Mechanical Subsystem. After the evolution to phase B/C the hardware of each service module shall be reviewed and updated.

A detailed geometric model was carried out using the commercial CATIA® software [70]. CATIA® modeling presents several important advantages for designing a structure. Firstly, the study of the satellite with CATIA® allows a good understanding of the components. Secondly, CATIA® can be used to verify the suitability of new concepts. CATIA® can also calculate several physical properties such as the total mass, the center of gravity (COG) location and the inertia properties. A complete material database has been created to enable CATIA® to calculate these properties from the geometry. Finally, the software facilitates the creation of technical drawings to be used on FEM which considerably simplifies the work [70].

This chapter gives a list of the high level requirements that shall be considered in the design of the mechanical subsystem. It describes the COTS hardware for each subsystem and their functionalities. The chapter also describes the process of design of MECSE's mechanical subsystem and conclusions.

3.1 Methodology

For the design of a CubeSat, two key aspects shall be taken into account. The first is to follow the CubeSat Design Specifications. The other is to accommodate the payload and make sure its requirements are met. The adopted approach for the design of MECSE's mechanical subsystem was to firstly define the different project requirements based on Mission Requirements and Design Requirements, Figure 3.2.

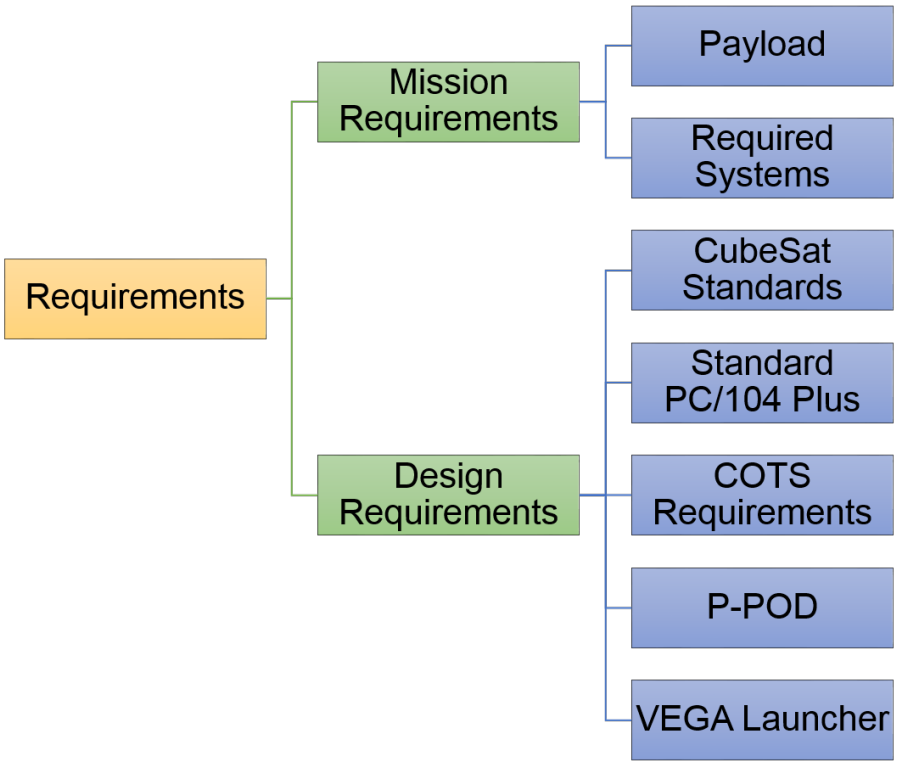

Figure 3.2: Project Requirements.

In order to define the design requirements a container and a Launcher had to be assumed to have more realistic constraints. Therefore the P-POD was selected as the CubeSat container and the Vega Launcher was selected as the launcher.

MECSE's project presents Mission Requirements (MR), Table 3.1, that were determined based on the payload requisites and on the subsystems needed to fulfill all the mission's phases.

Table 3.1: Mission Requirements

#ID	Mission Requirement	Rationale
MR-01	Commercial of-the-shelf (COTS) components or custom solutions will be preferred to space-qualified materials	Educational Objective
MR-02	The project shall use the organizational frame and requirements of the CubeSat Standard	Systems Engineering
MR-03	The payload's volume shall be less than 1U	Payload
MR-04	The CubeSat shall contain an EPS	Required Subsystem
MR-05	The CubeSat shall contain an AOCS	Required Subsystem
MR-06	The CubeSat shall contain an CDH subsystem	Required Subsystem
MR-07	The CubeSat shall contain a TTC subsystem	Required Subsystem
MR-08	The CubeSat shall contain a MSS subsystem	Required Subsystem
MR-09	The CubeSat shall contain a TCS	Required Subsystem

In order to construct a feasible mechanical subsystem all the subsystems must be physically defined. Starting from Mission Requirements, preliminary selection of the subsystems' hardware for the MECSE was done based on a state-of-the-art of previous missions' electronic hardware (see Appendices A).

Each subsystem was divided into CAD Parts taking into account the description of each subsystem from section 1.2. Figure 3.3 summarizes that division.

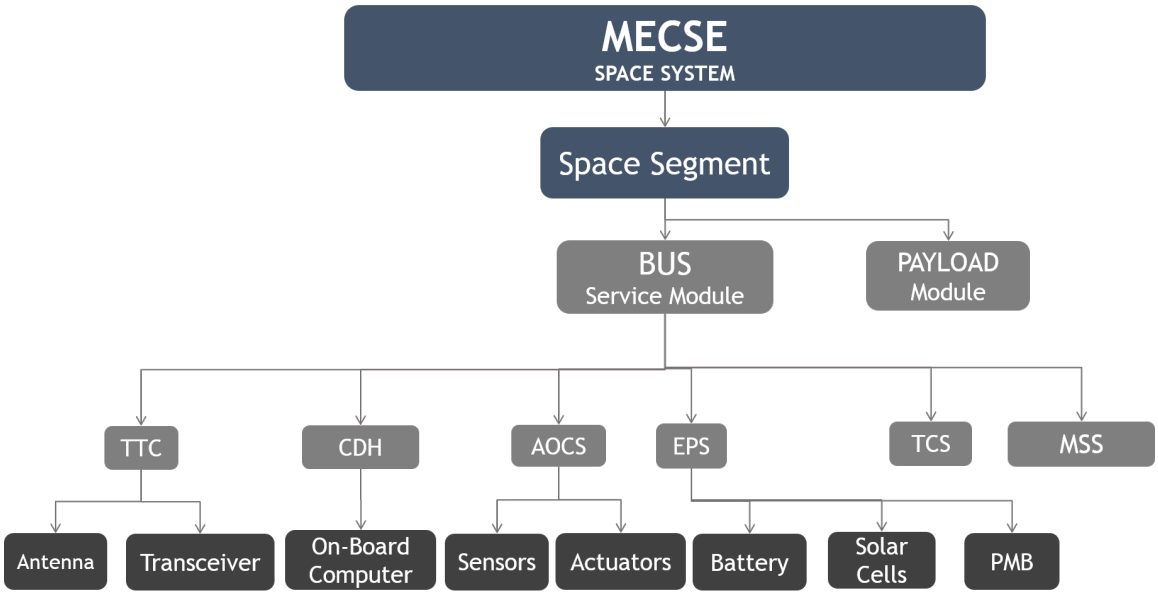

Figure 3.3: MECSE Space Segment.

The TTC subsystem is broken down into two parts: a deployable Antenna and a Transceiver. The CDH consists of an On-Board Computer. The AOCS is broken into two parts: the sensors and the actuators. Three-axis gyroscope sensor, sun sensor and a three-axis magnetometer are integrated as sensors, and two torque rods and one air core torquer are integrated as actuators. The EPS requires a Power Management Board, two Batteries and Solar cells [71].

As the mission requirements and the COTS hardware were defined, the focus of the next phase was on the definition of the stacking method of hardware, to determine the most suitable configuration of the CubeSat. Therefore, stacking methods were studied and the PC/104-plus staking was the adopted option. The PC/104-Plus was developed by Ampro Computers, Inc. [72] and offered to the PC/104 Consortium in September 1996. The Consortium formed a working group to review and finalize the specification and PC/104-Plus was subsequently approved by the Consortium's voting members in February 1997 [73].

Besides the requirements imposed by the CubeSat Design Specifications document (CDS) [4], the COTS requirements, the Standard PC/104 Plus requirements, the P-POD and the VEGA Launcher requirements were taken into account by the time of the definition of the Design Requirements (DR), table 3.2.

Table 3.2: Design Requirements

#ID	Design Requirement	Rationale
DR-01	The Structural Subsystem shall integrate all the spacecraft equipment	Subsystem Requirement
DR-02	The Structural Subsystem shall connect mechanically and electrically the spacecraft equipment	Subsystem Requirement
DR-03	The Structural Subsystem shall protect mechanically the spacecraft equipment during launch	Subsystem Requirement
DR-04	The Structural Subsystem shall ensure the integration within the P-POD and the test pod	Subsystem Requirement
DR-05	When inside the P-POD the CubeSat's power system shall be at a power off state, to prevent the CubeSat from activating any powered functions	CDS
DR-06	The Structural Subsystem's mass shall not exceed 600g	Systems Engineering
DR-07	The CubeSat shall have an access port area on a side face	CDS
DR-08	No external components other than the rails shall touch the inside of the P-POD	CDS
DR-09	Rails shall have a minimum width of $8.5mm$	CDS
DR-10	The edges of the rails will be rounded to a radius of at least 1mm	CDS
DR-11	No components shall exceed 6.5mm normal to the surface	CDS
DR-12	The ends of the rails on the +/-Z face shall have a minimum surface area of 6.5mm x 6.5mm contact area for neighboring CubeSat rails	CDS
DR-13	Aluminum 7075, 6061, 5005 and/or 5052 will be used for both the main CubeSat Structure and the rails. If other materials are used the developer will submit a DAR and adhere to the waiver process;	CDS
DR-14	The CubeSat rails and standoff, which are in contact with the P-POD rails and adjacent CubeSat standoffs, shall be hard anodized aluminum to prevent any cold welding within the P-POD.	CDS
DR-15	Separation springs are not required for 3U CubeSats	CDS
DR-16	The CubeSat center of gravity shall be located within 20mm from its geometric center in the X and Y directions	CDS
DR-17	The 3U CubeSat center of gravity shall be located within 70mm from its geometrical center in Z direction	CDS
DR-18	The Subsystems shall be distant from each other $15.24mm$	PC/104Plus
DR-19	The Batteries shall be distant from each other $23.5mm$	COT Requirement
DR-20	The Structural Subsystem shall be able to resist the lateral and longitudinal loads imposed by the launcher during all the phases of ascension	VEGA Requirement

3.2 Electrical Components and Electronics

Starting from the Mission Requirements, a preliminary design was built mostly based on COTS components. The process of subsystem's hardware selection for MECSE was based on the study of previous missions. This section briefly describes the chosen hardware and their functionalities.

For the TTC subsystem the antenna selected was the ISIS deployable Antenna, Figure 3.4, and the ISIS transceiver, Figure 3.5.

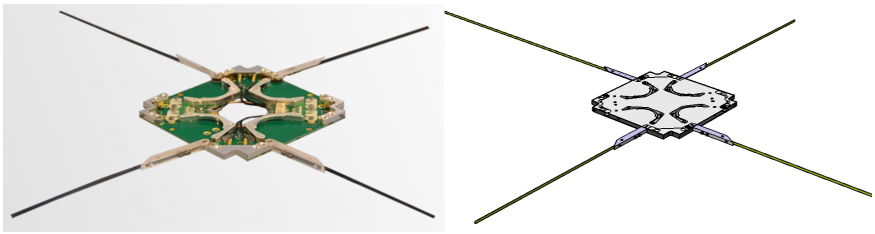

Figure 3.4: ISIS Deployable Antenna [74].

The antenna contains up to four tape antennas of up to 550 mm length, supporting a wide range of frequencies in both VHF and UHF bands and providing the optimal transmission quality and system reliability for a small size. The release mechanism of the antenna is triggered by the process of burning through a very small length of nylon wire, using electric current from the satellite's battery. Each burn (a total of four, one for each element) take a few seconds, and draws between 0.5 and 1 A from the battery. It has a mass of 85 g and dimensions of $98 \times 98 \times 7mm^3$.

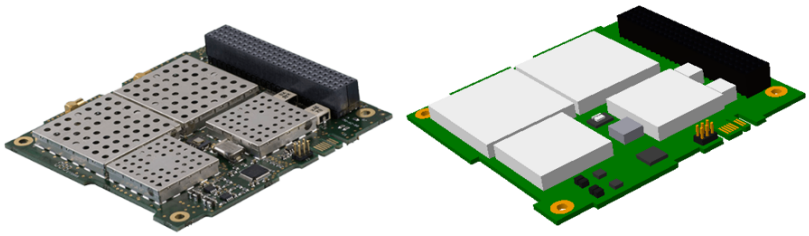

Figure 3.5: ISIS Transceiver [75].

The transceiver can operate in commercial and amateur bands of the VHF/UHF frequency spectrum and is low powered, low mass, and highly configurable, offering the flexibility of changing data rates and frequencies in flight. It has a mass of $75g$ and dimensions of $90 \times 96 \times 15mm^3$.

For the CDH subsystem the selected On-Board Computer was the Motherboard Module from Pumpkin Space Systems, Figure 3.6. It is the fifth generation of Pumpkin's line of single-board computers. This module is compatible with all CubeSats that conform to the CubeSat Kit Bus standard with its 104-pin connector. It has a mass of 77 g and dimensions of $92 \times 96 \times 17mm^3$.

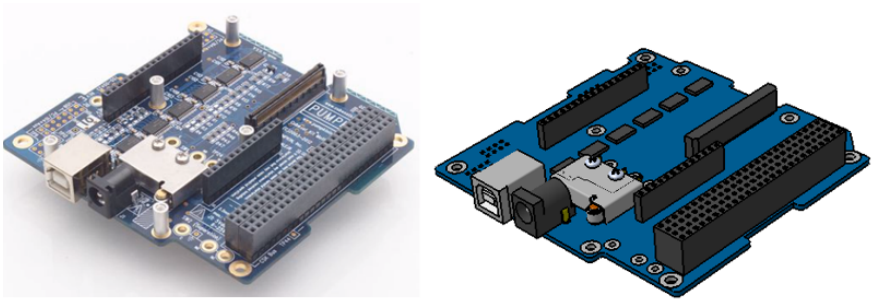

Figure 3.6: Pumpkin Motherboard Module [76].

For the AOCS the ISIS MagneTorquer board (iMTQ) was chosen as actuator, Figure 3.7. The Integrated Triple-Axis Digital-Output Gyroscope (ITG-3200), Figure 3.8, and Sun Sensors were

chosen as sensors. The Sun Sensor is commonly already integrated in the Solar Panels. Therefore independent sun sensors were not considered.

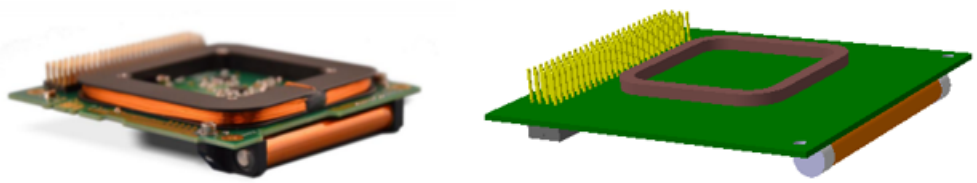

Figure 3.7: ISIS MagneTorquer board (iMTQ) [77].

The iMTQ is a PCB based 3-axis magnetic actuation and control system for Cubesats. It is designed as a standalone detumbling system and can also be used with more advanced ADCS hardware providing a nominal actuation of $0.2Am^2$. It has a mass of $196g$ and dimensions of $95.6 \times 90.1 \times 17mm^3$.

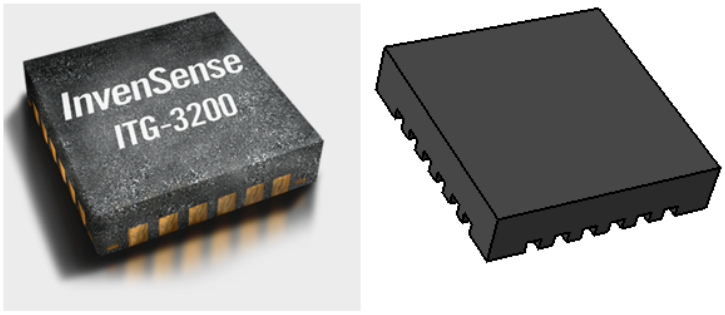

Figure 3.8: Invensense's Integrated Triple-Axis Digital-Output Gyroscope (ITG-3200) [78].

The ITG-3200 is the world's first single-chip, digital-output, 3-axis MEMS gyro optimized for motion-based remote control applications. It has a mass of $10g$ and the dimensions of $4 \times 4 \times \times 0.9$ mm^3.

For the EPS the GomSpace's NanoPower BP4 was chosen as battery, Figure 3.9, the NanoPower P31uX was chosen as power management board, Figure 3.10, and the 30% Triple Junction GaAs Solar Cell from AzurSpace, Figure 3.11 were chosen as solar cells.

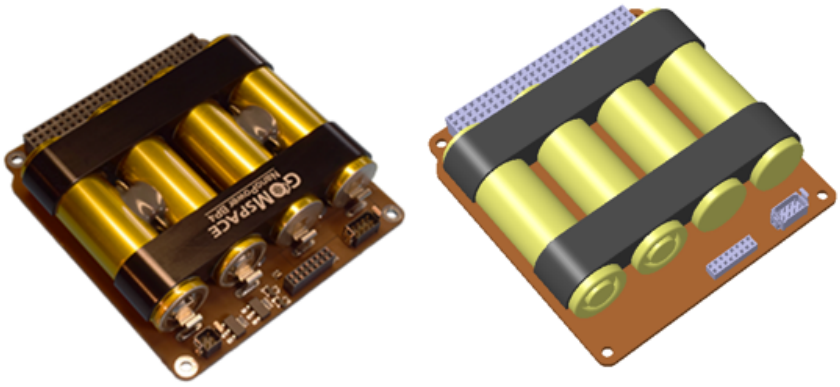

Figure 3.9: GomSpace NanoPower BP4 Battery [79].

NanoPower BP4 is a battery pack tailored to fit in CubeSat satellites. It employs four lithium-ion cells and features a power switch which can be used for control of high power consuming elements like antenna separation.The batteries are attached to a PCB following the CubeSat Kit standard (modified PC-104 plus) and are re-packed with Kapton insulation and fitted to the board with Scotch-Weld 2216 epoxy. In addition, aluminum brackets are glued to the batteries and screwed to the PCB to add mechanical and thermal stability. The inter-cell connections are made with strips spot-welded to the cell terminals. The battery comes with battery heaters that can be controlled from the P31 power management. The heaters can either be controlled directly from the output side by switching on or off the heater through commands, or by an autonomous heater controller with the heater on and off temperatures settable through the configuration system. It has a mass of $270g$ and dimensions of $87.4 \times 93.4 \times 22.9\ mm^3$.

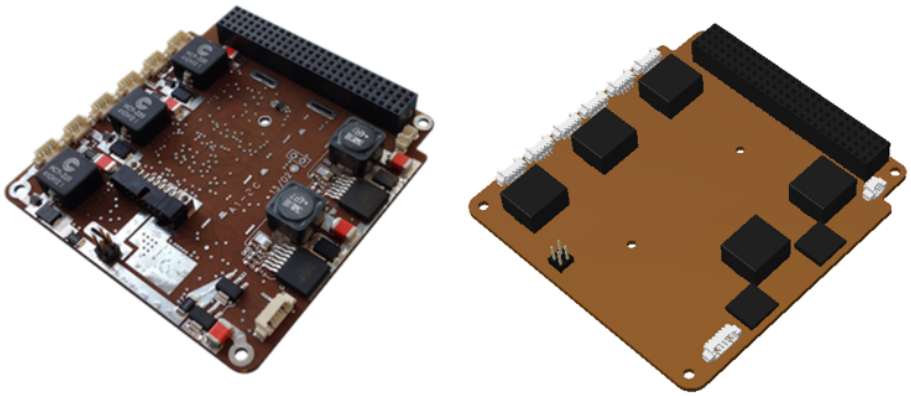

Figure 3.10: GomSpace NanoPower P31uX Power Supply [80].

The P31 power management board is designed for small, low-cost satellites with power demands from 1-30 W. The P31 provides a number of measurement points that enable monitoring the condition of the system. These measurements are available as buffered voltages to be sampled by an external system or as digital readings retrievable through the I^2C interface.

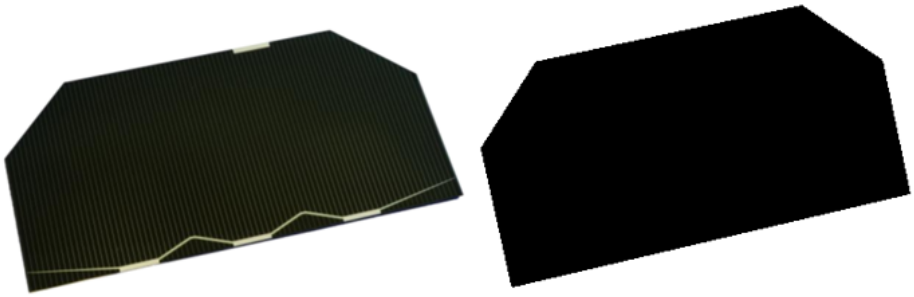

Figure 3.11: AzurSpace 30% Triple Junction GaAs Solar Cell [81].

The 30% Triple Junction GaAs Solar Cell is an InGaP/GaAs/Ge on Ge substrate triple junction solar cell (efficiency class 30% advanced). The cell has an improved grid-design and is equipped with an integrated bypass diode, which protects the adjacent cell in the string. Each cell has a mass of 3 g and dimensions of $40 \times 80 \times 0.1\ mm^3$.

As per DR-05 the CubeSat power system shall be turned off while integrated in the P-POD, the use of Deployment Switches to cut off the power is required. The switch selected was the SUB-Miniature Switch 0E6200H0 from Allied Electronics.

Figure 3.12: Allied Electronics ZF SUB-Miniature Switch 0E6200H0 [82]

3.3 Mechanical Components

3.3.1 Material

After the definition of the Design Requirements the materials for the main structure and the rails of the CubeSat had to be selected. Per CubeSat Design Specifications, the possible range of materials is highly constrained. A trade-off was performed comparing several material properties from reference [83] as thermal conductivity, electrical conductivity, workability and others, Table 3.3.

Table 3.3: Parameters considered for the Trade-Off

Parameter	Value
Density	
>	1
Thermal Conductivity	
>	1
Thermal Expansion	
>	1
Electrical Conductivity	
>	1
Fatigue Resistance	
>	1
Specific Strength	
>	1
Corrosion	
=	0
Workability	
>	1
Toxicity	

For the tradeoff, the material properties were ranked in order of priority and indicated if a parameter was more important (>) or equally important (=) than the next one. For example density was considered more important than the thermal conductivity thus it was ranked with a >symbol, on the other hand, corrosion was considered as important as the workability, thus it was ranked with a = symbol.

A table of weighting factors is created automatically taking into account the rank of each parameter. Thereafter a score ranging from 1 to 4 is assigned to each option for each key tradeoff parameter, Figure 3.13, taking into account the properties of the aluminum alloys considered in this study (The properties of the materials used for this tradeoff are on Appendix). Finally, the bottom row provided the ranking of the options, taking into account the weight factors.
In this case, the material best ranked in the tradeoff for the main structure was the Aluminum alloy 7075-T6. Therefore this was the material adopted for the preliminary design.

Aluminum 7075-T6 is an aluminum alloy, with zinc as the primary alloy. The first four digits (7075) represent the material composition. The T6 digits represent the treatment the alloy was submitted to, the ”T” means that the alloy was subjected to thermal treatment and the ”6” represents the kind of process of thermal treatment. In this case the 7075 solution was heat treated and then artificially aged [51]. The heat treatment was made between $460 - 565°C$ in order to dissolve soluble alloying elements, then, quenching (rapid cooling normally using water) is applied to retain the alloying elements in solid solution. After that, the material is artificially aged at $115 - 195°C$ to precipitate these elements in an optimum size and distribution [51].

Trade-Off table	Options definition	AL6061 T6 Aluminium	AL7075 T6 Aluminium	AL2024 T6 Aluminium	AL5052 H38 Aluminium	Weight Factor
Key Trade-Off Parameters	Density	3	4	2	1	0,21
	Thermal Conductivity	4	3	3	1	0,19
	Thermal Expansion	3	3	1	4	0,16
	Electrical Conductivity	4	1	3	2	0,14
	Frature Resistance	2	4	3	1	0,11
	Specific Strength	2	4	3	1	0,09
	Corrosion	4	4	4	3	0,05
	Workability	4	5	6	4	0,05
	Toxicity	4	4	4	4	0,01
	Total score	3,2	3,3	2,7	1,9	
	Ranking	**2**	**1**	**3**	**4**	

Figure 3.13: Material Tradeoff for Main Structure.

3.3.2 Structural Design

In the case of a CubeSat which has a fixed platform configuration the payloads and subsystem have to be chosen carefully in order to fit-in with the rest of the satellite.

Since the payload is still being studied by the stakeholders, it was not yet integrated in the CubeSat at the time of this dissertation. However, as one of the mission requirements states that the payload shall be located at one of the extremities of the CubeSat, the upper CubeSat's unit was reserved for the payload and it was represented as a blackbox.

Figure 3.14: MECSE's First Unit.

Taking into account all the requirements defined previously, the electronics hardware were organized by CubeSat units. The antenna and the battery were positioned in the second unit. Since the antenna's hardware presents large dimensions ($87.4 \times 93.4 \times 22.9mm^3$), when positioned in the CubeSat platform, it presents small space between the rails and the hardware. Thus, it is more feasible to position the antenna on a top or end of a unit. Plus the Antenna shall be able to be deployable after the CubeSat is released from the P-POD, hence its field of view shall be free. After careful study of the available positions for the antenna it was positioned at the top of the second unit.

Besides the payload, the batteries are the components with the largest mass, hence they were positioned as closer as possible of the geometrical center of the CubeSat, so they would not have a significant influence on the attitude of the vehicle, but at the same time not too distant from the EMB in order to reduce the length of cable connections.

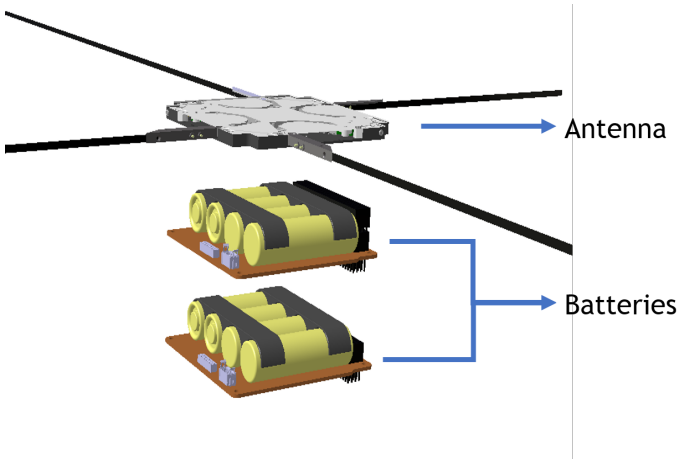

Figure 3.15: MECSE's Second Unit.

The remaining COTS were positioned on the last unit. The EMB was positioned as close as possible to the batteries, as mentioned before. The Transceiver was positioned right below the EMB. The OBC was placed on the lowest position. Since the chosen OBC provides the access port required by the CDS, it is placed within the required geometrical limits (Appendix C). The Gyroscope and Magnetorquer board were positioned as near as possible between the OBC and the transceiver.

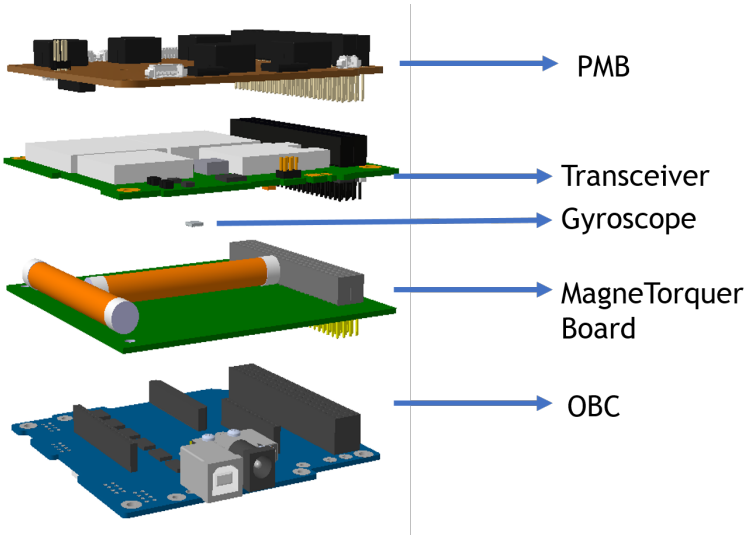

Figure 3.16: MECSE's Third Unit.

The Solar Panels were placed on the faces of the last two units. As the payload is under development, it was decided not to place solar panels on the first unit in order to prevent future challenges while designing the payload. The next step was to join the COTS of the three units, Figure 3.17.

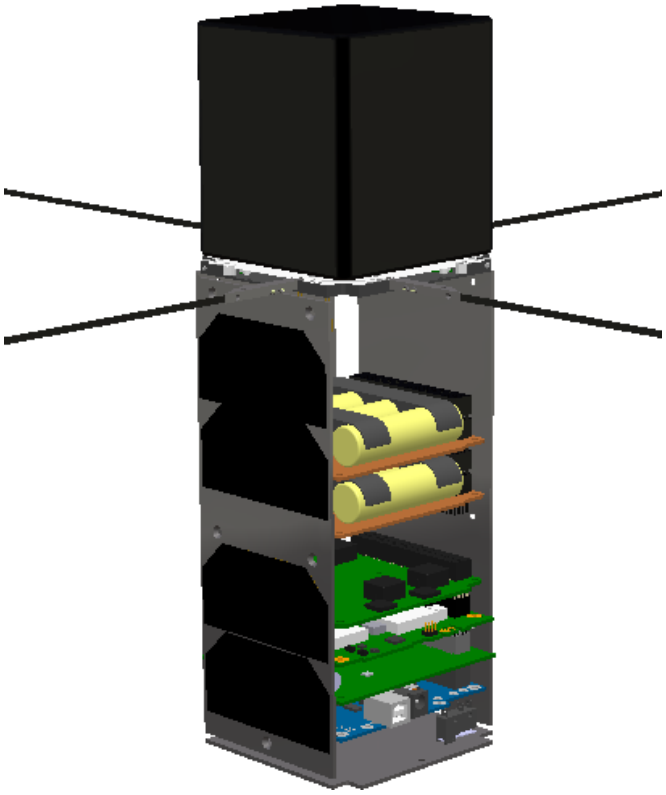

Figure 3.17: MECSE COTS Electronics.

After all the COTS were positioned, the side frames were designed. In the following figures the solar panels will not be included, so the details of the structure can be seen.

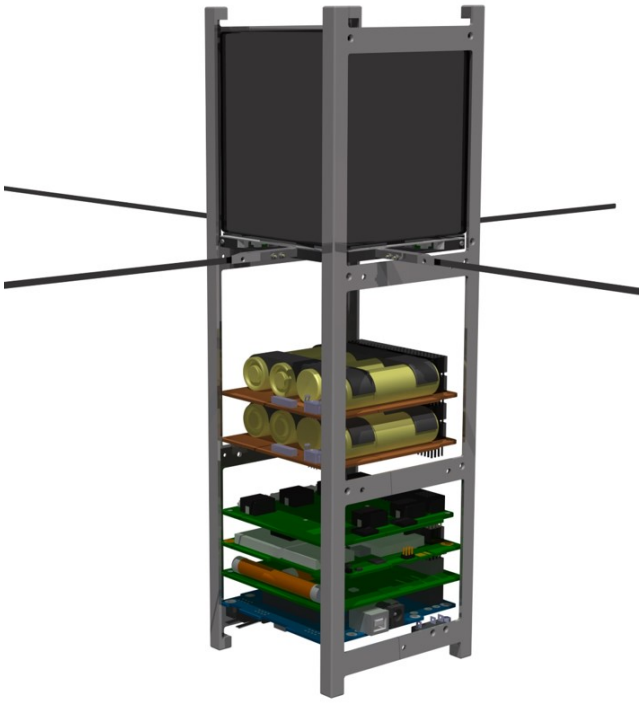

Figure 3.18: Integration of MECSE's Side Frames.

The Side Frames are made of Aluminum alloy 7075 T6. Each side frame has two hard anodized rails and four hard anodized feet to prevent cold welding when the CubeSat is inside the P-POD.

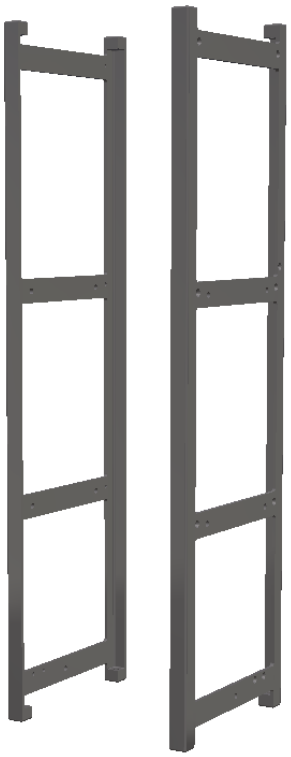

Figure 3.19: MECSE's Side Frames.

In order to create a connection between the rails, ribs were designed, Figure 3.20. Each Rib is

screwed to the side frame with two M2 bolts.

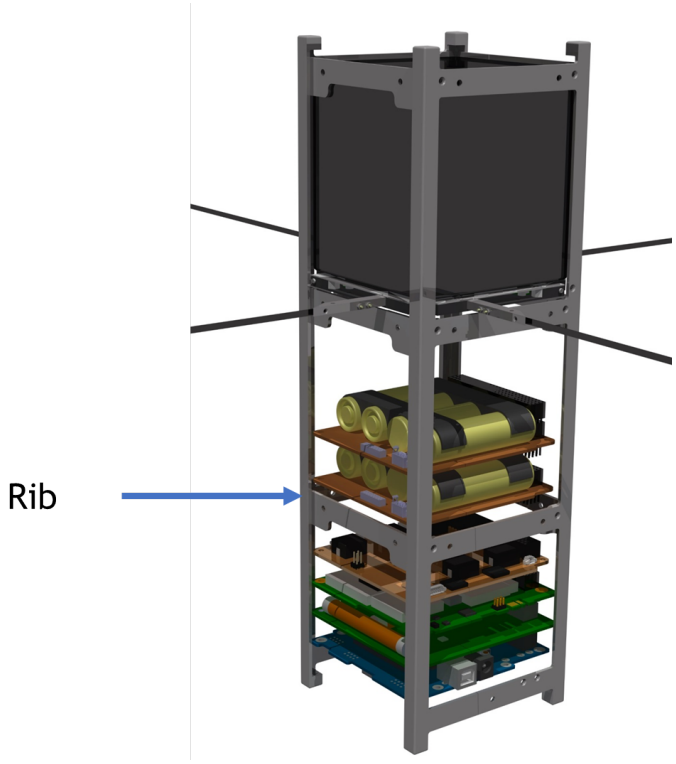

Figure 3.20: Integration of MECSE's Ribs.

Several configurations of ribs were designed as the structural and assembling requirements were being iterated. In the end, the best configuration of rib is presented on Figure 3.21. The ribs will allow connection between the rails, but they will also secure the electronics hardware and be the mounting points for the solar panels. The PC/104 stacking method consists of four endless screws securing the COTS electronics, therefore protuberances were designed in the ribs so they would be housings to secure the endless screws. Two ribs with different dimensions had to be designed due to the COTS electronic hardware design. The COTS present different spacing between the PCB holes, therefore one side has one type of rib (in Appendix D designed as Rib) and the other side has a second design (in Appendix D designed as Rib2).

Figure 3.21: MECSE's Rib.

The M3 endless screws constitute the secondary structure. Those are essential to secure the electronics inside the CubeSat. In order to space the PBC plates, spacers with an external diameter of 4.5 mm and internal diameter of 3 mm were positioned between the PCB along the endless screw. After the design of the parts presented above, the Top and End Plate were designed, Figure 3.22.

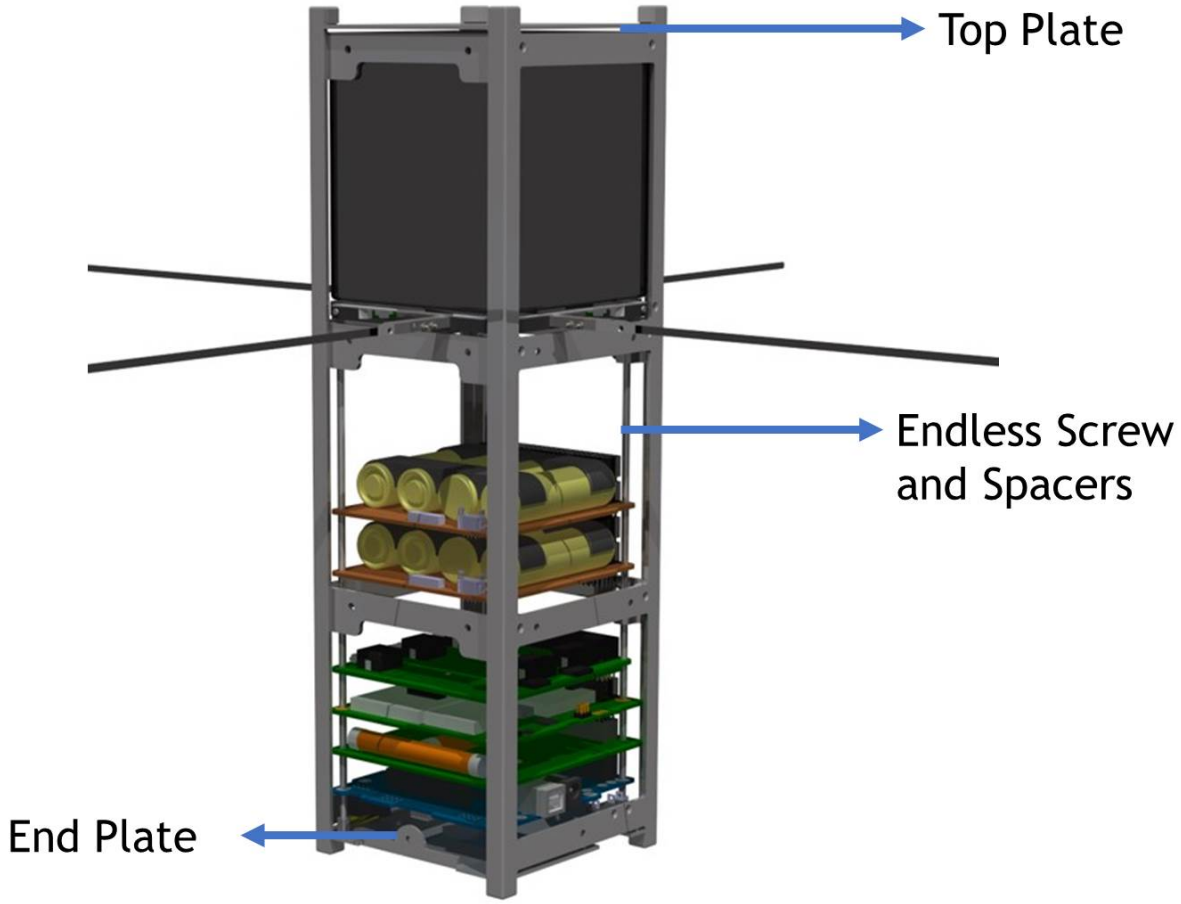

Figure 3.22: Integration of MECSE's Top and End Plates.

The Top Plate, Figure 3.23, is fastened to the side frames foot with four M2 bolts. Since the payload is under development, the first unit does not have many constraints yet. Therefore, the Top Plate was kept simple and light weighted.

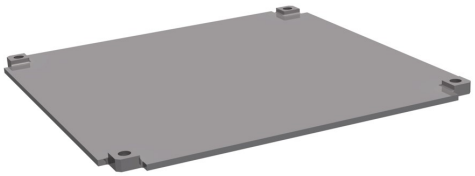

Figure 3.23: MECSE Top Plate.

The End Plate presents more complexity than the top plate. As this plate will be machined, protuberances were designed to house the M3 endless screws, adding rigidity to the structure.

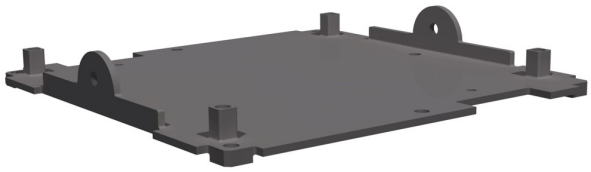

Figure 3.24: MECSE End Plate.

The End Plate is assembled to the rails through two M2 bolts, and two M3 Vented Socket Head Screws. The End plate will be the mounting points to a solar panel.

Some challenges were found when it was the time to secure the antenna as the usual point of attachment for the ISIS antenna were not a match in this design. Hence, a light machined support were designed, Figure 3.25. The support will use the attachment points that come with the antenna and will be fastened with one M2 screws to the rails.

Figure 3.25: MECSE Antenna Support.

The vehicle has two deployment switches attached to the side frame. In order to support it, a sheet metal support was designed and is screwed with three M2 bolts to the side frame and end plate.

The deployment switch's activation mechanism is placed on two of the feet of the CubeSat as per CubeSat Design Specifications (Figure C.1 from Appendix C). The mechanism consists of a Vented Socket Head Screw, a shaft, a support designed to secure the shaft and a Nylon washer (Figure 3.26).

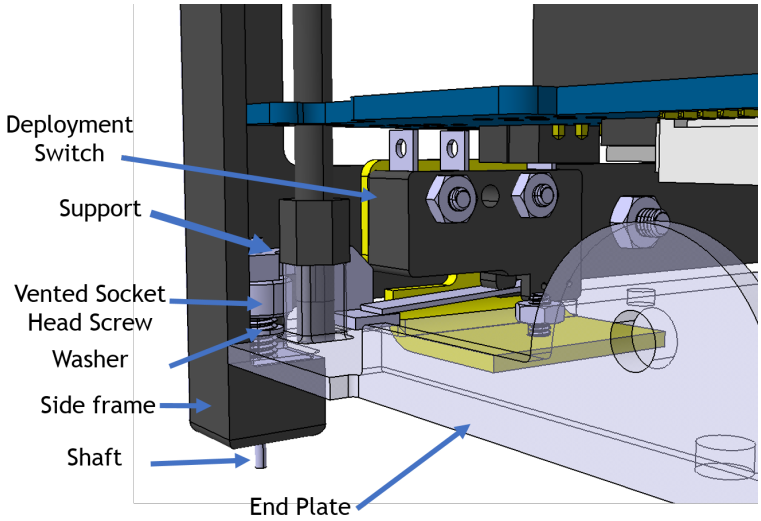

Figure 3.26: MECSE Deployment Switch Mechanism.

When the CubeSat is inside the P-POD, the shaft creates a force on the support, moving it vertically and consequently activating the deployment switch, cutting this way the electrical power.

After the integration of all the COTS hardware and the design of the mechanical subsystem, the preliminary design of MECSE was concluded, Figure 3.27.

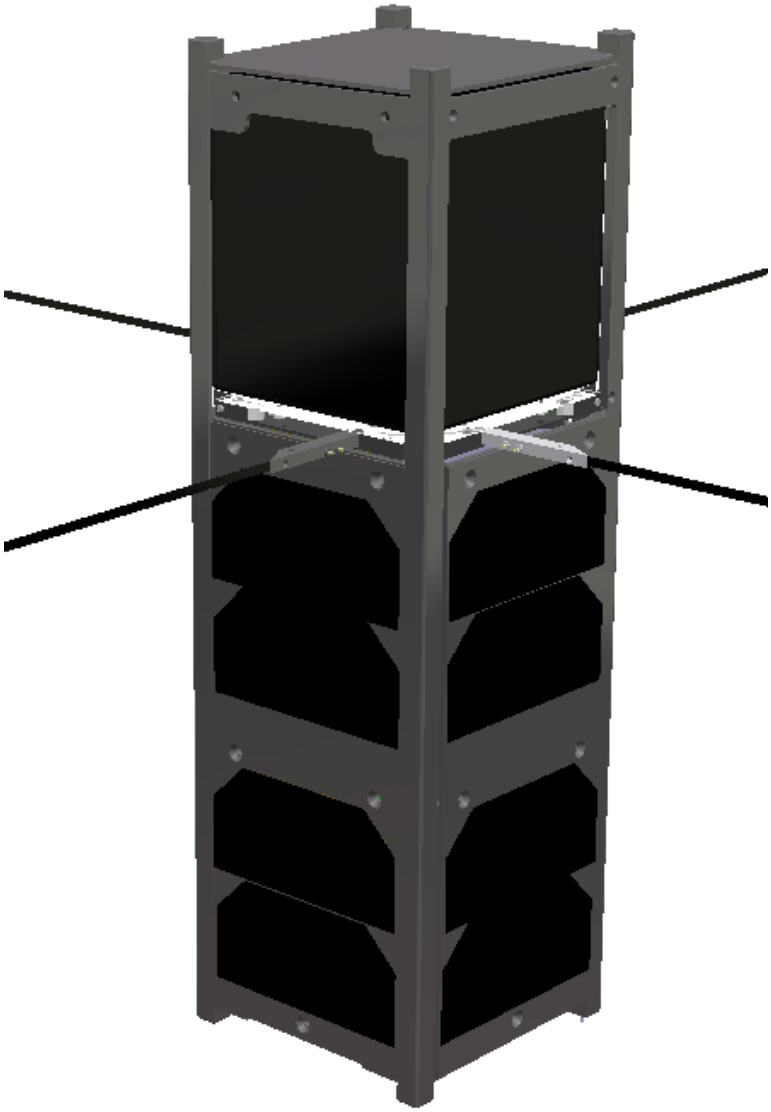

Figure 3.27: MECSE Preliminary Design.

This preliminary design of MECSE's mechanical subsystem presents several advantages: it presents low complexity in the manufacturing process, it is easy to assemble and allows access to the spacecraft's avionics even after the final integration by removing one or more detachable solar panels. Each component's 2D drawings of the mechanical subsystem can be consulted on Appendix D.

Chapter 4

Structural Analysis

This chapter presents the approach adopted in the MECSE linear static analysis using the Finite Element Method. Information on the used software, the meshing process and the final model are provided. Furthermore, study cases and their results are presented. This chapter also presents the results of the preliminary thermal calculations of the temperature at the spacecraft and their impact on the CubeSat's electronic hardware.

4.1 Software

The standard FEM process is divided into three steps: pre-processing; solution/analysis and post-processing [59]. The software used in this dissertation for the pre-processing was Altair HyperMesh [84], the solver was MSC Nastran [60] and for the post-processing was Altair HyperView [85].

Figure 4.1 demonstrates the methodology used in the process of structural Analysis.

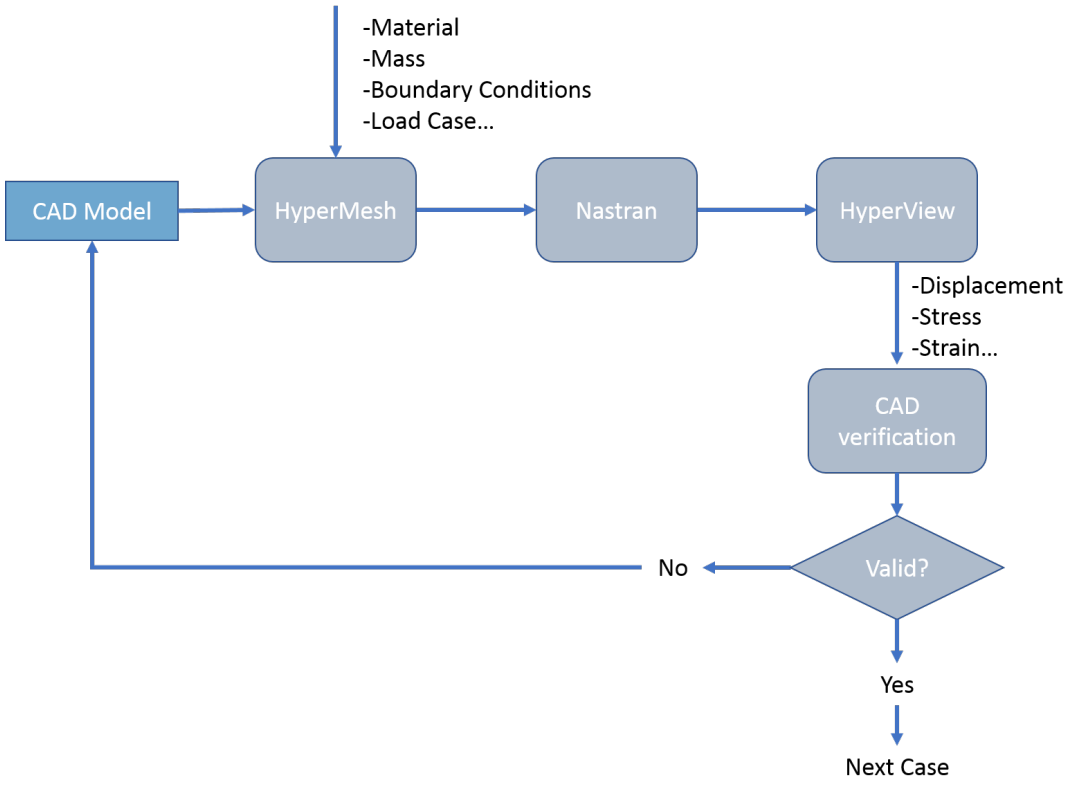

Figure 4.1: Process of Structural Analysis.

The first step in the FEM process is to import the model to the MSC HyperMesh. In this stage the properties of the model are defined (e.g. material properties, boundary conditions, load

cases) and the model is divided into discrete elements. Then the MSC Nastran is used to process the output of the Altair Hypermesh and to visualize the results processed by MSC Nastran, the results are imported to the Altair Hyperview.

4.2 Meshing

The basic idea of FEM is to make calculations at a finite number of points called nodes. These nodes form entities in predetermined shapes called elements and then the group of elements is called mesh.

The meshing step is crucial to the finite element analysis because the quality of the mesh influences directly the quality of the results generated. Thus, the first step is to define the mesh element type. This decision is based on geometry size and shape, type of analysis and time allotted to the project [86].

As explained in section 2.3.2, plates represent a structure whose thickness is small compared to its other dimensions and can be easily reduced to two-dimension elements, also called surface elements [60]. Since the thickness of MECSE structural components is low when compared to the width and length, it is possible to use two-dimension elements for these analysis. Two-dimension elements are planar hence, the software has the information of two out of the three required dimensions of the model (width and length). The third dimension (thickness) is given by the user as input data.

MSC Nastran, defines the model geometry with grid points [60, 86]. A grid point is a point on or in the structure which is used to define a finite element (CQUAD) [60]. Each grid point of the structural model has six possible components of displacement: three translations (x, y, or z directions) and three rotations (x, y, or z axis). These components of displacement are called degrees of freedom (DOFs). In the case of the grid points used to represent plate elements, stiffness terms only exist for five of the six possible degrees of freedom per grid point. There is no stiffness associated to the rotation about the normal to the plate, for that reason, rotational DOF must be constrained to prevent stiffness singularities.

The CQUAD4, Figure 4.2, is MSC Nastran's most commonly used element for modeling plates, shells, and membranes [60]. It can represent in-plane, bending, and transverse shear behavior, depending upon the data provided on the PSHELL property entry [86].

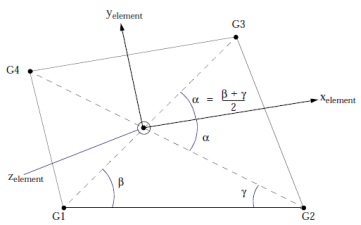

Figure 4.2: CQUAD4 Element Geometry and Coordinate System [86].

The CQUAD4 element is a quadrilateral flat plate connecting four grid points and its size depends on the density of elements the user choose to have. To define the most suitable density of

elements for MECSE, a convergence study was performed.

4.2.0.1 Mesh Convergence Study

The component chosen for the convergence study was a Rib because this component is essential for the integrity of the structure and it has a complex geometry. The rib was modeled following the theory of the thin plates, therefore, it was firstly converted into a Mid-Surface and it was given a shell element property (PSHELL) which defines the membrane, bending, transverse shear and coupling properties of thin shell elements [86]. FE Solvers assume the shell element to lie at the middle of the thickness and due to that a Mid-Surface was created.

In order to constrain the rib its position inside MECSE was considered and according with that, some elements of the Side Frame were used to reproduce its boundary conditions. Single point constraints (SPC's) are used to apply a set of single point constraints or enforced displacements (i.e., nonzero values of displacement) for static analysis [60, 86], therefore SPC's were used to constraint the elements of the Side Frames.

Although the system SI defines MPa as units for force, which is equal to N/mm^2, in this dissertation it was adopted the units daN/mm^2 for a better understanding of the results from MSC NASTRAN.

The rib was connected to the Side Frame with a shell patch fastener connection (CFAST) which defines a fastener with material orientation connecting two surfaces patches [86]. A force with magnitude of $14.02daN$ was applied to the rib divided by two grids.

Figure 4.3 presents the rib used for this study.

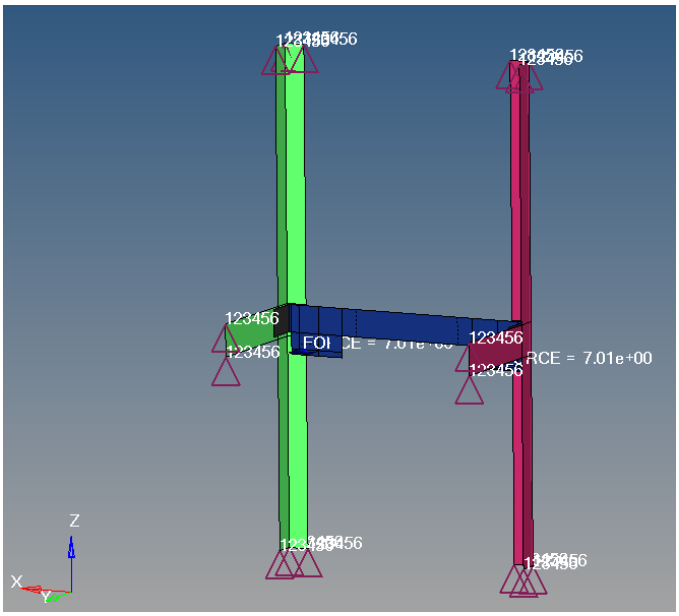

Figure 4.3: Component for the convergence study.

To define the dimensions of the mesh that shall be used to model MECSE, the element sizes were changed until the values of stress, strain and time converged. Five multiples of the part's

thickness for the mesh dimension were considered ($5t$, $4.5t$, $4t$, $3t$, $2.5t$).

In Figure 4.4 it can be seen that there is a convergence from the first to the third point. However, from the forth point it diverges due to presence of elements with dimension $t \times t \times t$ which no longer respect the thin plate theory (small ratio between the width and length in relation to thickness) which is why it is not a valid mesh for this type of elements.

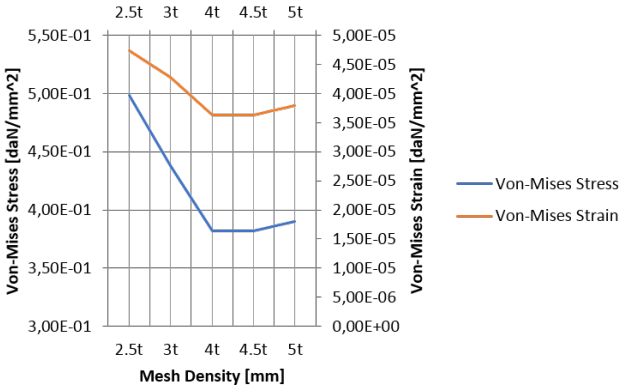

Figure 4.4: Stress and Strain vs Mesh Density.

The time of computation was also taken into account, as it is possible to see from Figure 4.5 the computational time decreases after the third point ($4t$) remaining constant along the iterations.

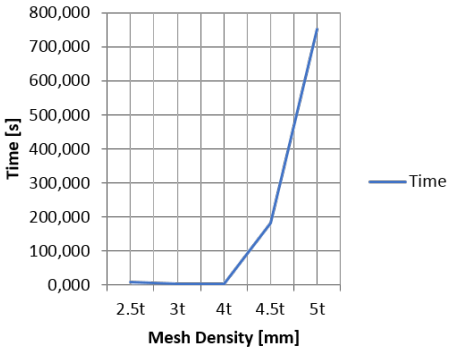

Figure 4.5: Time vs Mesh Density.

From this study a dimension of $4t$ was chosen, as it presents low computational time and in point $4t$ the stress and strain converged, although especially in the areas where the model experiences a reduction area the dimensions of the mesh shall be adapted to best suit the geometry.

4.3 Final Model

After the STEP file was created, it was imported into the Altair Hypermesh, the structure was simplified. The fillets and bolts's holes eliminated in order to simplify the meshing process.

All the structures were converted into Mid-Surfaces and PSHELL properties were assigned to those Mid-Surfaces with exception of the endless screws which were converted into Simple

Beam Element Connections (CBAR's) [86].

The endless screws were connected to the ribs through rigid body elements (RBE2). An RBE2 is a 1D element used to connect nodes. This connection is a rigid link that transfers motion from the independent node to the dependent nodes [86].

All the fasteners were converted into CFAST and their properties had to be added to the input data. Therefore, the Stiffness Values ($KT1$, $KT2$ and $KT3$), the Rotational Stiffness values ($KR1$, $KR2$ and $KR3$) were calculated using reference [86]:

$$KT1 = \frac{EA}{L}$$

$$KT2 = \frac{G_2 A_s}{L}$$

$$KT3 = \frac{G_3 A_s}{L}$$

$$KR1 = \frac{GJ}{L}$$

$$KR2 = \frac{EI}{L} + \frac{G_2 A_s L}{3}$$

$$KR3 = \frac{EI}{L} + \frac{G_3 A_s L}{3}$$

where

$$A = \frac{\pi D^2}{4}$$

$$I = \frac{\pi D^4}{64}$$

$$J = \frac{\pi D^4}{32}$$

$$L = |\vec{x_B} - \vec{x_A}|$$

$$A_s = \frac{A}{\alpha_s}$$

$$\alpha_s = 4/3$$

and E is the Young's modulus and G is the Shear Modulus of the fasteners' material.

As all the components representations were defined and the mesh size was studied, the model was created, Figure 4.6.

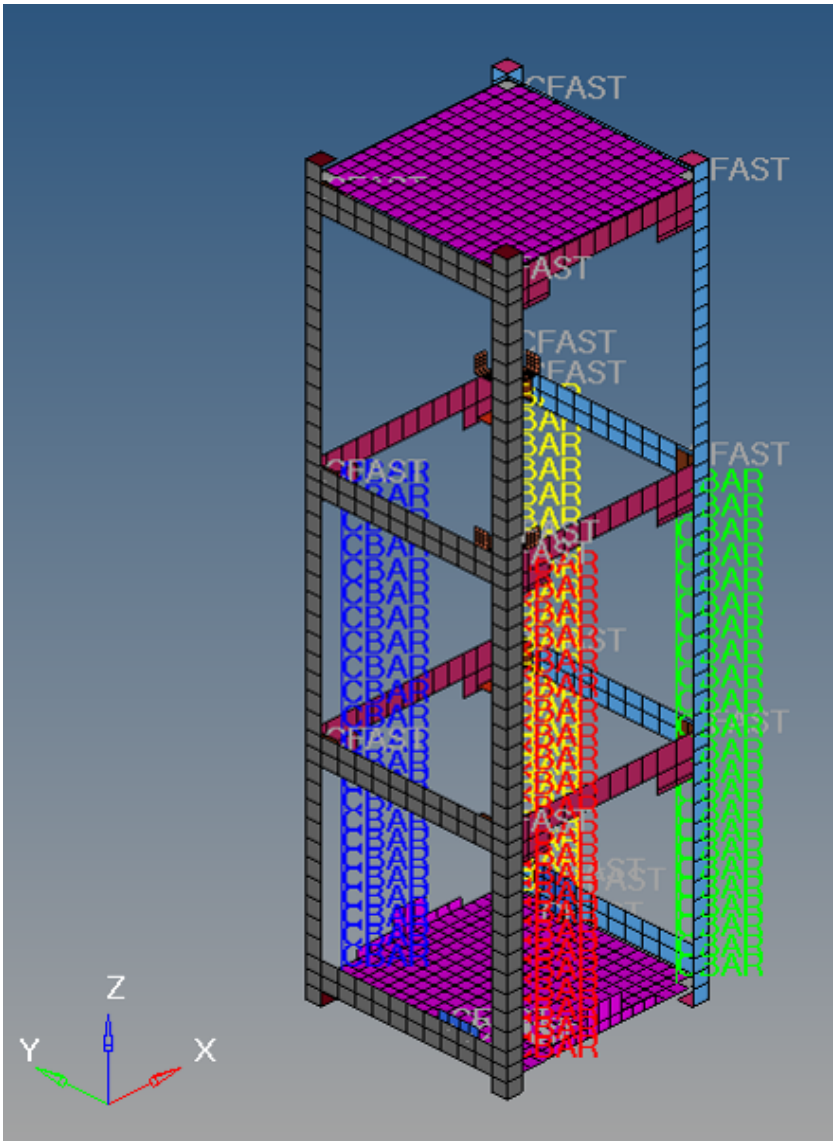

Figure 4.6: Model FEM.

Each Electronic COTS' hardware were converted as concentrated mass elements connections (CONM2), that define a concentrated mass at a grid point and to each CONM2 was assigned the respective mass of the components they represent. The CONM2 were connected through RBE2 to the CBARs, 4.7.

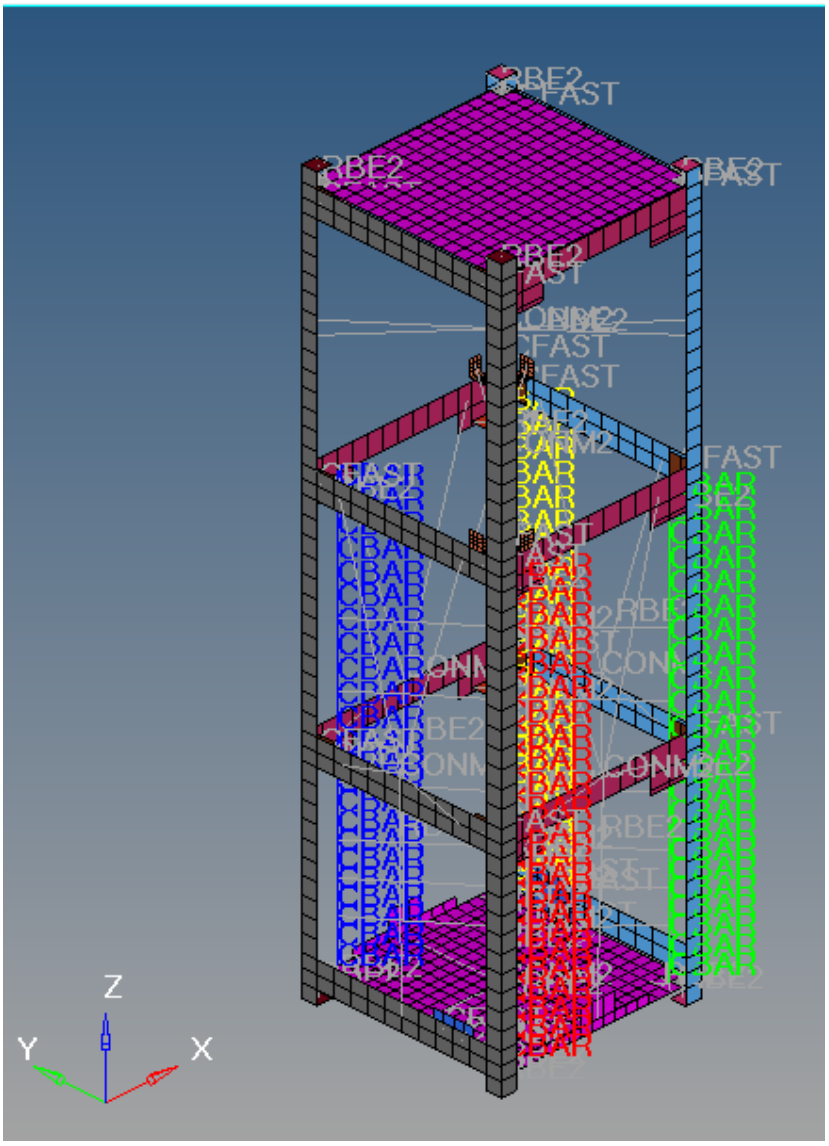

Figure 4.7: Final Model.

In order to facilitate the identification of the parts, each different components were given an ID number, Figure 4.8.

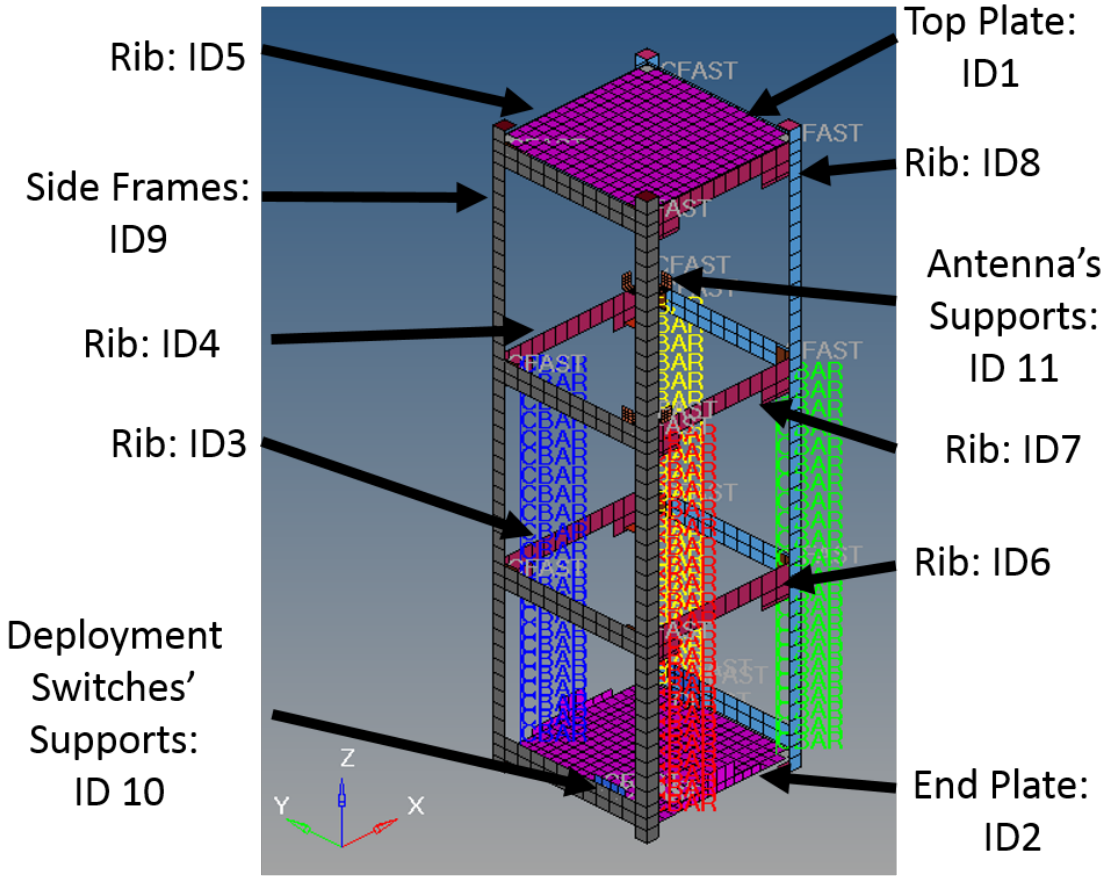

Figure 4.8: ID number of the model's components.

4.4 Linear Static Analysis

These analysis aim to understand if the main structure is able to withstand the steady state accelerations and to define the margin of safety for MECSE. After the study of the VEGA's User Manual [43], and the Announcement of Opportunity for the Launch of Multiple Light Satellites on a VEGA Flight [87], it was possible to understand that the highest loads MECSE would encounter occur during the launch sequence.

Reference [87], defines that the CubeSat when within the launcher is lay down horizontally on the lower module. The maximum quasi-static acceleration in the longitudinal axis is 14.5 G (Load 1) in compression and 10.5 G (Load 2) in tension. The maximum lateral loads are 3 G (Load 3) along the x-axis and 3 G (Load 4) along the y-axis, Figure 4.9. As the quasi-static accelerations from the reference [87] have a higher value when compared to reference [43] for the same conditions, a safety value was not added as it is already an intrinsic value.

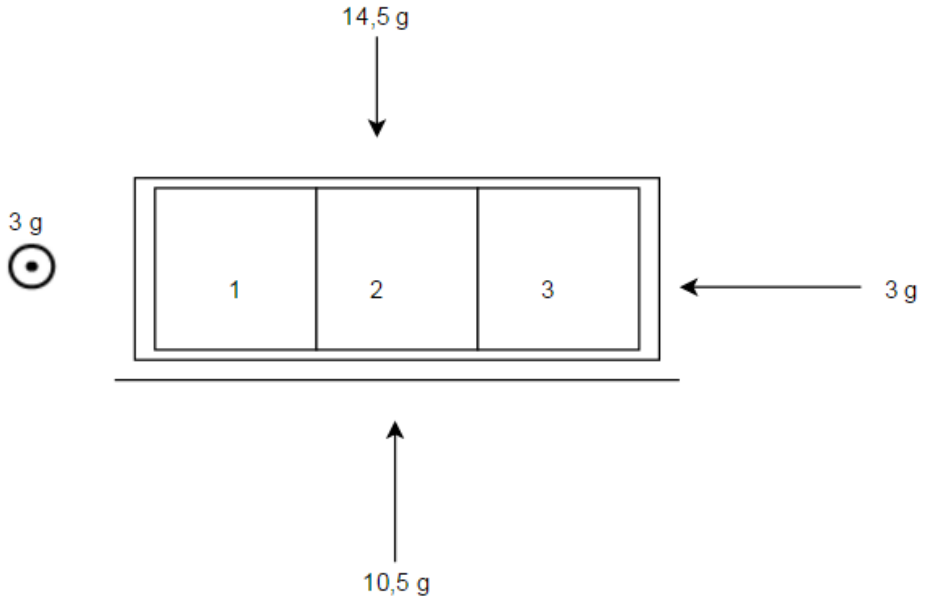

Figure 4.9: MECSE Position Within VEGA Launcher [87].

Reference [88] defines that a CubeSat shall survive within a temperature range from $-20°C$ to $50°C$ from the time of launch until its end of life, hence these temperatures were also simulated. For these analysis it was considered $T1 = -20°C$ and $T2 = 50°C$

The loads were defined as Acceleration or Gravity Load (GRAV) which defines acceleration vectors for gravity or acceleration loading. On the other hand, temperatures were defined as grid point temperature field (TEMP) which defines temperature at grid points for determination of the thermal loading, temperature-dependent material properties, or stress recovery.

Table 4.1 summarizes all the different case scenarios used in the FEM analysis.

Table 4.1: Study Cases

	Load 1	Load 2	Load 3	Load 4	Temperature 1	Temperature 2
Case 1	x				x	
Case 2		x			x	
Case 3			x		x	
Case 4				x	x	
Case 5	x					x
Case 6		x				x
Case 7			x			x
Case 8				x		x

4.5 Results

In the analysis the theorem of maximum principal stress was considered, which states that the failure of a material or component will take place when the maximum value of stress exceeds the limiting value of stress. Therefore, when performing the post-processing the Extreme Von-Mises Stress and Strain values, the Maximum Principal Stress and Strain that corresponds to tension and the Minimum Principal Stress and Strain, that corresponds to compression, were taken into

consideration.

$$\sigma_{Von-Mises} = \sqrt{\sigma_{P1}^2 - \sigma_{P1} \cdot \sigma - P3 + \sigma_{P3}^2} \quad (4.1)$$

where σ_{P1} is the Maximum Principal Stress , σ_{p3} is the Minimum Principal Stress.

$$\sigma_{P1} = \frac{\sigma_x + \sigma_y}{2} + \sqrt{\frac{(\sigma_x - \sigma_y)^2}{4} + \tau_{xy}^2} \quad (4.2)$$

where τ_{xy} is the shear stress

$$\sigma_{P3} = \frac{\sigma_x + \sigma_y}{2} - \sqrt{\frac{(\sigma_x - \sigma_y)^2}{4} + \tau_{xy}^2} \quad (4.3)$$

The Margin of Safety (MS) were calculated using the equation 2.10.

$$MS = \frac{Allowable of the Material}{Applied Load} - 1$$

Reference [66] defines that the Ultimate and the Yield margin of safety shall be > 0.2.
The values for the allowable of the material are defined by reference [83], table 4.2.

Table 4.2: Allowable of the material

Allowable	Value
F_{tu}	55.2 daN/mm^2
F_{ty}	48.0 daN/mm^2
F_{cy}	48.0 daN/mm^2

When calculating the MS of the Extreme Von-Mises Stress and Strain the F_{tu} is the allowable, F_{ty} is the allowable for the margin of safety of Maximum Principal Stress and Strain and F_{cy} is the allowable for margin of safety of the Minimum Principal Stress and Strain.

In the cases where the margin of safety is superior to 10 it will be identified as High Margin of Safety (HMS). The model presents several RBE2 elements and as those elements are rigid elements they increase the value of stress and strain so they were excluded from the analysis. Table 4.3 presents the values of Displacement, Von-Mises Stress and Strain and the Margin of Safety for each case study. The Figures that gave origin to the table can be found on Appendix F. Only the primary structure was taken into account for these studies.

Table 4.3: Displacement, the Extreme Von-Mises Strain, the Extreme Von-Mises Stress and the Margin of Safety of Cases 1 to 8

Cases	Maximum Displacement [mm]	Extreme Von-Mises Strain [daN/mm^2]	Extreme Von-Mises Stress [daN/mm^2]	MS
1	0.17	4.72E-4	4.27	7.6
2	0.11	4.73E-4	4.01	8.2
3	0.13	4.73E-4	4.05	8.1
4	0.18	4.73E-4	4.09	8.0
5	0.70	2.84E-3	24.13	0.5
6	0.72	2.84E-3	24.14	0.5
7	0.70	2.84E-3	24.14	0.5
8	0.69	2.84E-3	24.19	0.5

It is possible to conclude from table 4.3 that the margins of safety decrease at the case 5. In case 5 the load applied to the satellite is the same as in case 1, but the temperature of the case 5 is superior, therefore it is possible to understand that when the temperature increase, the stress also increases.
Considering the equation of the linear thermal expansion

$$\triangle u = L_0 \cdot \alpha \cdot (T_1 - T_0) \quad (4.4)$$

where $\triangle u$ is the displacement, L_0 is the initial length of the object, T_1 is the final temperature and T_0 is the initial temperature, with the increase of the temperature the displacement $\triangle u$ will increase. This is a problem for the fasteners, because if the results present severe displacement, the fasteners will be loosen and the structure will no longer be constrained.From the simulations' results it possible to conclude that the displacement is not significant to constitute a risk for the structure and fasteners connections since the highest value is $0.72\ mm$.

It is necessary to study each components to understand which are the critical components that created the lower margins of safety to conclude which components shall be redesigned. Table 4.4 presents the Extreme Von-Mises Stress and Strain, the Maximum Principal Stress and Strain (P1), the Minimum Principal Stress and Strain (P3) and the stress Margin of Safety for the worst case scenario of each component.

Table 4.4: Individual Cases

ID	1	2	3-8	9
Extreme Von-Mises Strain [daN/mm^2]	2.39E-3	2.23E-3	2.05E-3	2.84E-3
Maximum Tension Strain [daN/mm^2]	4.03E-3	3.82E-3	3.51E-3	4.31E-3
Minimum Compression Strain [daN/mm^2]	2.26E-4	1.16E-3	1.53E-3	2.86E-4
Extreme Von-Mises Stress [daN/mm^2]	15.14	8.75	16.80	24.19
MS	1.4	3.2	1.2	0.5
Maximum Tension Stress [daN/mm^2]	8.72	8.49	12.00	8.84
MS	3.4	3.5	2.2	3.3
Minimum Compression Stress [daN/mm^2]	14.57	5.84	12.70	25.70
MS	1.6	5.6	2.0	0.5

From table 4.4 it is possible to conclude that all components respect the limits of margin of safety imposed by reference [66]. The side frames are the components with lower margin of safety to stress as their highest value of stress is the a minimum compression stress with a magnitude of $25.70\ daN/mm^2$ (case 5), Figure 4.10. When the CubeSat is within the launcher it is horizontally and the largest acceleration has a magnitude of 14.5 G in Z- direction, therefore it was expected that the side frames would present higher values of compression, which was proved in the simulations.

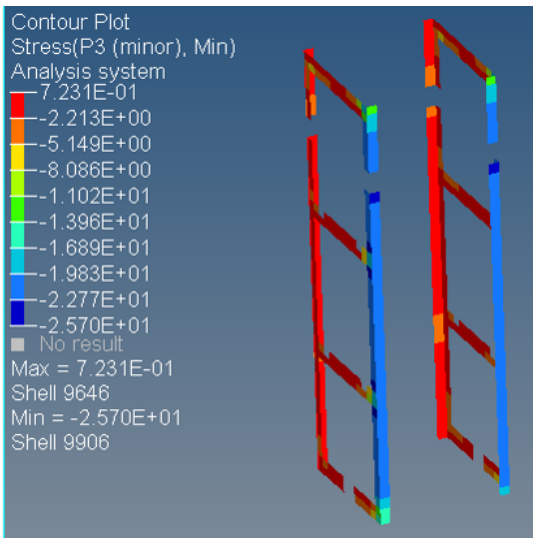

Figure 4.10: Case5-Minimum Compression Stress of the Side Frames.

As it was referred in the mesh convergence study, the ribs are essential for the integrity of the structure. The ribs present a margin of safety to the Extreme Von-Mises Stress, Figure4.11, 6 times the limit value of margin of safety. Thus the ribs are not critical components.

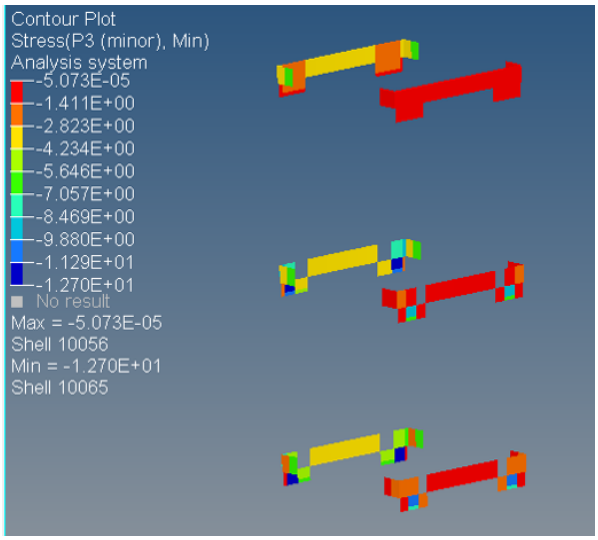

Figure 4.11: Case5-Minimum Compression Stress of the Ribs.

The remaining components present a margin of safety superior to the margin defined by [66]. Considering these case studies, it is recommended to reduce the thickness of the components with exception of the side frames, which will consequently reduce the mass of the satellite.

From reference [25], it was possible to identify two possible temperatures the satellite would be exposed while on orbit. Thus, two extra simulations are performed to study the structural behavior of the satellite when subjected to $-120°C$ (T3) and $120°C$ (T4).

Table 4.5 presents the Displacement, the Extreme Von-Mises Strain, the Extreme Von-Mises Stress and the Margin of Safety associated to stress for the last two case studies.

Table 4.5: Displacement, the Extreme Von-Mises Strain, the Extreme Von-Mises Stress and the Margin of Safety of Cases 9 and 10

Cases	Maximum Displacement [mm]	Extreme Von-Mises Strain [daN/mm^2]	Extreme Von-Mises Stress[daN/mm^2]	MS
9	0.71	2.84E-3	24.16	0.5
10	0.71	2.86E-3	24.16	0.5

The margin of safety of the last two cases respects the limits defined previously, and as it was expected the Extreme Von-Mises strain presents higher values than the previous case studies (2.86E-3) Which was expected to occur. Each component was studied individually for the case study 9 and 10. Table 4.6 presents the Extreme Von-Mises Stress and Strain, the Maximum Principal Stress and Strain (P1), the Minimum Principal Stress and Strain (P3) and the stress Margin of Safety for the worst case scenario of each component.

Table 4.6: Worst Case Scenario for Each Component

ID	1	2	3-8	9
Extreme Von-Mises Strain [daN/mm^2]	2.38E-3	2.06E-3	2.05E-3	2.84E-3
Maximum Tension Strain [daN/mm^2]	4.03E-3	3.20E-3	1.53E-3	4.30E-3
Minimum Compression Strain [daN/mm^2]	2.26E-4	1.14E-3	3.5E-3	9.33E-4
Extreme Von-Mises Stress [daN/mm^2]	15.14	6.74	16.73	24.16
MS	1.4	4.3	1.2	0.5
Maximum Tension Stress [daN/mm^2]	8.72	7.18	12.75	8.84
MS	3.4	7.2	2.0	3.3
Minimum Compression Stress [daN/mm^2]	14.57	5.79	12.96	25.62
MS	1.6	5.6	2.2	0.5

The Side Frames are the most fragile component of the primary structure as they present a margin of safety of 0.5 to the Minimum Compression Stress, but the increase of the coldest and hottest temperatures did not present sever effect or damage on the Mechanical Subsystem. As the maximum displacements were inferior to 1mm. These two cases confirm that the structural components' thickness shall be reduced with exception of the Side Frames.

While modeling the geometry some simplifications were done, for example the fillets were eliminated and by doing that the thickness of the structure decreases, so the real model will present higher margins of safety. Additionally, as the first unit is still under-development it was assumed the payload (1.2kg) would be only connected to the Side Frames, which increases the values of stress of the Side Frames.

4.6 Thermal Impact Evaluation

Systems Tool Kit (STK) software was used to propagate the orbital elements through time which allow the definition of the worse cases scenarios the satellite would be exposed during its orbit. Figure 4.12 represents the initial orbit of MECSE and table 4.7 defines the orbital elements for the initial orbit.

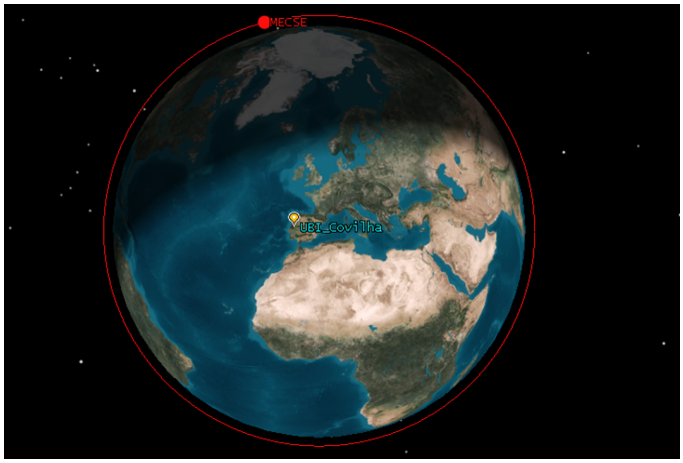

Figure 4.12: MECSE Initial Orbit.

Table 4.7: Orbital elements of MECSE's reference orbit [71]

Epoch	1-Jan-2020
Orbit Type	LEO
Altitude of Apogee/Perigee	350 km
Eccentricity	0
Inclination	52.6°
Argument of Perigee	0°
RAAN	0°
True Anomaly	0°

MECSE will have a life time duration of 1.5 years, beginning its orbit at 350 km with an inclination of $52.6°$. MECSE follows the 3U CubeSat standardization, therefore the body reference frame shall comply with the CubeSat Design Specification (CDS) [4] but in the case of attitude simulations the axis used does not correspond to the CDS. For the attitude referential X_O axis is the velocity direction and is equivalent to the Z_B from the CDS axis. Figure 4.13 illustrates the orbit reference frame used for attitude analysis.

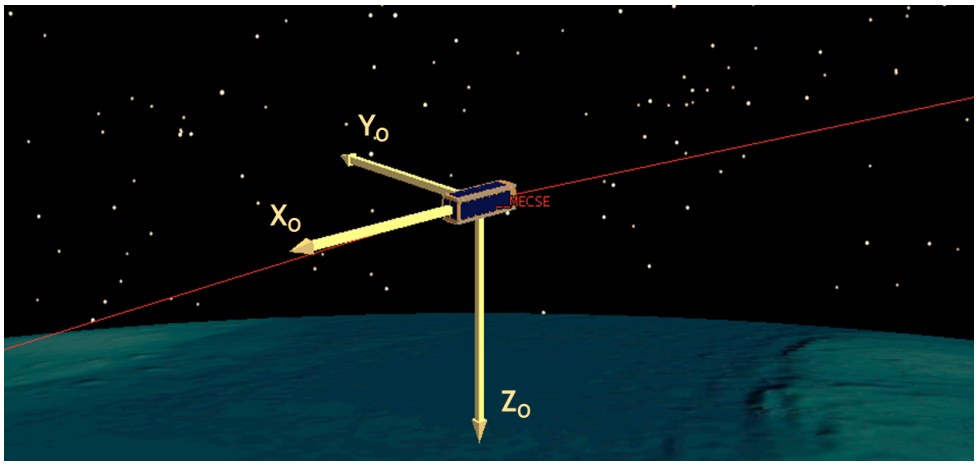

Figure 4.13: Orbit reference frame used for attitude analysis.

For the thermal impact evaluation, the methodology adopted was to simulate cases with different beta angle and understand which were the worst case scenarios and study that specific

case. After carefully analyse MECSE's orbit it was possible to characterize the hottest and coldest cases MECSE would be exposed to. Using equations, 2.13, 2.14, 2.15, 2.16 and 2.17 it was possible to calculate the hottest and coldest temperatures inside MECSE.

Generally, the outer surface area of a CubeSat is covered with solar cells, which behave as flat absorbers, converting radiance into power, reducing this way the heat loads on a surface. As MECSE's payload is still under development and the first unit outer surface is not yet defined, it was assumed that this unit would be covered with aluminum alloy panels (four side panels and one top panel, total area $47227\ mm^2$), creating a hotter case than if we assumed it was covered with solar cells.

The total area of hard anodized aluminum alloy 7075 T6 is $23732\ mm^2$ and it was assumed the material of the Solar Panels was PCB, presenting an area of $25107\ mm^2$ of PCB material and $51306\ mm^2$ of Solar Cells.

Through the literature review, it was possible to learn that aluminum alloys may have different emissivities, as a result of the coating or finishing choice of the aluminum. In table 4.8 the optical properties used for the static thermal analysis are presented.

Table 4.8: Optical Properties of MECSE's Materials [1, 2]

Material	Emissivity	Absorptivity
Aluminum Black	0.86	0.86
Aluminum Panel	0.03	0.09
Solar Panel (PCB)	0.80	0.60
Solar Cells	0.91	0.89

Using equation 2.17 and considering the areas presented before and table 4.8,

$$Q_{Sat} = 5.024 \cdot 10^{-}3 \cdot T^4[W]$$

4.6.1 Case Studies

For the first case of analysis, the position of the CubeSat that constitutes the hottest case was considered, it occurs when the CubeSat is positioned at $\beta = 75°$. From STK, it is possible to understand that at this orbit, day and attitude three faces of the CubeSat will be under sun's influence (X_O+,Y_O+, Z_O-).

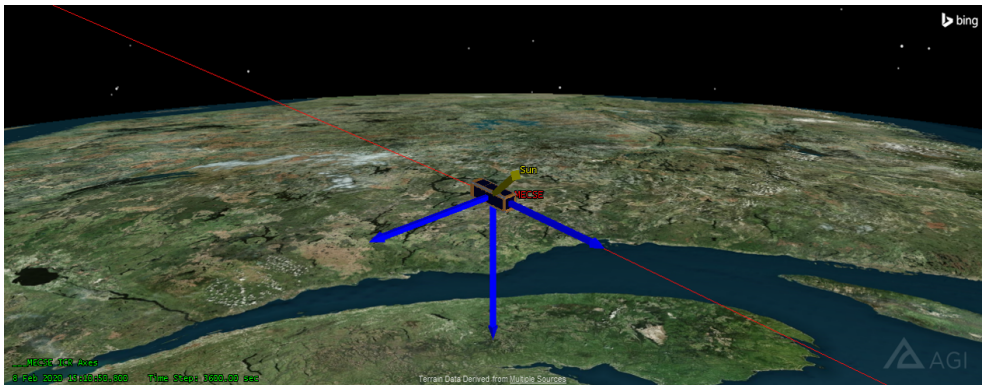

Figure 4.14: Attitude at $\beta = 75°$.

In summary the area facing the Sun is:

Table 4.9: Areas of Case 1

MECSE	Area facing Sun [mm^2]	Area facing Earth [mm^2]
Side Frame	11866.0	5788.5
Aluminum Panel	28469.0	9379.0
PCB	10716.0	5358.0
Solar Cells	24144.0	12072.0

In this case we will have heat contributions from Sun, Earth, Albedo and Internal dissipation.

As the orbit is assumed to be at an altitude of 350 km then

$$Q_{sun} = 1367 \cdot [24144 \cdot 0.89 + 10716 \cdot 0.60 + 28469 \cdot 0.09 + 11866 \cdot 0.86] = 5.56 \cdot 10^7 [W]$$

$$Q_{Earth} = 230 \cdot [12072 \cdot 0.91 + 5358 \cdot 0.8 + 9379 \cdot 0.03 + 5788.5 \cdot 0.86] \cdot [\frac{6371^2}{(6371+350)^2}] \cdot 3 = 1.27 \cdot 10^7 [W]$$

$$Q_{Albedo} = 1367 \cdot 0.3 \cdot [12072 \cdot 0.89 + 5358 \cdot 0.60 + 9379 \cdot 0.09 + 5788.5 \cdot 0.86] \cdot [\frac{6371^2}{(6371+350)^2}] \cdot 3 = 2.19 \cdot 10^7 [W]$$

$$Q_{Internal} = 3[W]$$

Using equation 2.13, the hottest temperature is:

$$T = 94°C$$

The second and last simulation is the coldest case. At $\beta = -70°$ no face will be exposed to the sun and albedo, and one face (Z_o+) will be under Earth IR.

Figure 4.15: Attitude at $\beta = -70°$.

$$Q_{Earth} = 230 \cdot (12072 \cdot 0.91 + 5358 \cdot 0.8 + 9379 \cdot 0.03 + 5788.5 \cdot 0.86) \cdot [\frac{6371^2}{(6371+350)^2}] \cdot 3 = 1.27 \cdot 10^7 [W]$$

$$Q_{Internal} = 3[W]$$

So the coldest temperature is

$$T = -48°C$$

All electronic devices are designed to operate in a temperature range, table 4.10. Basically, the allowable temperature range is defined by the subsystem component with the lower values of operational temperature.

Table 4.10: Thermal Range of the Subsystems

Subsystem	Operational Temperature ºC
Solar Cells	[-40,85]
Battery	[-40,125]
EMB	[-40,85]
AOCS Board	[-40,70]
OBC	[-40,85]
Antenna	[-20,60]
Transceiver	[-20,60]

The analytic calculations presented in this section allow to understand that the temperatures at the spacecraft (cold and hot) exceed the operational temperatures of the subsystem's electronic hardware. The manufacturers datasheets did not present information related to the survival temperature of each hardware, but from the state-of-the-art studies performed, it was concluded that the survival temperature of the electronic hardware ranges from $-55°C$ to $120°C$. Hence, the electronic hardware would survive in the hottest and coldest cases, but they would not operate. Therefore the operations of the hardware will depend on the β angle.

MECSE requires high peaks of energy in order to perform the scientific experiment, that energy will be provided by the batteries. The operational temperatures of the battery ranges from $-40°C$ to $125°C$. Comparing with the results from the analytical study, the battery will not operate during the coldest case ($\beta = -75°$), but it will operate during the hottest case. Hence, with the current materials, the experiment can not be performed at a $\beta = -75°$.

Other requirement of MECSE is the transmission of the data collected from the Langmuir Probes. The antenna present a range of operational temperatures that is inferior than the analytical results, therefore communications will not occur when the spacecraft presents an orbit of $\beta = -75°$ and $\beta = 75°$.

In order to increase the operational envelope of the subsystems it is required to protect the interior of the spacecraft from the temperature variations. In MECSE case, it requires a protection from the cold and hot temperatures. The market offers several options of surface coating and finishes, but as MECSE structure is covered with solar panels it is impractical to coat the surfaces. Bearing that in mind, other market options were studied and the implementation of aerogel on the interior of the CubeSat surfaces would present good advantages for MECSE. Aerogel is an ultralight (slightly heavier than air) and ultra-isolating material (thermal conductivity of the order of a few mW/m^2) polymer that can have a small thickness which makes this material a good option of thermal control to CubeSats [89].

Chapter 5

Conclusion

With the elaboration of this dissertation, a preliminary design of MECSE was accomplished on CATIA. FEM analysis of the preliminary structure was performed and the on-orbit temperature at the spacecraft was calculated. The work presented in this dissertation already gave origin to a presentation on the 10th Pico- and Nano-Satellite Workshop in Würzburg on September 2017 [90].

The selection of the subsystem's hardware based on the requirements imposed by the project was the starting point for the preliminary design. Hence, an exhaustive market research was necessary and a selection of the electronics' hardware was made based on the study of previous missions. After considering this entire hardware selection, the preliminary design was carried out and, with that in mind, it was possible to define MECSE's preliminary configuration and design.

The Mechanical Subsystem was divided in several parts, and each part went through several structural configurations until a feasible mechanical design was possible to be defined.

The main structure was composed of a Top Plate, an End Plate, six Ribs and two Side Frames, all assembled with M2 bolts. Further on, it was necessary to design supporting structures for the antenna and the deployment switch device.

Thus, using CATIA®, it was possible to obtain a three-dimensional CubeSat Mechanical Subsystem whose configuration presents several advantages: it is light weighted; it has a modular structure; it presents low manufacture complexity; it is ease to assemble, and allows easy access to the spacecraft's avionics even after the final integration by removing one or more detachable solar panels.

Then, linear static FEM structural analysis was performed to this preliminary design, ensuring that its robustness could be virtually guaranteed and validated, proving it can sustain the launch QSL.

The FEM model is composed of 1D and 2D elements respecting the Thin Plates Theory. The worst case scenario for each primary structure was assessed and all components presented margins of safety to Extreme Von-Mises Stress and Strain, Maximum Principal Stress and Strain and Minimum Principal Stress and Strain superior to MS=0.2 which is the limit value for margin of safety. All components of the primary structure present high margins of safety to strain, bearing that in mind the strain is not a critical parameter.

The side frames are the components that present the lower margin of safety (MS=0.5), 2.5 times the limit value of margin of safety, being this way the most critical components. Consequently their thickness should not be reduced in this phase. After the full design of the payload, new

structural analysis shall be performed and the possibility of thickness reduction shall be evaluated.

The ribs are important components of the CubeSat as they are the connection of many elements. They present a margin of safety (in the worse case scenario) of 1.2, being their highest solicitation the tension ($\sigma_{P1} = 12.75\ daN/mm^2$). This margin of safety is 6 times the limit value of margin of safety. Consequently their thickness shall be reduced. The remaining components present high margins of safety therefore, their thickness should be reduced.

With this dissertation the temperatures at the spacecraft were obtained performing analytical studies. For these studies the different optical properties of the materials were taken into consideration. The conclusion of the analytical calculations was that the coldest temperature at the spacecraft is $-48°C$ and the hottest is $94°C$. These values exceed the operational temperatures of the electronic devices hence, the operational envelope of the electronics is limited depending on the β angles of the spacecraft. In order to increase the operational envelop of the subsystems it was recommended the use of aerogel in the interior of the spacecraft due to its good properties of thermal insulation.

At this point of the project, the Mechanical Subsystem fulfills all the defined objectives. Indeed, the environmental constraints, the design and mass requirements as well as the structural integrity are ensured through this work. The future work could then be developed on this basis. Due to its good geometry and available space, the mechanical subsystem allows the integration of other non considered payloads of MECSE, for example Langmuir Probes and one extra battery.

A very important characteristic of the Mechanical Subsystem developed with this master dissertation is that it can be adapted to other mission's payloads and subsystems, this way it is a scalable and a profitable product. Although this is only the preliminary design, once the subsystem is in detailed phase it has potential to bring a great revenue.

5.1 Accomplishments

During the development of this dissertation there were many accomplishments encountered.

The first objective of the dissertation was the investigation of the different standards for the Design of a CubeSat. A long state-of-the-art study was performed and the main challenge was the definition of the standards that MECSE shall fulfill.

The CubeSat Design Specifications document provided by Cal Poly covers the general standards for CubeSats, but depending on the launch platform the requirements change. Therefore, in the begin of the project the launch platform shall be decided.

While projecting the integration of the required Subsystems' hardware, the main challenge was on the integration of the Antenna device. Since the antenna did not present compatible mounting points with the structure, a support had to be designed and adapted to the anatomy of the Antenna and of the Side Frames. Other challenge was the design of the deployment switch mechanism. As there is no available COTS for this type of mechanism, a configuration

that would fit inside the CubeSat's feet had to be studied and projected. After the design of several configurations, a mechanism that is light, fits inside the structure and respects the P-POD requirements was created.
The evaluation of the thermal impact on the subsystems presented many difficulties, as different references had different values of optical properties for the same material. It was understood that in order to test the thermal impact on the subsystems while on-orbit it is possible to create an experiment that simulate that thermal impact. The base of the experiment is the simulation of the space environment with heating lumps. The heating lumps have their light focus on the surfaces of the CubeSat and periodically the CubeSat changes its beta angle in relation to the light. This way it is possible to test the impact of the application of different materials on the surfaces and to clearly define an envelope of operations.

5.2 Difficulties

EESA defines several requirements related to all the subsystems of a CubeSat. These are very important requirements, as they have to be fulfilled before the launch of the CubeSat, but due to the big number of documents related to the same subsystem it is an hard task to clearly define the requirements for each phase of the project. Many hours had to be spent carefully studying the requirements. And in some points of the project, specially during the structural analysis, it was necessary to use margins of safety from aeronautical books as those margins are not limited by EESA.
The Thermal analysis also presented some challenges as the used software for this dissertation could not simulate the effects of the temperature on orbit. Therefore, it was only possible to perform analytical studies. In the future it will be necessary to use specific software for thermal simulations as for example ESATAN-TMS. ESATAN-TMS is a standard European thermal analysis tool used to support the design and verification of space thermal control subsystems.

5.3 Future Work

MECSE project is still in the conceptual phase. Hence, many subsystems are not yet defined. However, the Mechanical Subsystem is in the preliminary phase. Once the project also moves on to the preliminary phase is required that the assumptions done through this dissertation are reconsidered and the preliminary design of the first unit concluded after thorough revaluation.

Concerning the FEM analysis, only the linear static analysis were assessed. Further on it is imperative that transient and random vibrations analysis are performed.

The thermal management is a complex task as it directly depends on the material emissivity and absorptivity properties. As future work, it is advised to perform computer simulations not only related to the surface temperature but also to study the heat modes between the subsystems, as those analysis were neglected for this master dissertation.
Although the geometry of the mechanical subsystem is defined, the material and the manufacturing process should be reevaluated so the weight and the performance of the CubeSat may increase.

Bibliography

[1] D. G.Gilmore, Spacecraft Thermal Control Handbook, 2nd ed., A. I. of Aeronautics and Astronautics, Eds. The Aerospace Press, 2012, vol. Volume I: Fundamental Technologies. xvii, 9, 10, 11, 37, 75

[2] T. Flecht, "Thermal modelling of the PICSAT nanosatellite platform and synergetic prestudies of the CIRCUS nanosatellite," Master's thesis, Lulea University of Technology, 2016. xvii, 75

[3] A. Toorian, K. Diaz, and S. Lee, "The CubeSat Approach to Space Access," in IEEE Aerospace Conference, vol. Vols 1-9, 2008. 1, 8

[4] C. P. SLO, CubeSat Design Specification Rev.13, 2014. 1, 4, 5, 44, 74, 93, 94

[5] A. Poghosyan and A. Golkar, "CubeSat evolution: analyzing CubeSat capabilities for conducting science missions," Progress in Aerospace Sciences, 2016. 1, 3, 4

[6] F. Dias, J. Páscoa, and C. Xisto, "Numerical computations of mhd flow on hypersonic and re-entry vehicles," in ASME 2016 International Mechanical Engineering Congress and Exposition, 2016. 1, 14

[7] F. Dias, "Modelação numérica de escoamento MHD em veículos de reentrada na atmosfera," Master's thesis, University of Beira Interior), 2016. 1

[8] J. R.Wertz, D. F.Everett, and J. J. Puschell, Space Missions Engineering: The New SMAD. Space Technology Library, 2015. 2, 3, 4, 5, 7, 8, 9, 10, 11, 21, 22, 28, 31

[9] F. E. Tubbal, R. Raad, and K.-W. Chin, "A Survey and Study of Planar Antennas for Pico-Satellites," IEEE Access, 2015. 3

[10] S. W. J. Henry Helvajian, Anti-Satellite Weapons, Countermeasures, and Arms Control. Aerospace Press, 2008. 3

[11] W. J. Larson and J. R.Wertz, Space Mission Analysis and Design, 3rd ed. Microcosm Press, 2005. 5, 6, 17, 18, 19, 23

[12] J. Bouwmeester and J.Guo, "Survey of worldwide pico and nanosatellite missions, distributions and subsystem technology," Acta Astronautica, 2010. 6, 7

[13] J. M. Paul Muri, "A Survey of Communication Sub-systems for Intersatellite Linked Systems and CubeSat Missions," Journal of communications, vol. 7, no. 4, 2012. 6

[14] E. S. E. O. Resources. (2012) Dice. [Online]. Available: https://directory.eoportal.org/web/eoportal/satellite-missions/d/dice 6

[15] R. Welle, A. Utter, T. Rose, J. Fuller, K. Gates, B. Oakes, and S. Janson, "A cubesat-based optical communication network for low earth orbit," in 31st Annual AIAA/USU Conference on Small Satellites, 2014. 6

[16] T. P. on Small Spacecraft Technology Committee on Advanced Space Technology, Aeronautics, S. E. Board, C. on Engineering, T. Systems, and N. R. Council, Technology for Small Spacecraft. National Academy Press, 1994. 6, 9, 10, 11, 28, 29, 31

[17] J. A.King, K. Leveque, M. Bertino, J. Kim, and H. Aghahassan, “Ka-band for cubesats,” 29th Annual AIAA/USU Conference on Small Satellites, 2012. 6

[18] NASA. Ground data systems and mission operations. [Online]. Available: https://sst-soa.arc.nasa.gov/11-ground-data-systems-and-mission-operations 7

[19] D.Bekker, P.Pingree, T.Werne, T.Wilson, and B.Franklin, “The COVE Payload-A Reconfigurable FPGA-Based Processor for CubeSats,” 25th Annual AIAA/USU Conference on Small Satellites, 2011. 7

[20] P. Fortescue, J. Stark, and G. Swinerd, Spacecraft System Enginering. John Wiley & Sons Ltd, 2004. 8

[21] CubeSatShop. [Online]. Available: https://www.cubesatshop.com/ 8

[22] Texas University, “Power Subsystem.” 9

[23] Clyde Space. Clyde space cubesat. [Online]. Available: https://www.clyde.space/ 9, 13

[24] GomSpace. [Online]. Available: https://gomspace.com/home.aspx 9

[25] M. M. Finckenor and K. K. de Groh, Space Environmental Effects, A. Rai and N. Hosein, Eds. NASA ISS Program Science Office, 2005. 9, 72

[26] S. Czernik, “Design of the thermal control system for compass-1,” Master’s thesis, University of Applied Sciences Aachen, Germany, 2004. 9, 23

[27] R. D. Karam, Satellite Thermal Control for Systems Engineers. American Institute of Aeronautics and Astronautics, INC., 1998. 10

[28] Sunpower, Inc. [Online]. Available: http://sunpowerinc.com/ 10

[29] Northrop Grumman. [Online]. Available: http://www.northropgrumman.com/Pages/default.aspx 10

[30] Lockheed Martin Space Technology and Research Lab. [Online]. Available: http://www.lockheedmartin.com/us/ssc/atc.html 10

[31] J.M.Madey and R. Baumann, Design Techniques for Small Scientific Satellite Structures, 1969. 11, 24, 25, 26

[32] Pumpkin Incorporated. Pumpkin cubesat kit. [Online]. Available: http://www.cubesatkit.com/ 12, 13

[33] Innovative Solutions in Space. Isis cubesat. [Online]. Available: https://www.isispace.nl/ 12

[34] N. Avionics. (2016) Cubesat structure. [Online]. Available: http://n-avionics.com/cubesat-components/structures-and-deployable-mechanisms/cubesat-structure/ 13, 14

[35] M. K. Kim, “Electronmagnetic manipulation of plasma layer for re-entry blackout mitigation,” Master’s thesis, The University of Michigan, 2009. 14

[36] U. Müller and L. Bühler, Magnetofluiddynamics in Channels and Containers. Springer, 2001. 14

[37] CEiiA. [Online]. Available: https://www.ceiia.com/ 15

[38] J. J. Wijker, Spacecraft Structures. Springer, 2008. 17, 27, 28, 29

[39] P. Gamboa, “O processo de projeto de aeronaves,” 2017. 17

[40] T. D. E. T. Com, Aiaa Aerospace Design Engineers Guide. AIAA, 2003. 17, 18, 24

[41] G. S. Aglietti, G. Richardson, and P. Quill, “Launch environment,” Encyclopedia of Aerospace Engineering, 2010. 19, 20, 21

[42] G. F.Abdelal, A. H.Gad, and N. Abduelfoutouh, Finite Element Analysis for Satellite Structures. Springer, 2013. 19, 22, 24, 25, 26, 27, 28, 29

[43] Arianespace, Vega User’s Manual Issue 4, 2014. 19, 68

[44] A. Calvi, “Spacecraft loads analysis- an overview,” ESA / ESTEC, Noordwijk, The Netherlands, 2011. 21, 41

[45] L.-H. Hu, M.-S. Chang, and J.-R. Tsai, “Thermal control design and analysis for a picosatellite-yamsat,” in Transaction of the Aeronautical and Astronautical Society of the Republica of China, 2013. 21

[46] M. Aguirre, “Satellite configuration and mechanical subsystem,” 2016. 22, 23

[47] C. L.Stevens, “Design, analysis, fabrication, and testing of a nanosatellite structure,” Master’s thesis, Faculty of the Virginia Polytechnic Institute and State University, 2002. 25, 26

[48] F. Hansen, “Dtu satellite systems and design course cubesat thermal design,” Danish Small Satellite Programme, 2001. 25, 26

[49] Vinodh Reddy Chennu. Identification charts for different typrs of fasters: Hear styles, bold and screw, drive, wahser and nut types. [Online]. Available: https://me-mechanicalengineering.com/identification-charts-for-different-types-of-fasteners/ 26

[50] CEiiA, “Stress training,” 2013. 27

[51] A. Silva, “Materiais de constução aeroespacial,” 2016. 28, 50

[52] Alison, “Course-introduction to manufacturing processes,” 2017. 29

[53] F. M. B. C. Santos, “Tecnologia mecânica parte iii,” 2016. 29, 30

[54] C. on Space-Based Additive Manufacturing, Aeronautics, S. E. Board, N. Materials, M. B. D. on Engineering, P. Sciences, and N. R. Council, Eds., 3D Printing in Space. The National Academies Press, 2014. 30

[55] C. Gutierrez, R. Salas, G. Hernandez, D. Muse, R. Olivas, E. MacDonald, M. D. Irwin, R. Wicker, M. Newton, K. Church, and B. Zufelt, “Cubesat fabrication through additive manufacturing and micro-dispensing,” The University of Texas. 30

[56] B. Vayre, F. Vignata, and F. Villeneuve, “Designing for additive manufacturing,” 45th CIRP Conference on Manufacturing Systems, 2012. 30, 31

[57] Loughborough University. About additive manufacturing. [Online]. Available: http://www.lboro.ac.uk/research/amrg/about/the7categoriesofadditivemanufacturing/powderbedfusion/ 31

[58] Loughborough University. About additive manufacturing. [Online]. Available: http://www.lboro.ac.uk/research/amrg/about/the7categoriesofadditivemanufacturing/directedenergydeposition/ 32

[59] A. Engineering, Practical Aspects of Finite Element Simulation. Altair Engineering, 2015. 32, 33, 61

[60] M. Software, Getting Started with MSC.Nastran-User's Guide. MSC Software, 2004. 32, 33, 34, 61, 62, 63

[61] P. Gamboa, "Placas," 2017. 33

[62] European Space Agency, ESA, Space engineering-Spacecraft mechanical loads analysis handbook (ECSS-E-HB-32-26A), 2013. 34, 35, 36

[63] NASA, Load Analyses of Spacecraft and Payloads (NASA-STD-5002), 1996. 34, 35

[64] ESA, Space Engineering-Structural General Requirements, ecss-e-st-32crev.1 ed. ESA Requirements and Standard Division, 2008. 36

[65] D. R. Solomon, "Analysis and design of the mechanical systems onboard a microsatellite in low-earth orbit: An assessment study," Master's thesis, Montana State University, 2005. 36

[66] E. Bruhn, B.S., M.S, C.E, and Dr.Eng, Analysis and Design of Flight Vehicle Structures. S.R.Jacobs and Associates, Inc, 1973. 36, 70, 71, 72

[67] J. J. Wijker, Spacecraft Structures. Springer, 2008. 37

[68] F. Molliet, "Phase C- Swisscube Thermal Analysis," École Polytechnique Fédérale de Lausanne and Haute Ecole Spécialisée de Suisse Occidentale, Tech. Rep., 2008. 37, 38, 39

[69] E. S. E. O. Resources. (2002) Oufti-1. [Online]. Available: https://directory.eoportal.org/web/eoportal/satellite-missions/o/oufti-1 38

[70] DISTRIM. Catia. [Online]. Available: http://www.distrim.pt/catia/ 41

[71] J. Monteiro, "Mission analysis," Master's thesis, University of Beira Interior), 2016. 44, 74

[72] PC/104. What is pc/104-plus. [Online]. Available: http://pc104.org/hardware-specifications/pc104-plus/ 44

[73] P. E. Comsortium, PC/104-Plus Specifications, 2008. 44

[74] Innovative Solutions in Space (ISIS). Dipole antenna system. [Online]. Available: https://www.isispace.nl/product/dipole-antenna/ 46

[75] Innovative Solutions in Space (ISIS). Isis vhf uplink/uhf downlink full duplex transceiver. [Online]. Available: https://www.isispace.nl/product/isis-uhf-downlink-vhf-uplink-full-duplex-transceiver/ 46

[76] Pumpkin, Inc. Motherboard module. [Online]. Available: http://www.pumpkinspace.com/store/p49/Motherboard_Module_%28MBM%29.html 46

[77] Innovative Solutions in Space (ISIS). Isis magnetorquer board. [Online]. Available: https://www.isispace.nl/product/isis-magnetorquer-board/ 47

[78] InvenSense. Motion. [Online]. Available: https://www.invensense.com/motion/ 47

[79] GomSpace. Standard battery module for small nanosatellites. [Online]. Available: https://gomspace.com/Shop/subsystems/batteries/nanopower-bp4.aspx 48

[80] GomSpace. Electrical power supply system for small nanosatellites. [Online]. Available: https://gomspace.com/Shop/subsystems/power-supplies/nanopower-p31ux.aspx 48

[81] AzurSpace. 30% triple junction gaas solar cell. [Online]. Available: http://www.azurspace.com/images/products/0003384-01-02_DB_3G30C-Advanced.pdf 49

[82] Allied Electronics. Zf electronics 0e6200h0. [Online]. Available: https://www.alliedelec.com/zf-electronics-0e6200h0/70207594/ 49

[83] U. S. A. Administration and B. M. I. C. Laboratories, Mettalic Materials Properties Development and Standardization (MMPDS-06). Federal Aviation Administration, 2011. 49, 70, 92

[84] Altair. [Online]. Available: http://www.altairhyperworks.com/product/hypermesh 61

[85] Altair. [Online]. Available: http://www.altairhyperworks.com/product/hyperview 61

[86] M. Software, MSC Nastran Quick Reference Guide. MSC Software, 2008. 62, 63, 65

[87] EESA, Announcement of Opportunity for the Launch of Multiple Light Satellites on a VEGA Flight. 68, 69

[88] QB50, System Requirements and Recommendations-Issue 7, 2015. 69

[89] University of Würzburg. Thermal protection. [Online]. Available: http://www.qarman.eu/index.php/design/thermal-protection 77

[90] University of Würzburg. 10th Pico- and Nano-Satellite Workshop on ”Technologies for Small Satellite Research. [Online]. Available: http://www7.informatik.uni-wuerzburg.de/conferences/pina2017/ 79

Appendix A

Missions and their Main Properties

A.1 Missions

Table A.1: Missions and their Main Properties

ID	Objective	Units	Structure	Payload	Systems
OUFTI-1	Demonstration in orbit of: D-Star digital telecommunications protocol; Azurspace's solar cell; Innovative electrical power system	1U	-Endless ScrewSpacers (AL-6061 T6) -Pumpkin 1U -Antenna's Panel (Aluminium hard anodized MECH subsystem) -Self-Blocking nut	-Experimental Power Supply (EPS2) -Solar cells from AzurSpace	-433 MHz Antenna -144MHz Antenna -Telecommunications Card -Main Power Supply (EPS1) -2 Battery -Permanent Magnet (Al-Ni-Co-5) -3 PC104 Connector -Flight Module 430RBF Module -External Power Supply -Second on-Board computer (OBC2) -FM430 card(OBC1) -Hysteretic rods
SwissCube	Optical Measurements of the airglow phenomenon over all latitudes and longitudinal for at least 3 month	1U	-Main Frame Monoblock -Spacers(Certal Aluminium Alloy) -Screws - PCB (FR-4 material(TBC)) -Composite Panels	-CMOS Detector MT9V032 -OscillatorHC-49/US SMD -RAM R1LV0416CSB-7LI	-COM -Motherboard -Beacon -Antenna -EPS (electronic power system) -ADCS:6 sun sensors attached to the internal face,3 magneto-torques (one per axis),wheel subassembly attached by its axis to the frame -Microcontroller MSP430F1611 -Temperature Sensor LM94022
CubeStar	Perform electron density measurements in the ionosphere	2U	-Monoblock Structure	-Multi-Needle Langmuir Probe (m-NLP) -Electron Gun	-EPS -ADCS: Sensor: 3 axis Magnetometer, 3 axis Gyroscope Sun Sensor Actuator, 3 Magnetorquers -OBDH -COMM
UWE-3	In orbit demonstration of a low-power coarse attitude determination and control system	1U	-Standadized Connectors -PCB4 -Side rails -6 side panels (double sided PCB with aluminium core)	-9 single axis magnetometers -3 single axis MEMS gyroscopes -6 two-angle sun sensors in an istotropic Kalman filter	-OBDH -EPS -COMM -FAB (front access board) -OBC -Batteries
CuSPED	Determination of the dynamics and coupling of the Earth's magnetosphere, ionosphere, and atmosphere and their response to solar and terrestrial inputs	3U	Pumpkin structure	-TECHS: Electrostatic analyzer Microchannel plate (MCP) Anode imaging system Active aperture biasing system UV absorptive coating, Sensor -FOTON GNSS receiver	-3 ISIS Sun Sensor -Clyde Space battery -GOMSpace Nanomind processor -Clyde Space EPS - L3 Cadet UHF Transceiver -3 MAI Earth Sensor -ADIS-16405IMU+ -3 axis Magnetometers -Antcom L1 /L2 GNSS Antenna
Compass-1	Demonstrate the usefulness of an optical sensor for earth observation and a Ka-band antenna(technology demonstration)	1U	-ADCS PCB -COM PCS -EPS PCB -Mainboard PCB -PCB Holder -Frames and Beams	-Optical Sensor -Ka-band antenna	-ADCS (sensor and actuator) -COMM(antenna, transceiver, modem) -Command & Data Handling - Power (solar cells (RWE), battery(E-Tech), power distribution, power regulation & control) -Thermal (Sensor(LM75) & heater (Kapton heater)
Delfi-C3	Test different concepts developed at UPC	3U	-Pumpkin Solid Chassis -Primary and secondary structure -Passive thermal control system - thermal tape	-Thin Film Solar Cells (TFSC) -Autonomous wireless sun sensor (AWSS) -2 radio amateur platforms(RAPs)	-ADCS: AWSS(technology developed) and Passive Magnetic Attitude Control System (PMAS) -FM-430 board from Pumpkin -Local microcontroller(PIC) -Antennas

Appendix B

Material

Table B.1: Material Properties [83]

Material	AA 6061 T6	AA7075 T6	AA 2024 T6	AA 5052 h38	Ti-6Al-4V	15-5PH H1025	AZ31B H24	Beryllium
Density [$10^3 kg/m^3$]	2.70	2.81	2.70	2.68	4.42	7.83	1.77	0.12
Longitudinal Ultimate Tensile Strength [$10^6 N/m^2$]	296.47	551.58	468.84	268.9	958.37	1089.4	268.9	482.63
Longitudinal Tensile Yield Strength [$10^6 N/m^2$]	262	482.63	420.58	220.0	903.21	1048	186.158	344.74
Young's Modulus E [$10^9 N/m^2$]	68.26	71.02	72.39	69.63	110.32	196.5	44.81	293.03
Shear Modulus G [GPa]	26.2	26.89	27.58	26.5	42.747	77.2	16.55	137.90
Specific Heat C [$J/g^\circ C$]	0.896	0.96	0.875	0.88	0.526	0.42	1	1.925
Thermal Expansion[$\mu m/m^\circ C$]	25.2	25.2	24.7	25.7.	9.2	11.3	27	14.5
Thermal Conductivity[W/mK]	167	130	150	138.0	6.7	10.4	96	216
Specific Longitudinal Strength[$10^3 Nm/kg$]	97.04	171.75	155.77	82.09	203.98	133.79	2971.90	2971.90
Electrical Resistivity[Ωcm]	94.48	171.75	155.77	82.09	203.98	133.79	124.79	2971.90
Electrical Conductivity[$\%IACS$]	3.99E-02	5.15E-02	4.50E-02	4.93E-02	1.78	7.79E-01	9.20E-02	4.01E-02

Appendix C

Design Specification Drawings

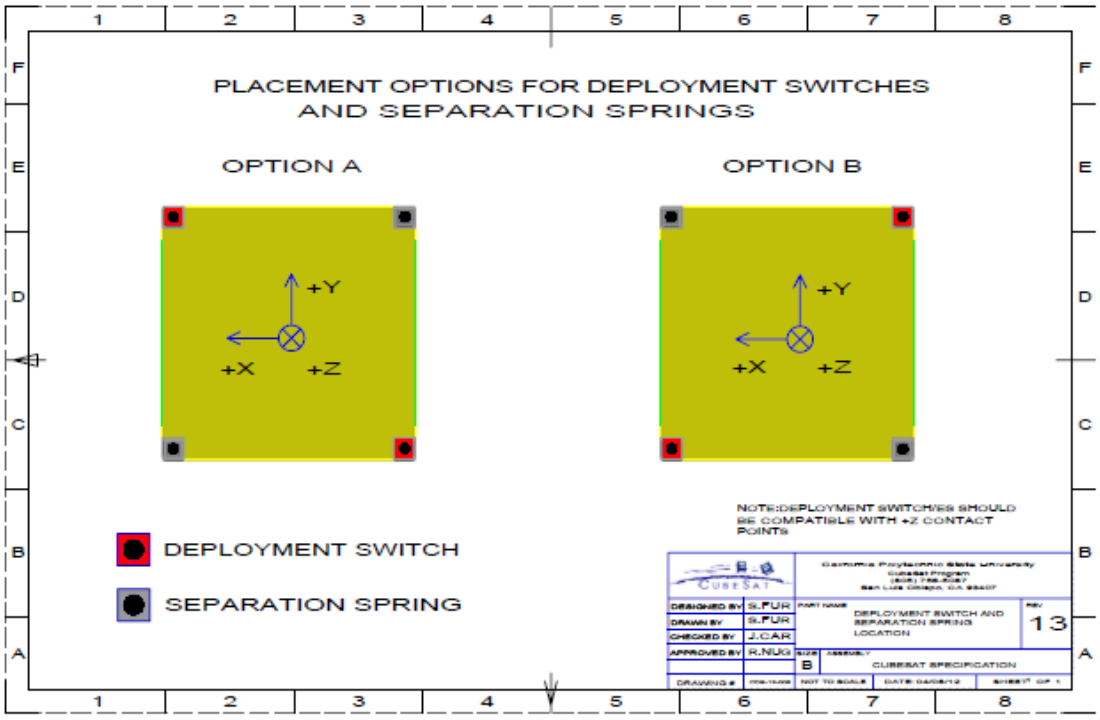

Figure C.1: Deployment [4]

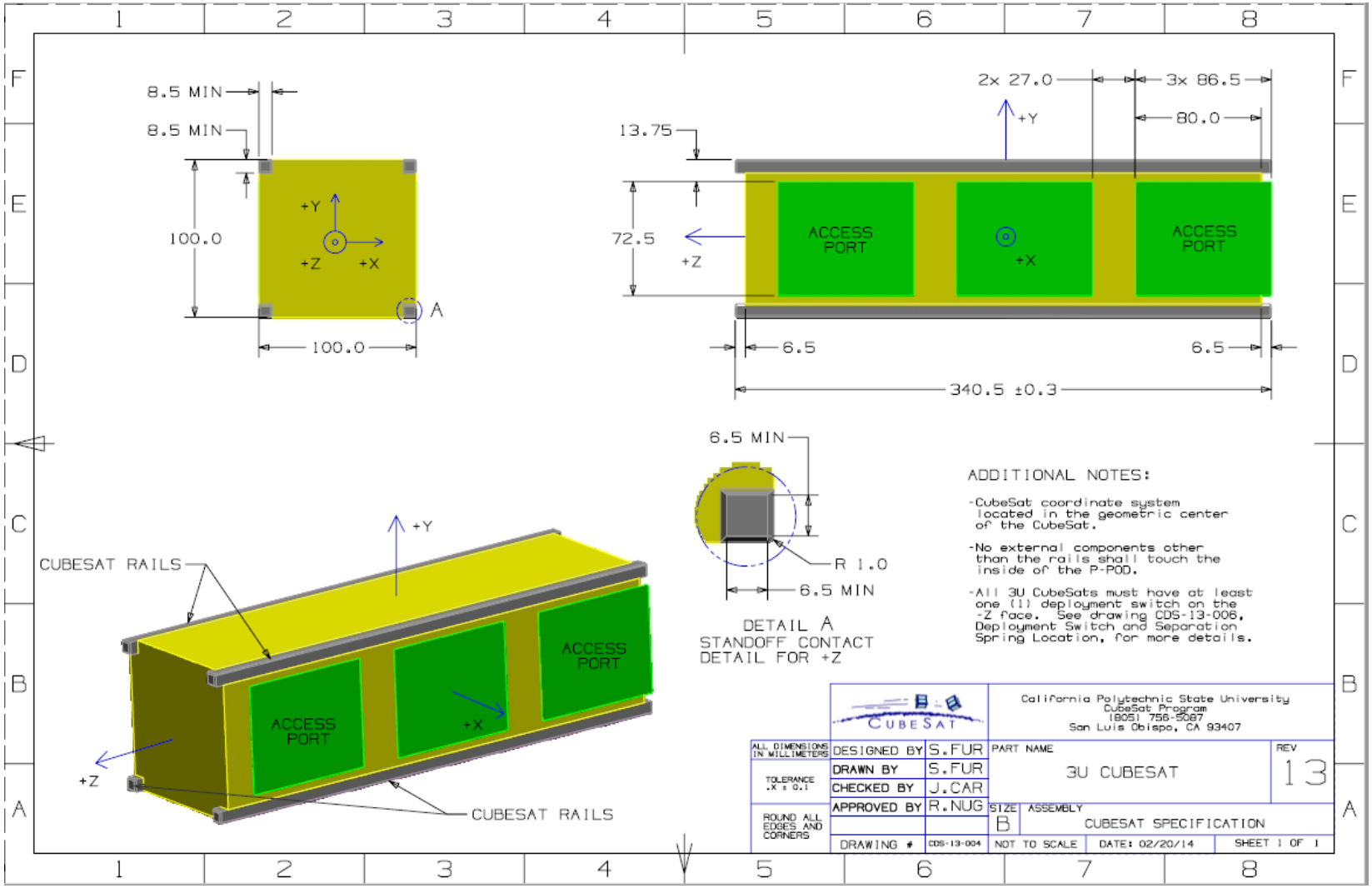

Figure C.2: 3U Cubesat Design Specification Drawing [4]

Appendix D

MECSE Drawings

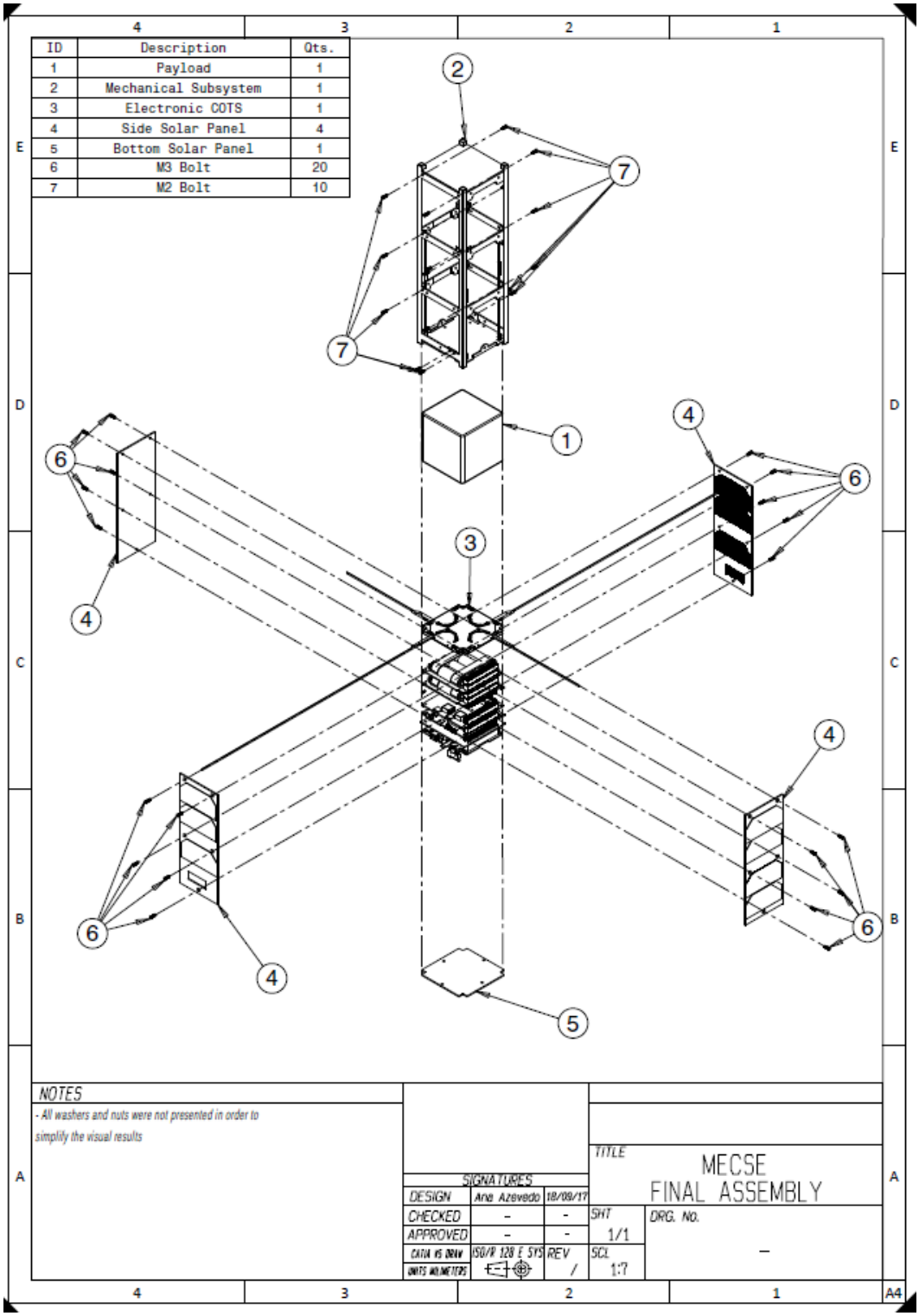

Figure D.1: MECSE Exploded View

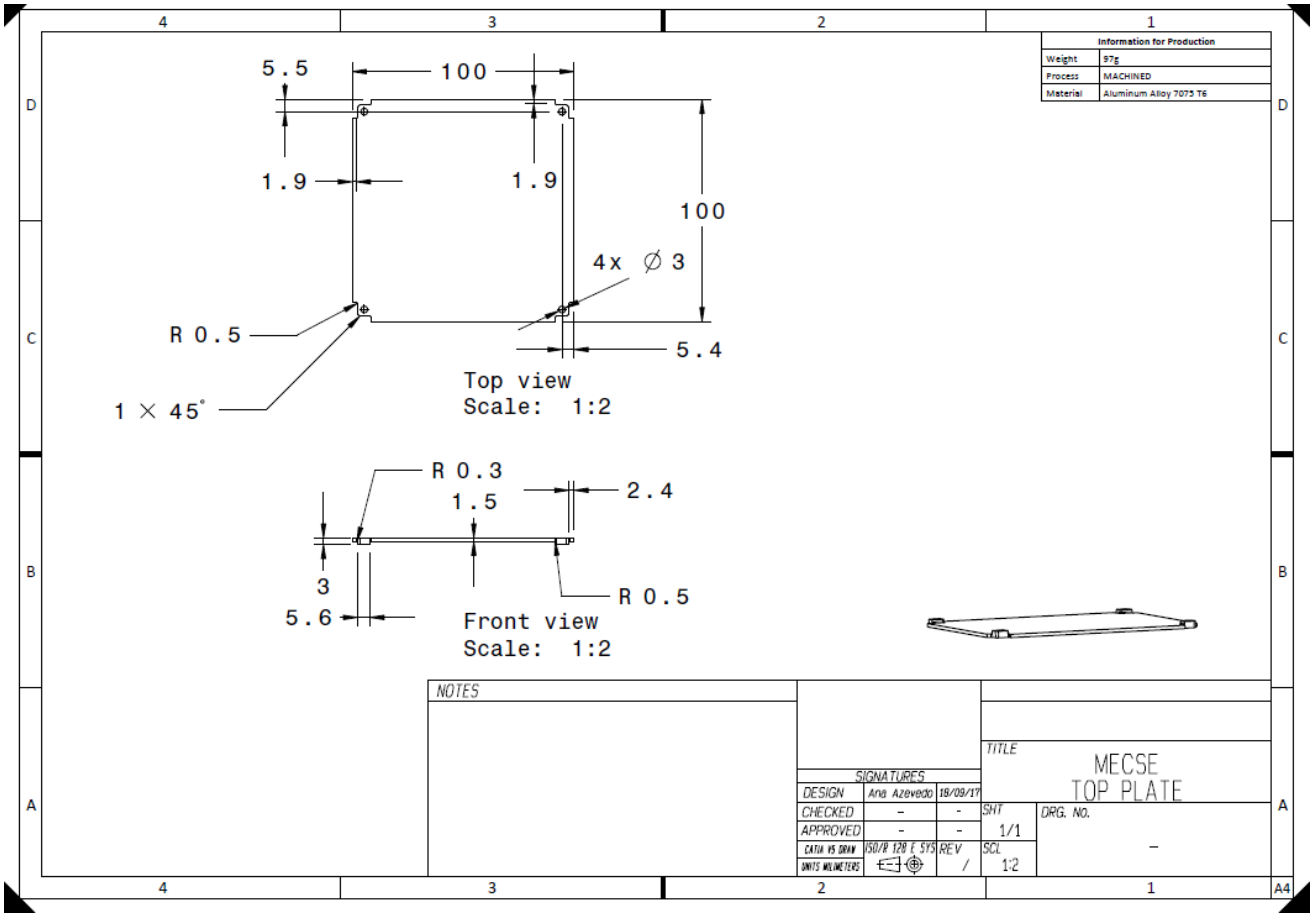

Figure D.2: Top Plate

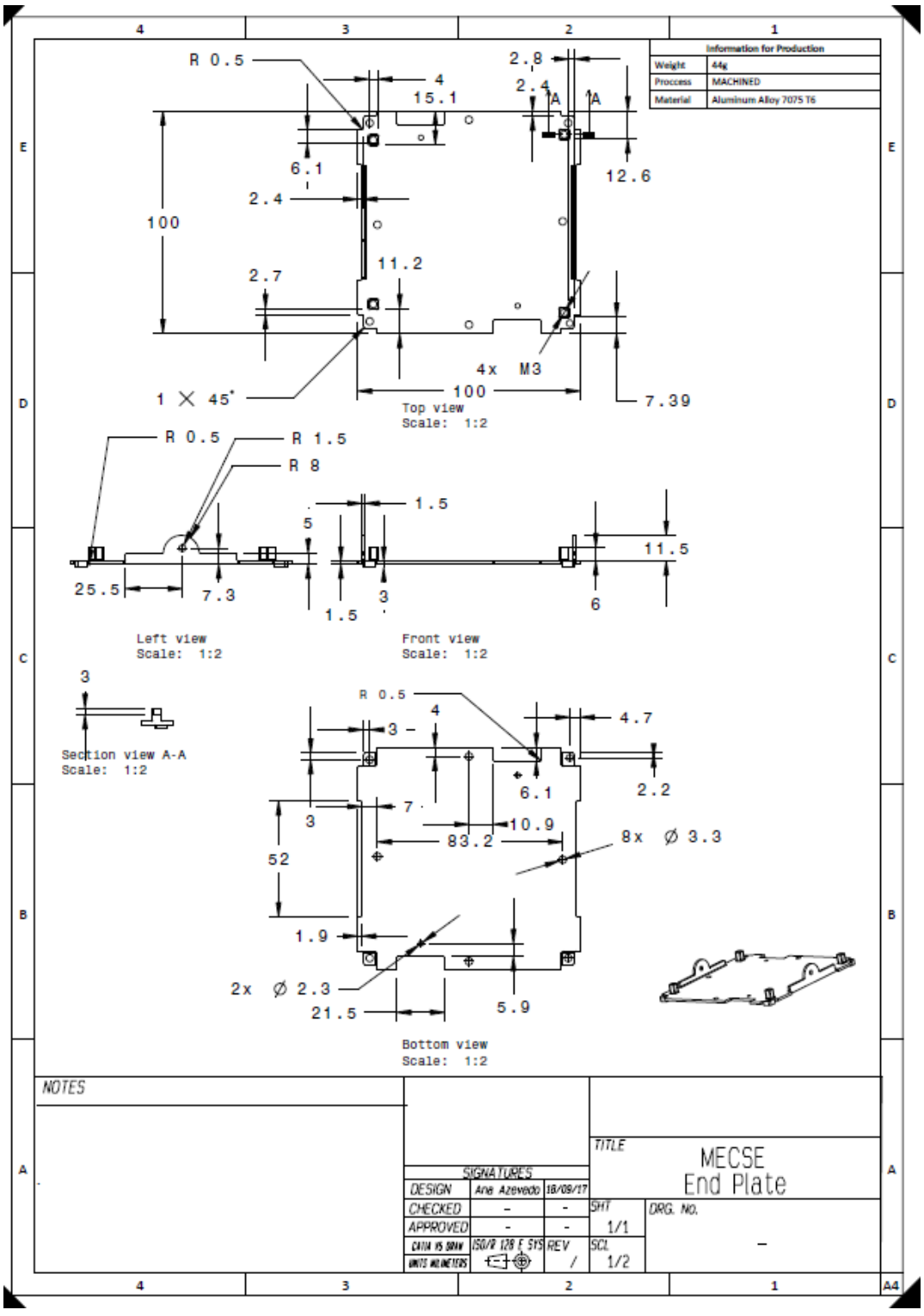

Figure D.3: End Plate

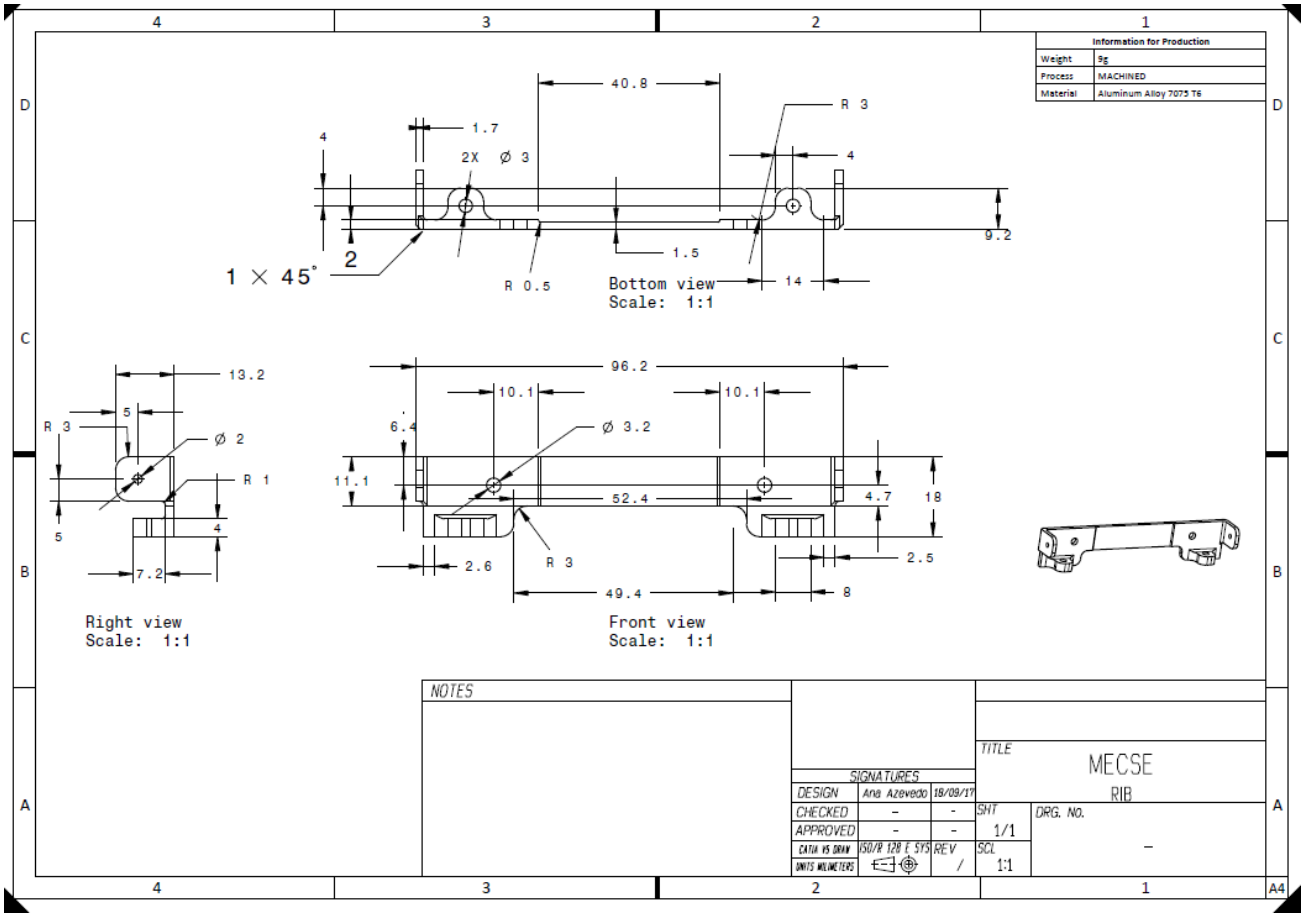

Figure D.4: Rib1

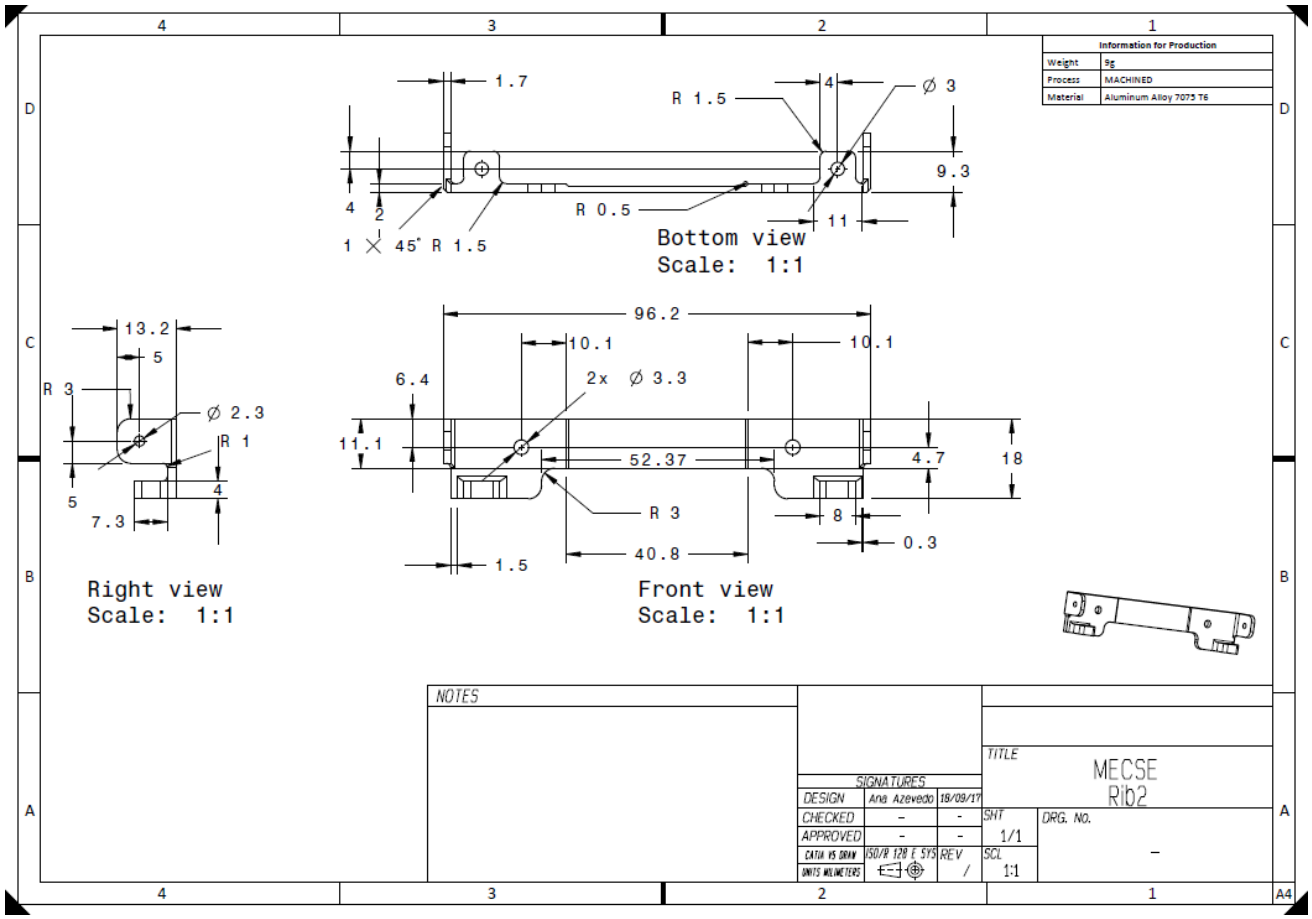

Figure D.5: Rib2

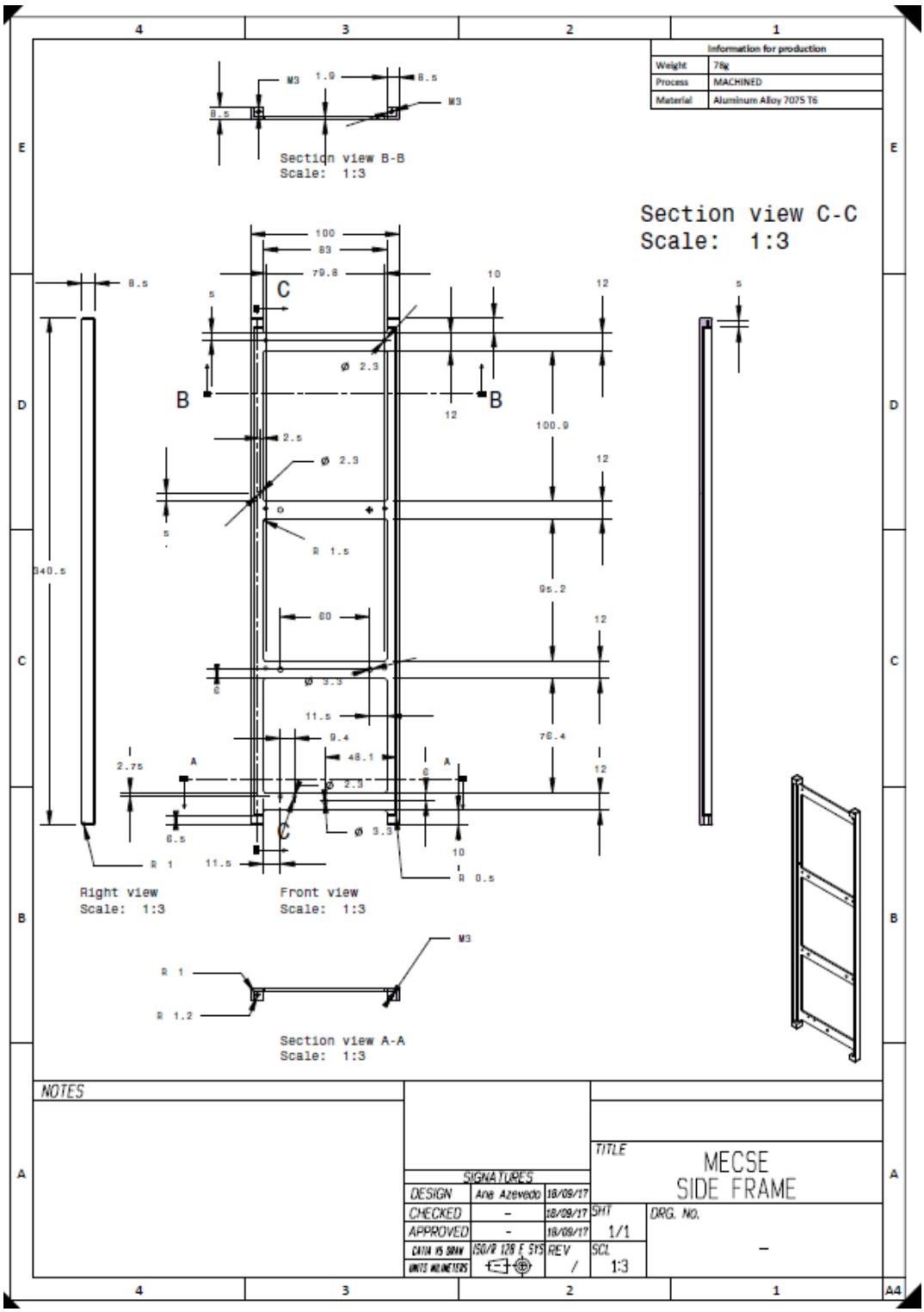

Figure D.6: Side Frame

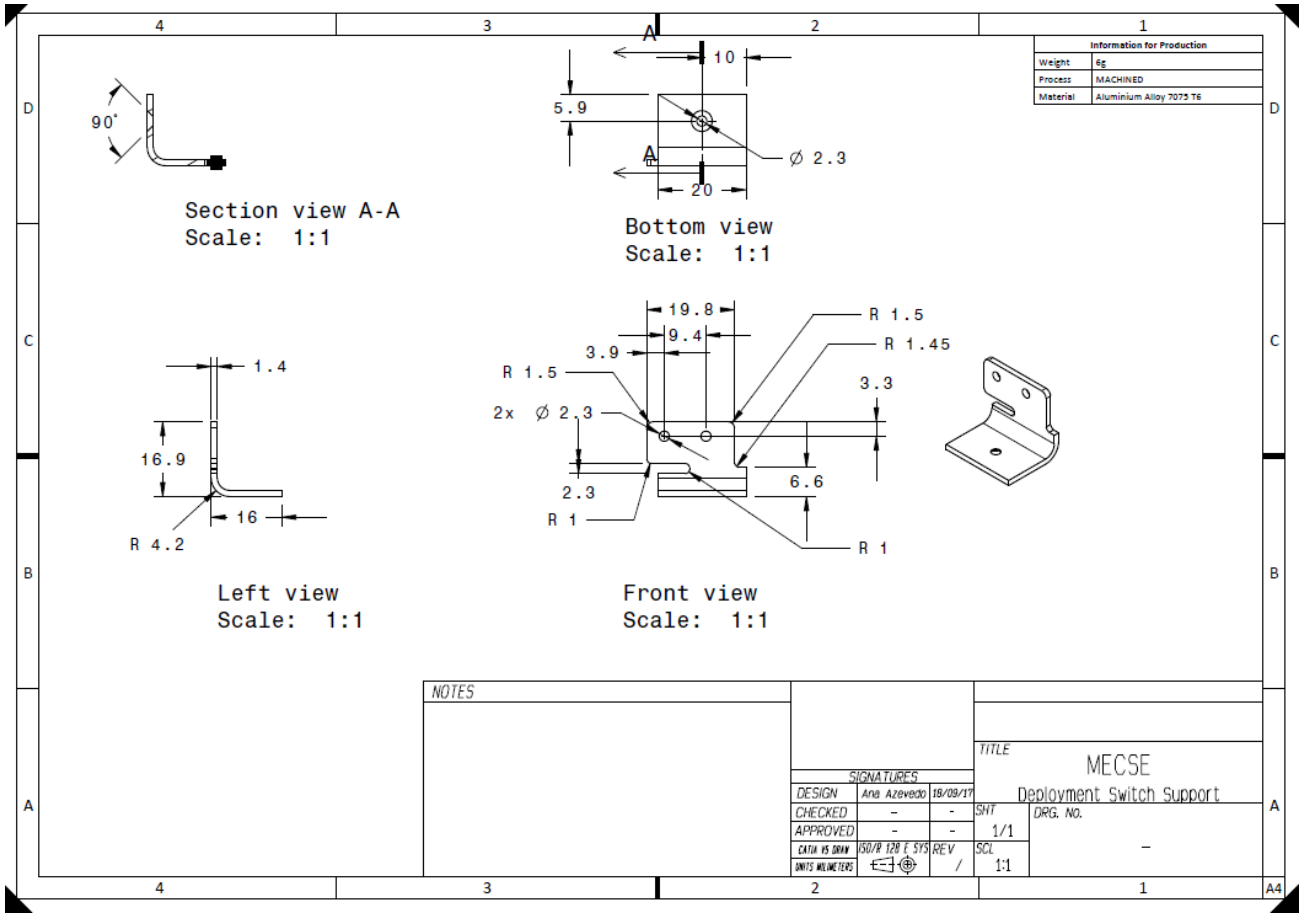

Figure D.7: Deployment Switch Support

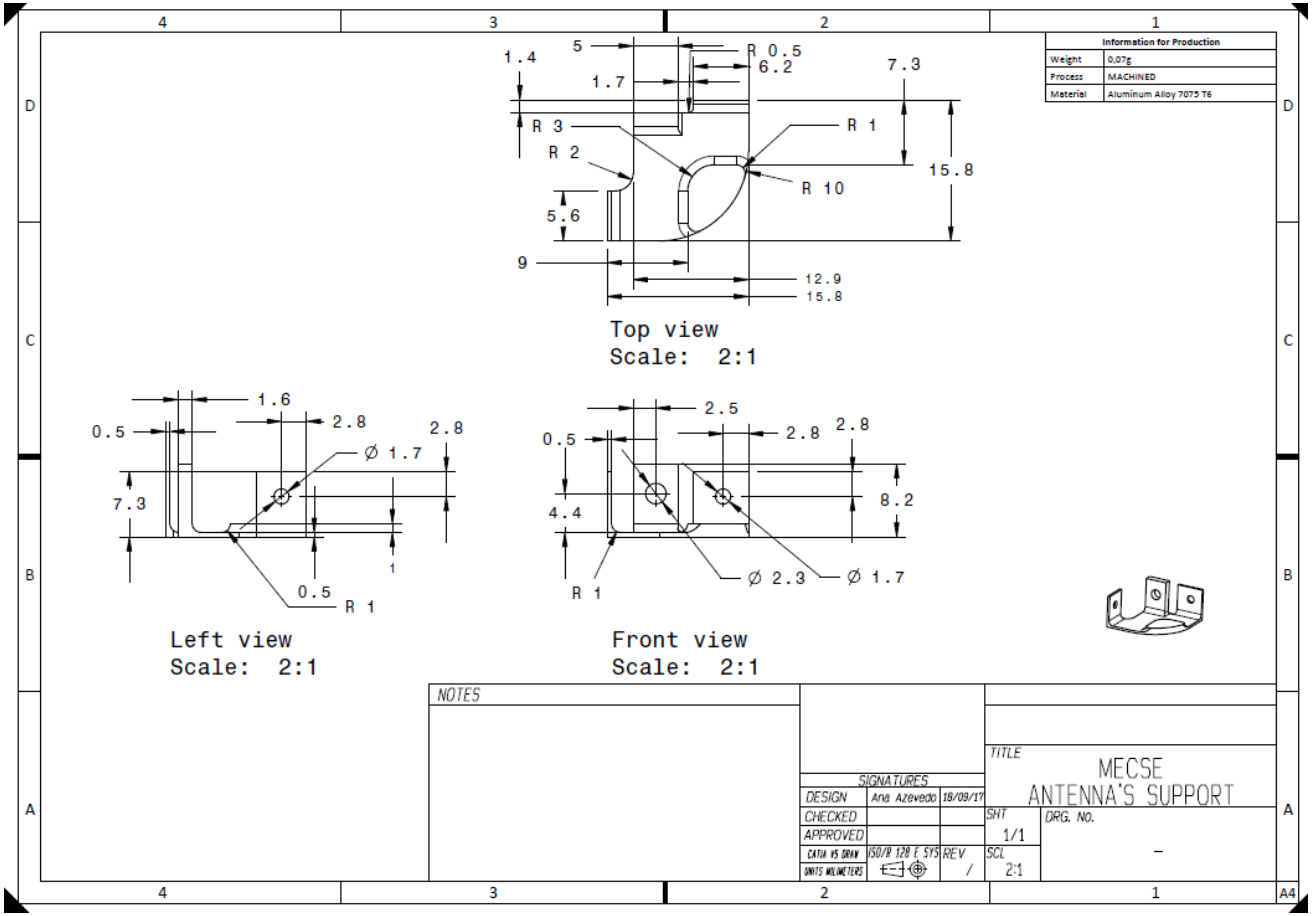

Figure D.8: Antenna's Support

Appendix E

MECSE Physical Properties

Table E.1: Mass Budget

Subsystem	ID	Mass [kg]
Structure	Side Frames	0.157
	Rib1	0.009
	Rib2	0.009
	Rib3	0.009
	Rib4	0.009
	Rib5	0.009
	Rib6	0.009
	Top Plate	0.097
	End Plate	0.044
	Endless Screw1	0.004
	Endless Screw2	0.004
	Endless Screw3	0.004
	Endless Screw4	0.004
	Support Antenna	6.5E-4
	Support Antenna	6.5E-4
	Support Switch	0.006
	Support Switch	0.006
Avionics	Payload	1.2
	Antenna	0.1
	Batteries	0.54
	EPM	0.2
	Transceiver	0.075
	AOCS Board	0.206
	OBC	0.077
	Deployment Switchess	7.3E-4
MECSE Total Mass	2.78	

Table E.2: MECSE Center of Gravity

Subsystem	ID	CG_x	CG_y	CG_z
Structure	Rail	-51.03	49.98	170.25
	Rib1	-51.07	95.88	102.52
	Rib2	-51.07	95.88	209.25
	Rib3	-51.07	85.88	322.13
	Rib4	-51.04	4.13	102.52
	Rib5	-51.04	4.13	209.24
	Rib6	-51.04	4.13	322.12
	Top Plate	-52.06	50.48	333.06
	Base Plate	-52.17	49.38	8.18
	Endless Screw1	-87.83	92.88	110.30
	Endless Screw2	-14.13	92.88	110.30
	Endless Screw3	-91.64	7.18	110.30
	Endless Screw4	-11.63	7.78	110.30
	Support Antenna	-93.84	8.38	219.76
	Support Antenna	-8.23	91.57	219.76
	Support Switch	-7.712	72.11	10.53
	Support Switch	-5.21	89.80	12.34
Avionics	Antenna	-51.03	50.0	222.55
	Bat1	-51.64	54.02	150.64
	Bat2	-51.64	54.02	125.29
	EMB	-52.82	56.18	78.68
	Transceiver	-52.94	50.57	61.91
	Magneto	-81.73	50.94	44.97
	OBC	-49.33	58.00	28.55
	Deployment	-94.55	26.10	15.12
	Payload[Assumed]	-47.00	48	240
	Deployment	7.51	73.85	15.12
MECSE CG		51.60	51.60	176.17

Appendix F

Finite Element Analysis

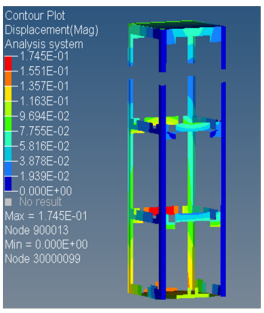

(a) Displacement

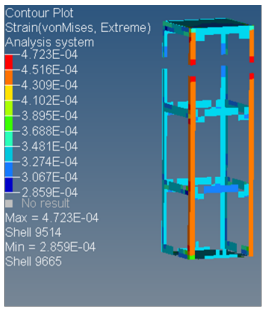

(b) Extreme Von-Mises Strain

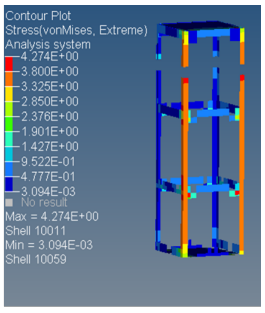

(c) Extreme Von-Mises Stress-MS=7.6

Figure F.1: Case Study 1.

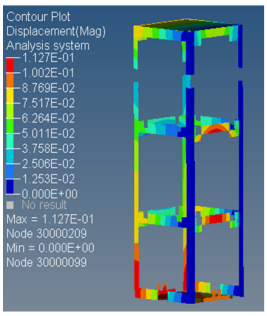

(a) Displacement

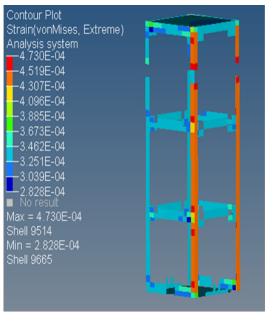

(b) Extreme Von-Mises Strain

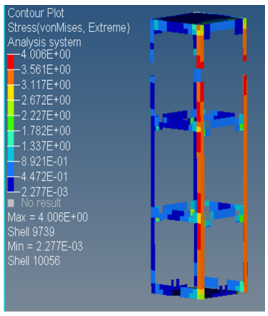

(c) Extreme Von-Mises Stress-MS=8.2

Figure F.2: Case Study 2.

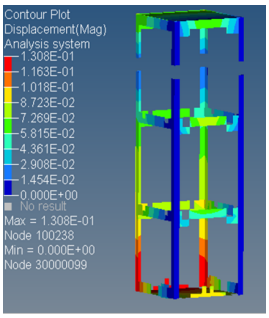

(a) Displacement

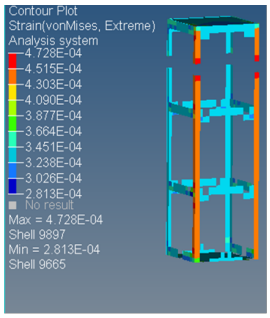

(b) Extreme Von-Mises Strain

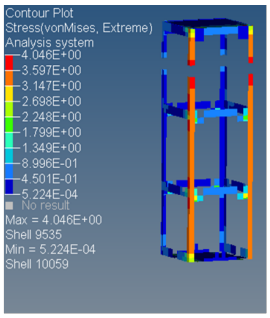

(c) Extreme Von-Mises Stress-MS=8.1

Figure F.3: Case Study 3.

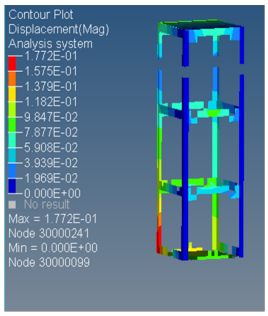

(a) Displacement

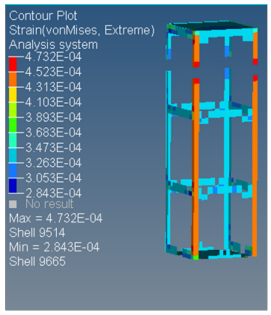

(b) Extreme Von-Mises Strain

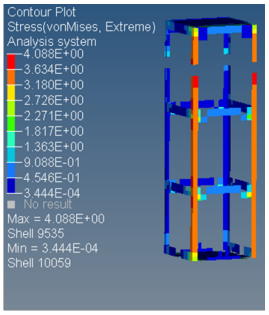

(c) Extreme Von-Mises Stress-MS=8

Figure F.4: Case Study 4.

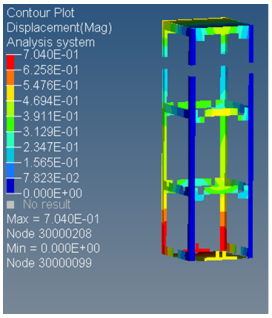

(a) Displacement

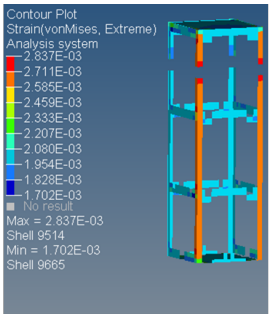

(b) Extreme Von-Mises Strain

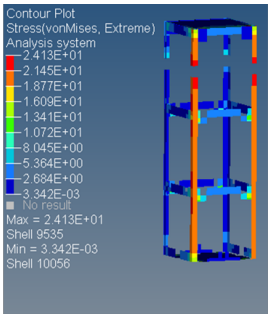

(c) Extreme Von-Mises Stress-MS=0.5

Figure F.5: Case Study 5.

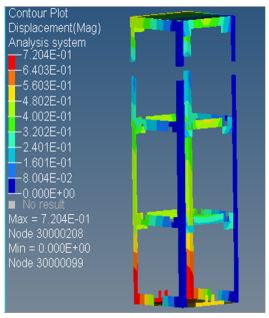

(a) Displacement

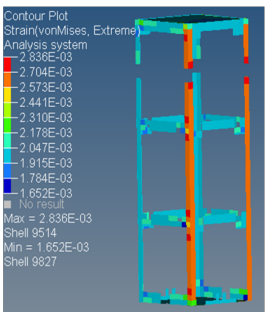

(b) Extreme Von-Mises Strain

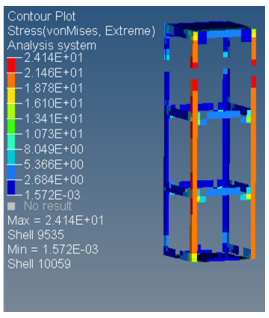

(c) Extreme Von-Mises Stress-MS=0.5

Figure F.6: Case Study 6.

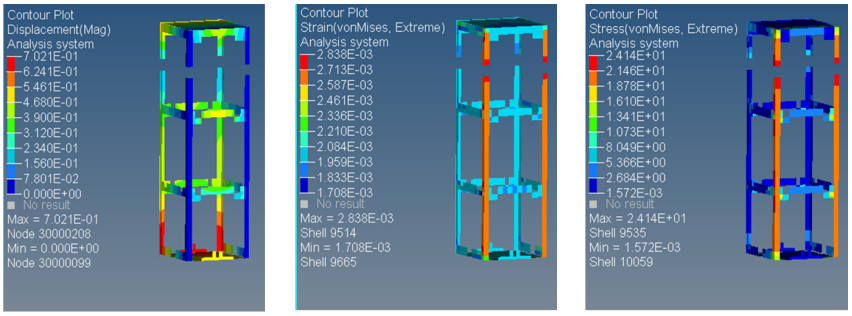

(a) Displacement (b) Extreme Von-Mises Strain (c) Extreme Von-Mises Stress-MS=0.5

Figure F.7: Case Study 7.

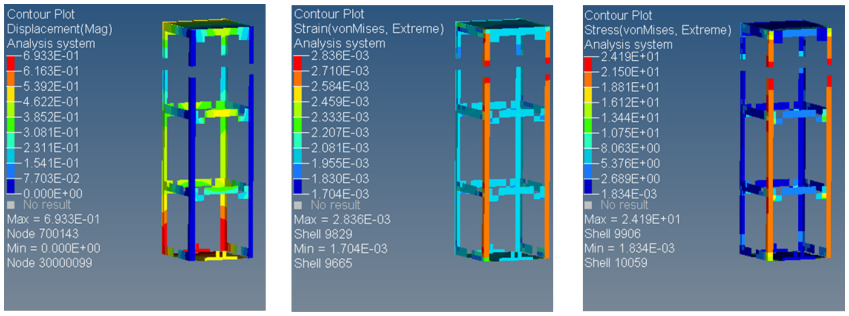

(a) Displacement (b) Extreme Von-Mises Strain (c) Extreme Von-Mises Stress-MS=0.5

Figure F.8: Case Study 8.

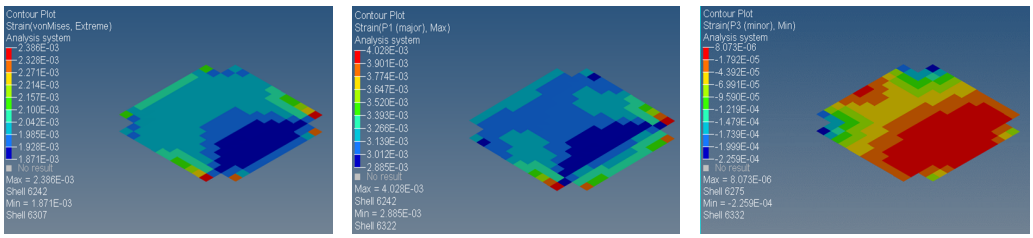

(a) Extreme Von-Mises Strain (b) Maximum Tension Strain (c) Minimum Compression Strain

Figure F.9: ID1-Highest values of Strain for Cases 1 to 8.

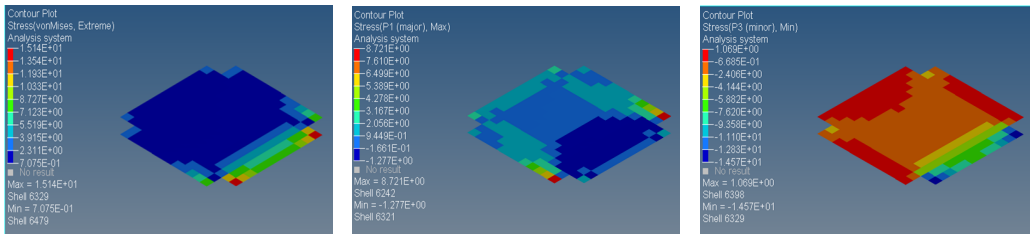

(a) Extreme Von-Mises Stress-MS=1.4 (b) Maximum Tension Stress-MS=3.4 (c) Minimum Compression Stress-MS=1.6

Figure F.10: ID1-Highest values of Stress for Cases 1 to 8.

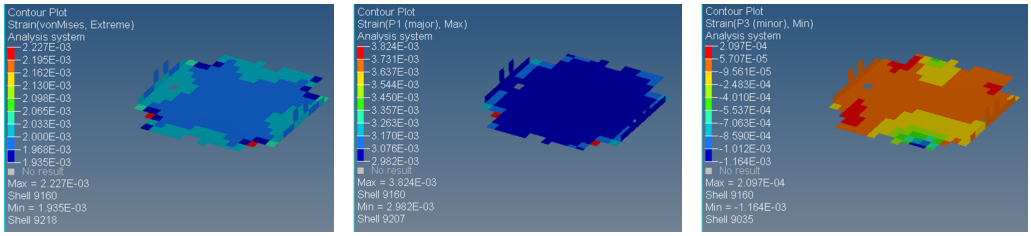

(a) Extreme Von-Mises Strain

(b) Maximum Tension Strain

(c) Minimum Compression Strain

Figure F.11: ID2-Highest Values of Strain for Cases 1 to 8.

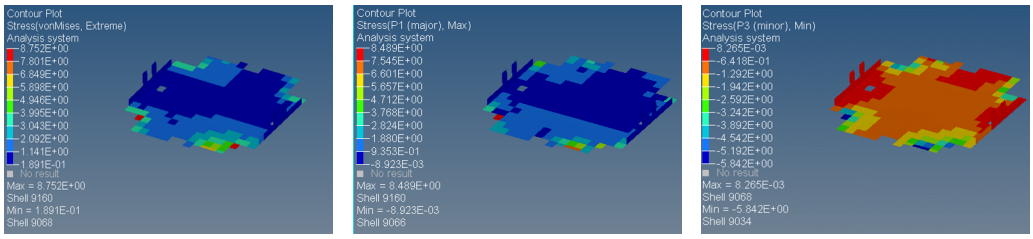

(a) Extreme Von-Mises Stress-MS=3.2

(b) Maximum Tension Stress-MS=3.5

(c) Minimum Compression Stress-SM=5.6

Figure F.12: ID2-Highest Values of Stress for Cases 1 to 8.

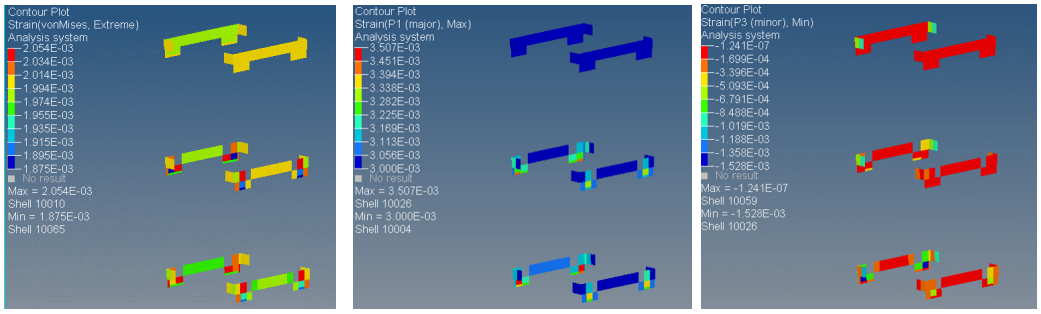

(a) Extreme Von-Mises Strain

(b) Maximum Tension Strain

(c) Minimum Compression Strain

Figure F.13: ID[4-8]-Highest Values of Strain for Cases 1 to 8.

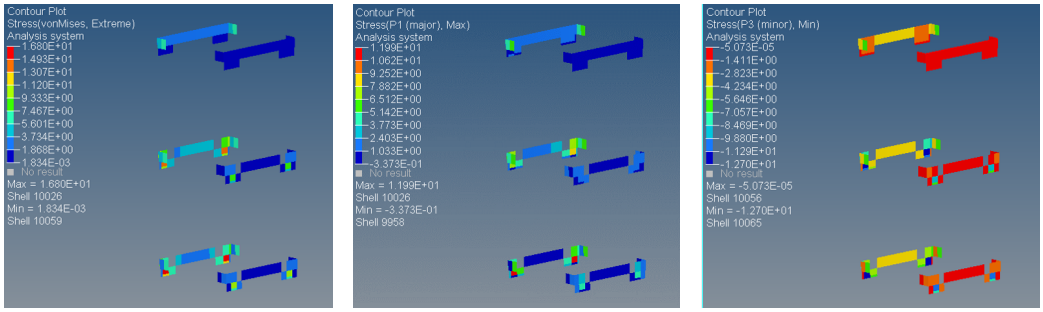

(a) Extreme Von-Mises Stress-MS=1.2

(b) Maximum Tension Stress-MS=2.2

(c) Minimum Compression Stress-MS=2.0

Figure F.14: ID[4-8]-Highest Values of Stress for Cases 1 to 8.

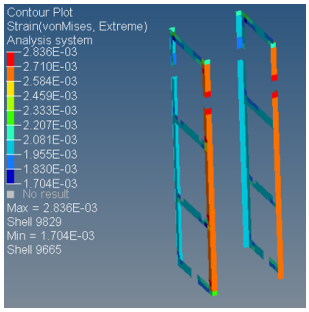

(a) Extreme Von-Mises Strain

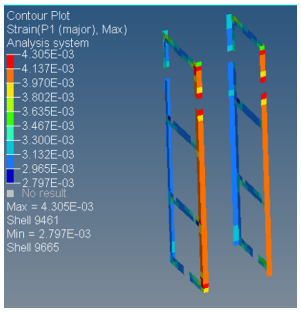

(b) Maximum Tension Strain

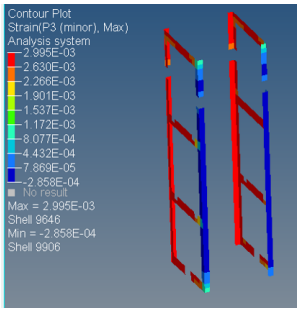

(c) Minimum Compression Strain

Figure F.15: Highest Values of Strain for Cases 1 to 8.

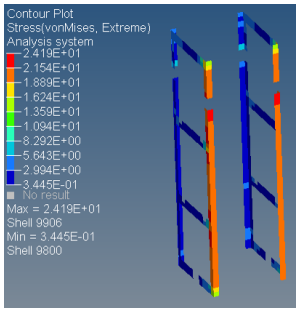

(a) Extreme Von-Mises Stress-MS=0.5

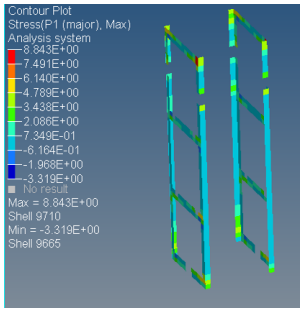

(b) Maximum Tension Stress-MS=3.3

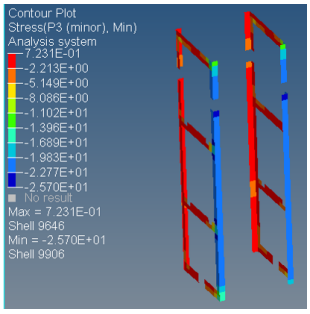

(c) Minimum Compression Stress-MS=0.5

Figure F.16: ID9-Highest Values of Stress for Cases 1 to 8.

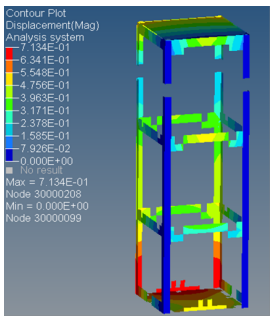

(a) Displacement

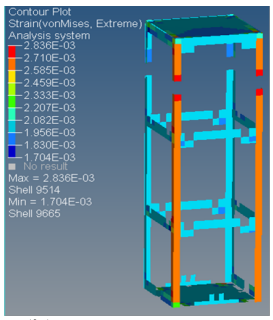

(b) Extreme Von-Mises Strain

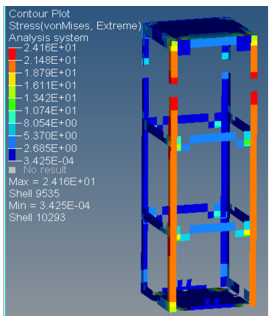

(c) Extreme Von-Mises Stress-MS=0.5

Figure F.17: Case Study 9.

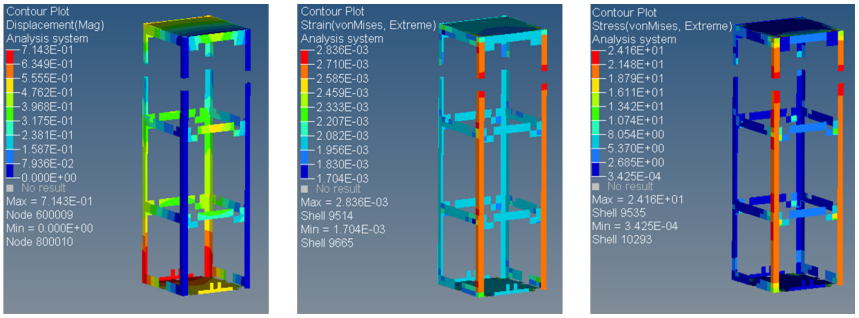

(a) Displacement (b) Extreme Von-Mises Strain (c) Extreme Von-Mises Stress-MS=0.5

Figure F.18: Case Study 10.

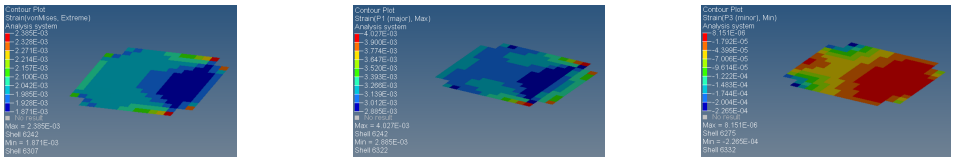

(a) Extreme Von-Mises Strain (b) Maximum Tension Strain (c) Minimum Compression Strain

Figure F.19: ID1-Highest Values of Strain for Cases 9 and 10.

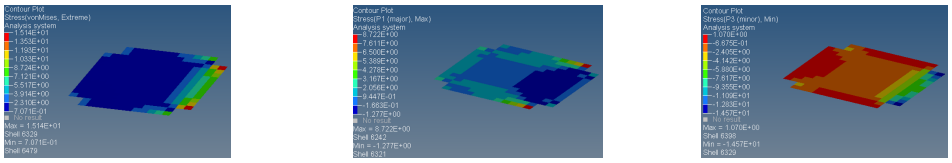

(a) Extreme Von-Mises Stress-MS=1.4 (b) Maximum Tension Stress-MS=1.4 (c) Minimum Compression Stress-MS=1.6

Figure F.20: ID1-Highest values of Stress for Cases 9 and 10.

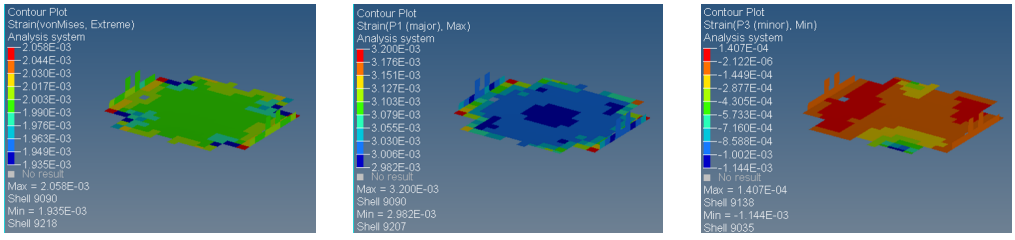

(a) Extreme Von-Mises Strain (b) Maximum Tension Strain (c) Minimum Compression Strain

Figure F.21: ID2-Highest Values of Strain for Cases 9 and 10.

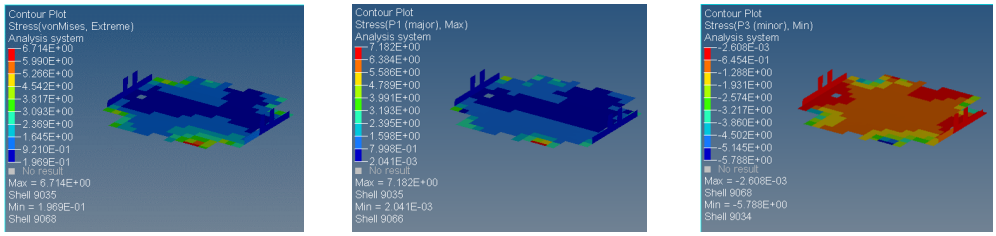

(a) Extreme Von-Mises Stress-MS=4.3 (b) Maximum Tension Stress-MS=7.2 (c) Minimum Compression Stress-MS=5.6

Figure F.22: ID2-Highest values of Stress for Cases 9 and 10.

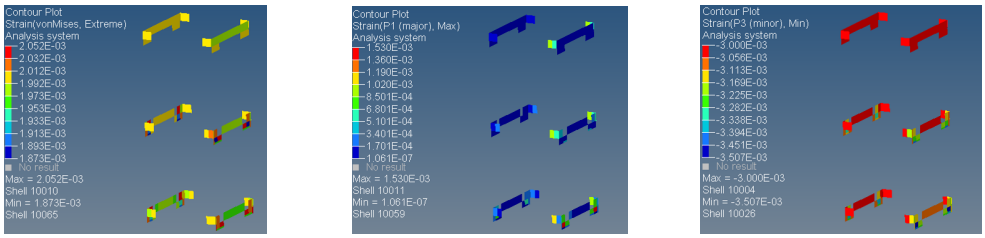

(a) Extreme Von-Mises Strain (b) Maximum Tension Strain (c) Minimum Compression Strain

Figure F.23: ID[4-8]-Highest Values of Strain for Cases 9 and 10.

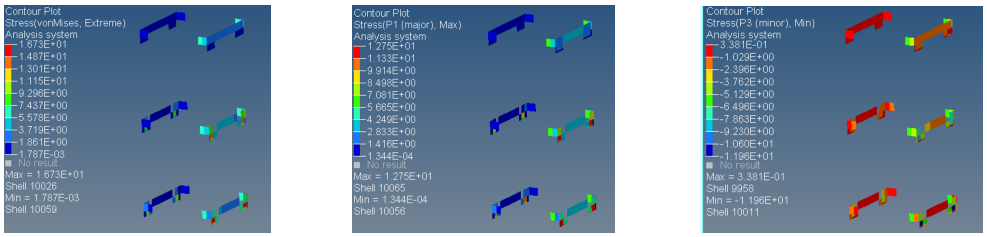

(a) Extreme Von-Mises Stress-MS=1.2 (b) Maximum Tension Stress-MS=2.0 (c) Minimum Compression Stress-MS=2.2

Figure F.24: ID[4-8]-Highest values of Stress for Cases 9 and 10.

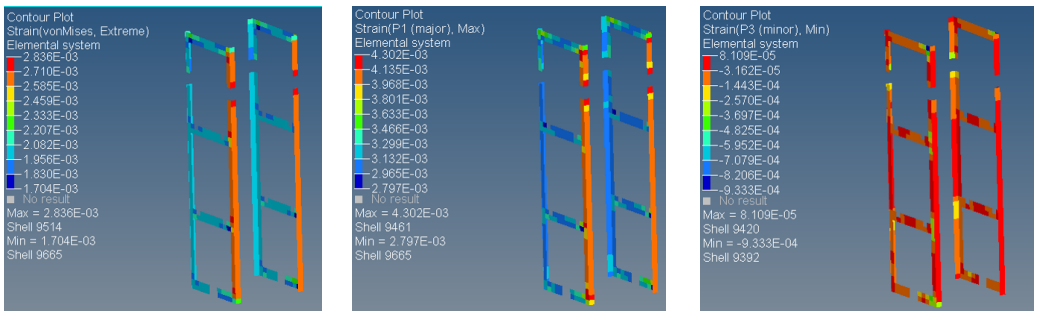

(a) Extreme Von-Mises Strain (b) Maximum Tension Strain (c) Minimum Compression Strain

Figure F.25: ID9-Highest values of Strain for Cases 9 and 10.

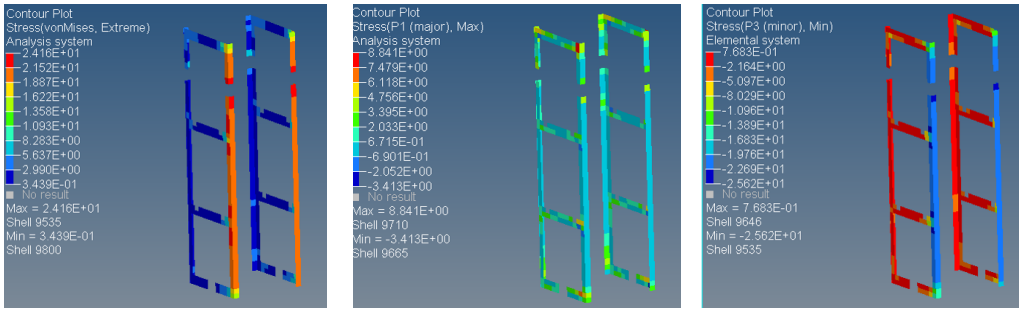

(a) Extreme Von-Mises Stress-MS=0.5

(b) Maximum Tension Stress-MS=3.3

(c) Minimum Compression Stress-MS=0.5

Figure F.26: ID9-Highest values of Stress for Cases 9 and 10.